USING SPECTRAL MEASUREMENTS TO DIFFERENTIATE BETWEEN AQUEOUS NACL AND AQUEOUS KCL IN DUAL-SALT SOLUTIONS

A Thesis Submitted to the College of

Graduate Studies and Research

In Partial Fulfillment of the Requirements

For the Degree of Master of Science

In the Department of Chemical and Biological Engineering

University of Saskatchewan

Saskatoon

By

REISHA DAYLE PETERS

PERMISSION TO USE

In presenting this thesis in partial fulfillment of the requirements for a Postgraduate degree from the University of Saskatchewan, I agree that the Libraries of this University may make it freely available for inspection. I further agree that permission for copying of this thesis in any manner, in whole or in part, for scholarly purposes may be granted by the professor or professors who supervised my thesis work or, in their absence, by the Head of the Department or the Dean of the College in which my thesis work was done. It is understood that any copying or publication or use of this thesis or parts thereof for financial gain shall not be allowed without my written permission. It is also understood that due recognition shall be given to me and to the University of Saskatchewan in any scholarly use which may be made of any material in my thesis.

Requests for permission to copy or to make other uses of materials in this thesis in whole or part should be addressed to:

Head of the Department of Chemical and Biological Engineering
University of Saskatchewan
57 Campus Drive
Saskatoon, Saskatchewan
S7N 5A9

ABSTRACT

Spectroscopy has been used for many years for analytical purposes and its applications are numerous. Though the use of spectroscopy for analysis of water and salt water samples is not a novel concept, most research on the subject has been limited to the concentration range that would typically be found in sea water. Because of the similarities between NaCl and KCl, they have often been assumed to have few if any differences in their effects on the absorption spectrum of water. Correlations between salinity and absorbance have been developed up to about 10% of saturation using water absorption overtones but these results have not been extended to higher concentrations and have not focused on differentiation of species. The research demonstrated in this work showed that modelling the concentration of $NaCl_{(aq)}$ and $KCl_{(aq)}$ in water could be extended up to the saturation point of both salts and the concentrations of individual species could be estimated both in single-salt solutions and dual-salt solutions.

Spectra for water from 15°C to 95°C were used to show the effect of temperature on the absorbance spectra in the wavelength range of 180 nm to 1800 nm. A model was developed from these data that was capable of estimating temperature for water samples based on absorbance. This model was capable of estimating the temperature of water between 15°C and 95°C to within +/- 1.4°C using spectral measurements.

Temperature variation for salt water samples would have also provided useful data, however evaporation at these high temperatures presented a problem as sample concentration would change with loss of water. A method was designed to allow for future testing of salt-water samples at high temperatures that mitigated evaporation while maintaining atmospheric pressure.

Spectral data for $NaCl_{(aq)}$ and $KCl_{(aq)}$ in solution were collected for single-salt samples as well as samples containing both salts. These data were used to develop three models for determining concentration of both $NaCl_{(aq)}$ and $KCl_{(aq)}$ in solution. The first model was capable of differentiating between single-salt samples and determining the concentration of the solution with an average error of 0.9%. The second and third models were able to determine concentrations of both $NaCl_{(aq)}$ and $KCl_{(aq)}$ in dual-salt solutions. These models were able to correctly determine $NaCl_{(aq)}$ and $KCl_{(aq)}$ concentrations to within 3.0% average error for the second model and 2.4% average error for the third model. These models were tested using single-salt solutions between 90 g/L and 300 g/L and dual-salt solutions that would be typical in potash processing (90-160 g/L $KCl_{(aq)}$ and 170-270 g/L $NaCl_{(aq)}$).

ACKNOWLEDGEMENTS

Firstly, I would like to acknowledge the fact that, had I not been given rigorous guidelines, this thesis would have contained many more jokes and likely would have included a number of margin doodles depicting my frustrations during data processing. Perhaps a few expletives would have also found their way into the footnotes as I struggled against the formatting as well!

All silliness aside, there are number of individuals who have made this degree a possibility for me and acknowledging those individuals is but a small token of my appreciation. First, to my parents. Thank you for following me to Saskatoon so that I didn't have to learn to cook for myself and adjust to university all in the same year. You have been so supportive in everything I have strived to accomplish and never doubted my ability to find success where it was pursued. Thank you to my husband, Seth, for working so I could finish my undergrad and for encouraging me to "do whatever I want as long as it makes me happy." I know we always said we would take turns going to school but I've loved being a student with you and wouldn't trade it for a positive bank balance. Orson, I know you don't understand sentences yet, but thanks for always being excited to see me and making me laugh when I got home.

My advisory committee provided so much guidance, direction, and affirmation about my project and always laughed at the jokes I put into my presentations. Thank you Dr. Aaron Phoenix and Dr. Terry Fonstad for helping everything stay on track and for reassuring my fragile ego. I would also like to thank Dr. Farhad Kermani for making me think critically about my data collection and analysis and for keeping a well-stocked chocolate stash in your desk.

This project would never have been born without the call for suggestions put forward by Mrs. Kathlene Jacobson and Mosaic. Thank you Kathlene for all of your help with the project and for my first ever mine tour (though, it would have been a better story if I had gone into labour).

Finally, I would like to say a huge thank you to my supervisor, Dr. Scott Noble. When I first applied for a summer job in your lab I knew I wasn't qualified for the position. Thankfully, you gave me an interview anyways (unlike any of the fast food restaurants in my area of town) and invited me to work for you as a lab assistant, introducing me to the world of research. Being able to work for and subsequently with you has been one of the biggest blessings in my life. You have opened so many doors for me and taught me so much in these past few years; thanking you is going to take more than just some words at the beginning of my thesis. But I can't attach the year's supply of coffee I'm sure you'll need after reading this, so for now, thank you for everything.

TABLE OF CONTENTS

LIST OF TABLES

LIST OF FIGURES

NOMENCLATURE

English Symbols

Symbol	Quantity	Units
A	Absorbance	-
c	Mass/water mass concentration	$g \cdot g_{water}^{-1}$
C	Molar concentration	$mol \cdot L^{-1}$
g^w	Mass of water	g
l	Path length	cm
n	Index of refraction	-
N	Number of samples	-
R^2	Coefficient of determination	-
R	Reflection	-
s_{yx}	Standard error of the fit	-
$t_{\nu,\%}$	Student's t distribution	-
T	Transmittance	-
u	Uncertainty	-
U	Partial uncertainty	-

Greek Symbols

Symbol	Quantity	Units
ϵ	Molar extinction coefficient	$L \cdot mol^{-1} \cdot cm^{-1}$
ν	Degrees of freedom	-
σ	Standard error of estimation	-

Abbreviation	Meaning
NIR	Near infrared
PTFE	Polytetrafluoroethylene
TDS	Total dissolved solids
UV	Ultraviolet
XRF	X-ray fluorescence

1 INTRODUCTION

Potash is a general term that can refer to many potassium salts with the most prominent being potassium chloride (KCl) and is also known as Muriate of Potash. For sale, however, the K_2O equivalent content of each of these salts is considered so conversions using molecular masses are not required (Armstrong, 1998). Potash mining is a major industry in Saskatchewan and potash production in this province supplies about 70% of the world's demand (Government of Saskatchewan, 2015). Potassium chloride and sodium chloride (NaCl) are the two major salts that are abundant in potash mines. These salts are very similar but have key differences that can be exploited in order to effectively separate them. Separation methods involve dissolving NaCl and KCl in water and selectively precipitating KCl. In order to do this most effectively, exact concentrations of the salts in solution must be known. Current analysis of $NaCl_{(aq)}$ and $KCl_{(aq)}$ in solution involves collection, transportation, and processing of samples resulting in a lag time of at least one hour between sampling and having information to act upon. The ability to access continuous in-line measurements of $NaCl_{(aq)}$ and $KCl_{(aq)}$ concentrations in process streams would eliminate this lag time and increases the ability to fine tune the process for optimal productivity.

Using spectral measurements in the ultraviolet (UV), visible, and near-infrared (NIR) regions for monitoring can provide near instantaneous measurements of $NaCl_{(aq)}$ and $KCl_{(aq)}$ in solution, does not present any health and safety risk, and could be relatively inexpensive. Correlations between salinity and absorbance up to 10% of saturation have been previously researched but higher concentration samples have not been investigated extensively. Differentiation between $NaCl_{(aq)}$ and $KCl_{(aq)}$ in solution has often been dismissed due to their similarities (Lin & Brown, 1993) or a lack of necessity for their discrimination (Max & Chapados, 2001). This project focused on developing correlations between high salt concentrations and spectral measurements, and on species differentiation to make the application of UV-visible-NIR spectroscopy applicable in the potash mining industry.

Process streams in potash processing have a temperature range between 15°C and 95°C. These temperature differences can affect the absorbance spectra, so correlations for temperature must be developed. Determining the effect that temperature has on water is simple to measure because evaporation is not an issue for pure water samples. However, collecting high-temperature data for brine solutions presents an issue with evaporation as the sample concentration can change.

Because of the time required to obtain the absorbance spectrum between 180 nm and 1800 nm with a good signal-to-noise-ratio, the concentration of the sample at the beginning and the end of the scan could differ. With very high-concentration samples, evaporation can also cause precipitation resulting in light scattering and precipitate suspension in the sample cuvette. For this project, a method was developed to mitigate this evaporation while maintaining atmospheric pressure. Data for salt water samples at temperature were not collected because of required improvements determined after this method was tested. Future designs will allow for the collection of these data and development of a model that is capable of determining $NaCl_{(aq)}$ and $KCl_{(aq)}$ concentration in dual-salt samples at various temperatures. Spectral data for water over the temperature range were collected and a model was developed that is capable of estimating the temperature of liquid water based on spectral measurements.

For brine solutions, spectral data were collected at 25°C to limit evaporation. Spectra of pure $NaCl_{(aq)}$ and $KCl_{(aq)}$ samples up to saturation were used to show the effects of each salt on absorbance. Using the data obtained from these measurements, a model was developed that accurately classified whether a sample contains $NaCl_{(aq)}$ or $KCl_{(aq)}$ and determined the concentration of that salt in the solution. Spectra of mixed salts extended these results to prove that discrimination of the effects of $NaCl_{(aq)}$ and $KCl_{(aq)}$ can be used to estimate the concentrations of each salt in mixtures. All models for determining salt water speciation and concentration were developed for 25°C. Future models will consider the effect of temperature on the absorbance spectra. The developed models were tested using a range of samples that represent the model's capabilities and the results were analyzed to determine the possibility of using spectral absorbance for speciation in dual-salt samples.

2 LITERATURE REVIEW

Many studies have been conducted to determine the spectral properties of water and the effects that temperature, pressure, and impurities have on that spectrum. The dissolution of salt in water has been found to produce changes both in the structure of the water (Hribar *et al.*, 2002) and the placement and intensity of absorption bands (Max & Chapados, 2001). These changes have been used to determine the concentration of $NaCl_{(aq)}$ and $KCl_{(aq)}$ in solution but have not been used for differentiation between these two salts (Lin & Brown, 1992). This differentiation is valuable for industrial potash mining applications as the current quantification methods for $NaCl_{(aq)}$ and $KCl_{(aq)}$ in solution are time consuming. A review of the currently available literature regarding water structure and spectroscopy as well as salt water structure and spectroscopy will highlight the need for a differentiation method between $NaCl_{(aq)}$ and $KCl_{(aq)}$ in solution. Other electrolyte quantification methods will also be investigated to further indicate that the use of spectroscopy is an appropriate method to meet this need.

2.1 Potash Industry

In the potash industry, raw ore containing large quantities of potassium chloride and sodium chloride must be processed to obtain pure KCl. One method used for this processing involves dissolving the ore in water and using saturation curves and temperature gradients to selectively precipitate the KCl from the brine. Solution mining of Potash ore involves the dissolution of NaCl and KCl (as well as other impurities in smaller quantities) into warm water pumped directly into the ore body. While conventional mining typically uses flotation for the first step in the KCl separation, solution mining uses selective crystallization (Perucca, 2003). During processing, chemicals and additional NaCl are added to the solution to increase the amount of KCl that can be precipitated. The quantities of these chemicals are related to the saturations of NaCl and KCl and have to be carefully calculated based on the current saturation of the brine. Adding too much NaCl can result in a precipitate with low purity and adding too little can result in low efficiency as less KCl can be recovered.

Currently, analysis of brine concentrations is performed using x-ray fluorescence (XRF), which requires the collection, dilution, and transportation of samples to a lab. While this method is effective, it is not efficient for monitoring the concentration at all times. This method also presents safety issues as an x-ray or gamma ray source is required. These sources must be carefully

monitored as over exposure to these radiation sources can damage human cells. There has been significant interest in developing an online technique that could be used for determining brine concentration using a safer and cheaper method that XRF that would not require the collection, transport, and dilution of samples.

The concentrations of $KCl_{(aq)}$ and $NaCl_{(aq)}$ during processing are typically high, ranging from 100 to 170 g/L for $KCl_{(aq)}$ and 200 to 240 g/L for $NaCl_{(aq)}$. Trace amounts of magnesium chloride ($MgCl_2$) and calcium sulfate ($CaSO_4$) are also present in the solution and can affect the solubility curves of the primary salts. The temperature of the solution reaches a low of approximately 15°C and extends to 95°C. At these temperatures and concentrations, the total dissolved solids (TDS) found in the ponds are often as high as 300,000 and the solution is near saturation (Jacobson, 2012).

2.2 Water

The properties of water have been extensively studied over many decades. Only a few pertinent features including structure, absorption, and a select set of environmental factors will be discussed to provide a brief introduction. For the purposes of this thesis, only liquid water is of interest.

2.2.1 The Structure and Absorption of Water

Water molecules are made of two hydrogen atoms and one oxygen atom. The hydrogen atoms are much smaller in mass than the oxygen atom due to the presence of only one proton in the hydrogen nucleus compared with the 8 protons in the oxygen nucleus. In normal water (sometimes referred to as light water) the hydrogen nucleus does not contain any neutrons (Maréchal, 2006). The oxygen atom, however, contains 8 neutrons in addition to the protons. This results in the oxygen atom having a mass that is about 16 times that of the hydrogen atom. Electric fields and hydrogen bonding allow the hydrogen to be transferred between oxygen atoms during a process called protonation and deprotonation. These processes are occurring constantly in the water and account for water's ability to act as both an acid and a base (Geissler *et al.* , 2001).

The structure of the water molecule is not linear along the H-O-H bond due to the presence of lone pair electrons in the outer shell of the oxygen atom. These two pairs of electrons cause the water molecule to form a dipole moment (Martin & Zipse, 2005). Each hydrogen atom carries a partial positive charge and the oxygen atom carries a partial negative charge. One molecule's

hydrogen will attract another molecule's oxygen allowing for an intermolecular interaction called hydrogen bonding. Hydrogen bonding is one of the main reasons that water remains liquid at room temperature as it prevents liberation of water molecules into the gas phase. The molecules are held together more tightly and are actually forced closer together than standard molecular distances would predict due to the presence of these hydrogen bonds (Isaacs *et al.*, 2000). The nature of these bonds is, however, very dependent on the environment and they are easily affected by temperature, contaminates in the water, and pressure.

The non-linear structure of the water molecule allows for three types of vibrations and librations (swaying back and forth of the molecule) in three axes. The three vibrations include symmetric stretching (ν_1), bending (ν_2), and asymmetric stretching (ν_3) (Walrafen & Pugh, 2004). Figure 2-1 illustrates how each of these vibrations occur in the water molecule.

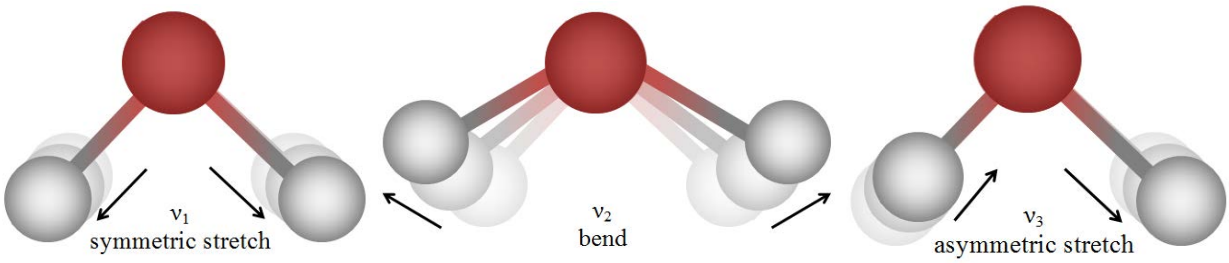

Figure 2-1: Vibrations in water molecules.

At 30°C the ν_2 bend initially causes absorption near 6080 nm with harmonics near 4650, 1900, 1200, 836, and 660 nm. The ν_1 and ν_3 stretching absorption bands occur near 3050 nm and 2870 nm respectively and both stretches contribute to absorption harmonics near 1900, 1470, 1200, 970, 836, 739, 660, 606, 514, 449, and 401 nm in various ratios (Walrafen & Pugh, 2004). These three vibrations are responsible for the main absorption bands of liquid water in the infrared region of the electromagnetic spectrum. Figure 2-2 shows the main absorption bands from the three vibrations as well as a number of their overtones.

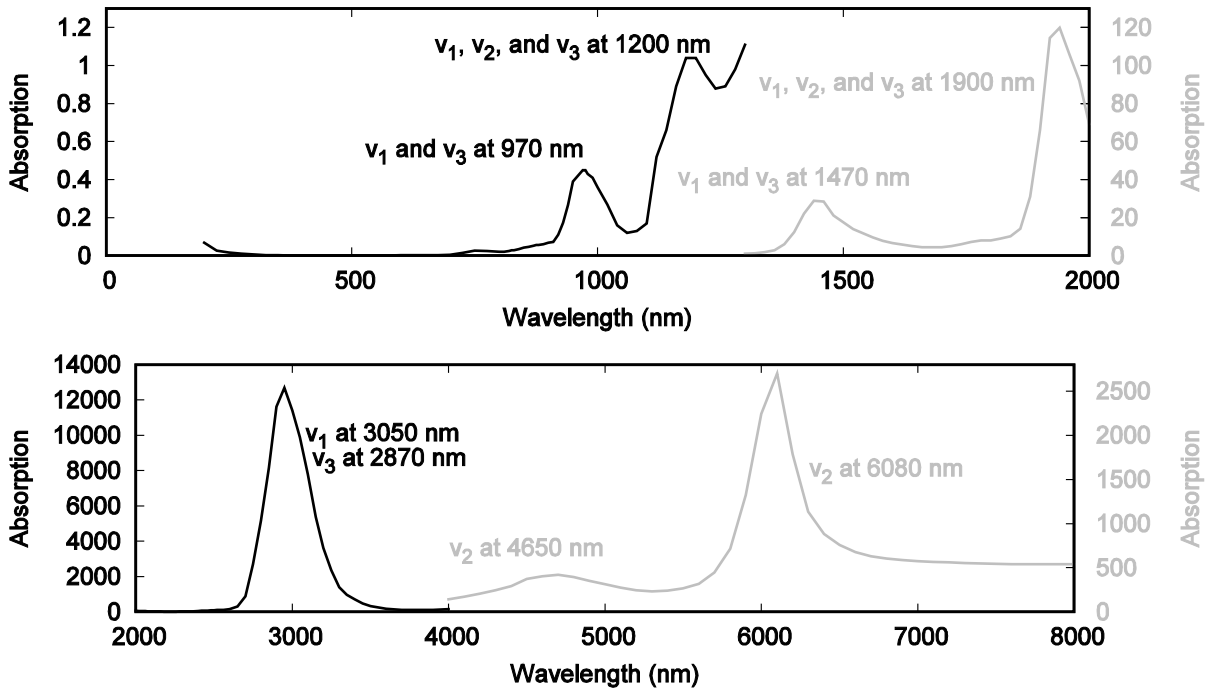

Figure 2-2: Absorption bands and harmonics in water at 25°C as found by Hale and Querry (1973).

The librations have primary absorption features near 23.3 μm, 15.4 μm, and 12.6 μm (Carey & Korenowski, 1998). These features also produce overtones but are much less prominent than the vibrational absorption. The main absorption bands in the infrared regions exhibit overtone absorption features (or harmonics) that appear in the near infrared and visible regions. The two stretching vibrations have their main absorption bands at different frequencies but the harmonics of the two stretching vibrations generally occur at the same higher frequencies or overlap to an extent where they cannot be differentiated. The bending vibrations exhibit harmonics at many of these stretching frequencies but also contribute to unique absorption feature overtones (Walrafen & Pugh, 2004). Like hydrogen bonding, the stretching and bending vibrations are easily affected by environmental factors such as temperature, pressure, and contaminants present in the water.

2.2.2 Temperature Effects

Changes in temperature cause a number of changes in the water structure. Increasing the temperature reduces the strength of the hydrogen bonds and decreases the energy required to break these bonds (Dougherty, 1998). The density of water also decreases as temperature increases. In addition to these changes, an increase in temperature also causes the stretching vibrations to shift to higher frequencies and the bending vibrations to shift to lower frequencies (Praprotnik *et al.*,

2004). Because many of the harmonics of the main absorption bands have contributions from both the bending vibrations and the stretching vibrations, a widening is expected in the absorption bands as temperature increases.

The effectiveness of hydrogen bonding is further described by Abe (2004) as the combination of five different structures of water molecules, each having a different number of active hydrogen bonds. These five arrangements of water have between zero and four hydrogen bonds per molecule and, as outlined by Abe, each type contributes a different Gaussian absorption feature to the stretching vibration harmonics. As the number of hydrogen bonds increases, the corresponding Gaussian peak centers around a higher wavelength. This corresponds with the temperature shift for stretching vibrations as an increase in temperature will result in fewer hydrogen bonds (or a lower concentration of quadruple-bonded water molecules) which translates to a shift to higher frequencies (Abe, 2004). A summation of the Gaussians for each of the five water species approximates the absorption spectral shape for water at 0°C in Figure 2-3. Abe's work focused on the absorption band around 970 nm which results from the harmonics of the stretching vibrations but does not consider the effects of bending vibration harmonics.

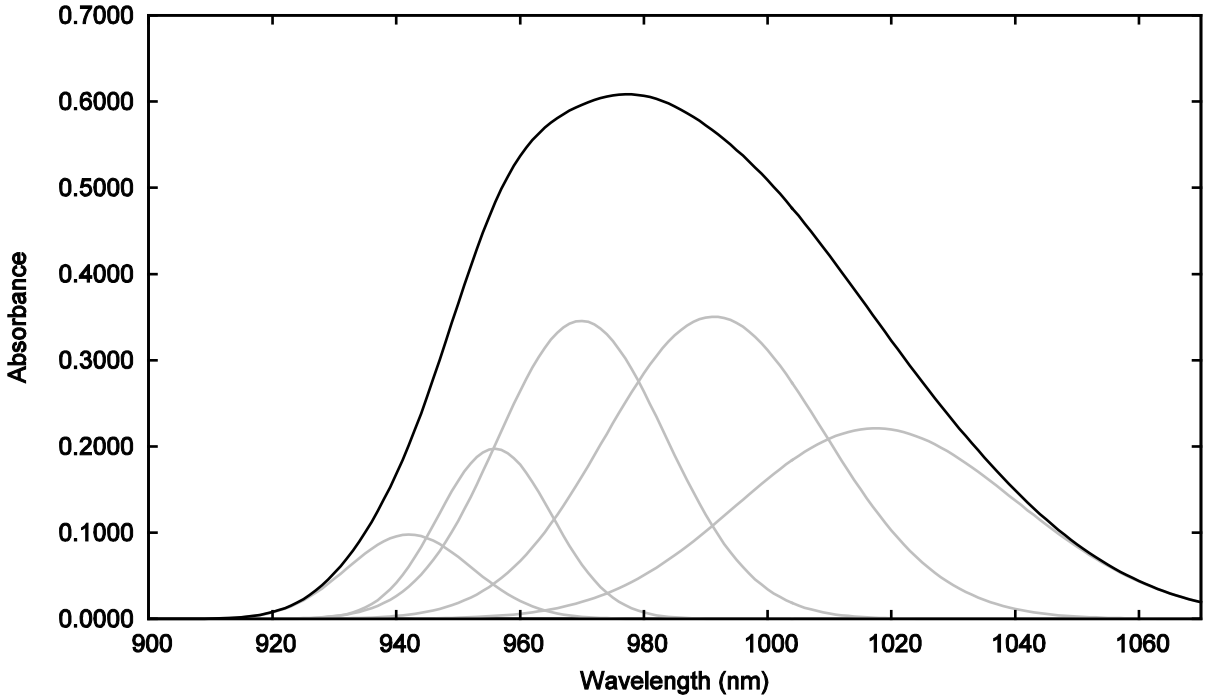

Figure 2-3: Approximate absorption band shape of water near 970 nm at 0°C generated using the Gaussians as described by Abe (2004).

2.3 Salt Water

For the purposes of this thesis, salt water is simply deionized water with the addition of dissociated NaCl and KCl. The term salt water applies to all concentrations of these dissolved ions and is independent of speciation.

2.3.1 The Interactions between Water Molecules and Na^+, K^+, and Cl^- Ions

Ionic solids such an NaCl and KC dissolve in liquid water (a polar solvent) until the system reaches the solubility limit. The dissociated Na^+, K^+, and Cl^- ions attract the polar water molecules. These attractions cause the water molecules to surround each ion with the attracted atom facing towards the ion and the other atoms facing away from the ion (and towards another, oppositely charged, ion) (Maréchal, 2006). This is called ion hydration (Collins *et al.*, 2007). When the solubility limit is reached any additional NaCl or KCl will no longer dissociate but will remain crystallized in the mixture. The point at which the maximum amount of salt is dissolved by a given quantity and state of water is known as the saturation point.

At low salt concentrations, a greater number of water molecules are able to interact with each individual salt ion but as the concentration increases, the number of water molecules interacting with each ion decreases (Pestova *et al.*, 2004). At low $NaCl_{(aq)}$ concentrations (0.5 M), about 25 water molecules will interact with each NaCl molecule dissolved in solution. For $KCl_{(aq)}$, this value is closer to 45 water molecules per KCl molecule at low concentrations. As the concentration increases this value drops to about 5-7 water molecules per salt molecule for both types of salt at standard temperature and pressure (Pestova *et al.*, 2004). When $NaCl_{(aq)}$ and $KCl_{(aq)}$ are present in the same sample, their saturation concentrations are dependent on each other as well. Figure 2-4 shows the approximate solubility curve for mixtures of $NaCl_{(aq)}$ and $KCl_{(aq)}$ at 25°C and 50°C (Sterner *et. al*, 1988). The black box on the figure represents the typical range of concentrations that is expected in potash processing. For any mixture of $KCl_{(aq)}$ and $NaCl_{(aq)}$, the solution will be saturated along the lines in this graph at the given temperature. The saturation point for pure $NaCl_{(aq)}$ is the point of intersection with the y-axis and the saturation point for pure $KCl_{(aq)}$ is the point of intersection with x-axis.

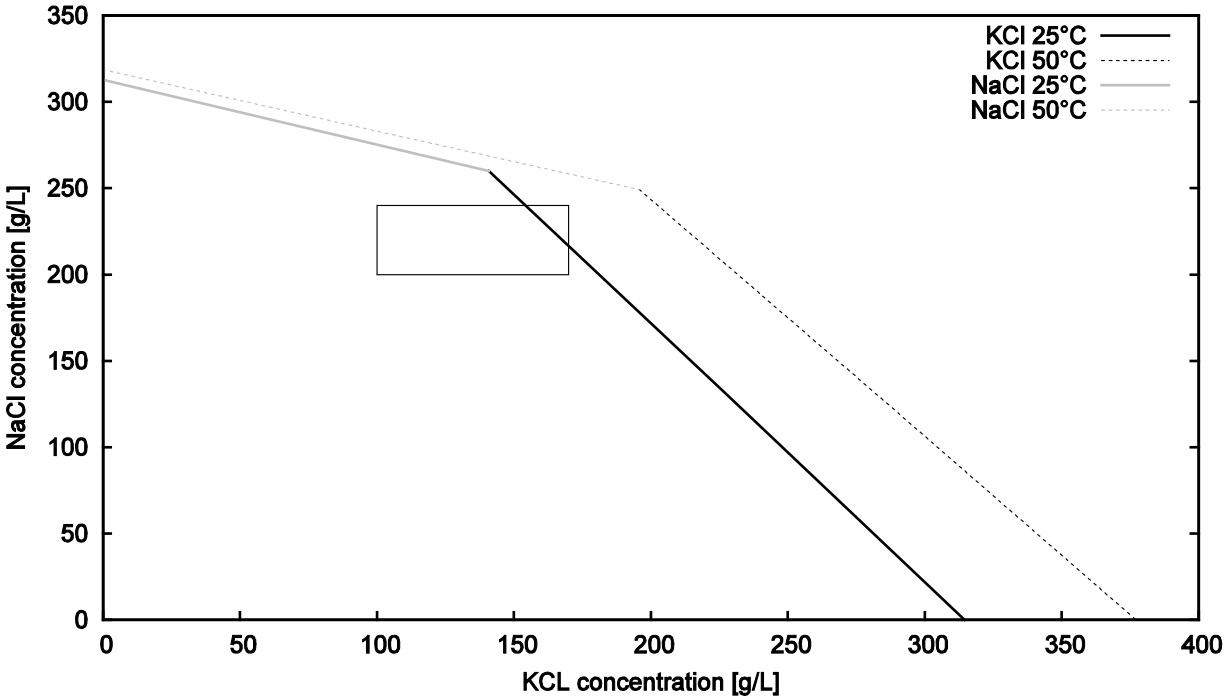

Figure 2-4: $NaCl_{(aq)}$ and $KCl_{(aq)}$ solubility curve at 25°C and 50°C (Sterner *et. al,* 1988).

The saturation point is not solely dependent on the number of water molecules in the sample but also temperature, pressure, and other impurities in the sample. As the temperature of the water increases, the water molecules gain more kinetic energy and are able to move more quickly in solution. Increasing the temperature of a salt water solution therefore allows the bonds between the water molecules and the salt ions to form and break more frequently. This allows a given number of water molecules to interact with more salt ions at a higher temperature thereby increasing the maximum concentration of salt that can be dissolved by the water. As mentioned earlier, hydrogen bonding is also dependent on temperature. As the temperature increases, hydrogen bonding between the water molecules decreases (Dougherty, 1998). This also allows for easier interaction between the water molecules and the salt ions as there is less interference from intermolecular hydrogen bonding of water.

Hydrogen bonding decreases the average distance between water molecules. However, the positive and negative ions from $NaCl_{(aq)}$ and $KCl_{(aq)}$ attract the hydrogen and oxygen atoms more strongly and further reduce the distance between the molecules in solution. These salts also reduce the protonation/deprotonation rate which increases the overall stability of the bulk structure (Zatula *et al.*, 2012). This contributes to the reduction in overall volume observed when salt and water are

mixed. The positive and negative ions also interfere with the vibrations that normally occur in the water molecules. As the Na^+, K^+, and Cl^- ions shift the water molecules into a more structured arrangement, the vibrations that occur within the molecule are damped due to reduced freedom of motion. Adding salt to water also has a number of other physical effects including decreasing the melting point and increasing boiling point.

2.3.2 Effect of Salt on the Water Absorption Spectrum

The addition of salt to water has a number of effects on the absorption spectrum. The most obvious change would be the addition of the absorption exhibited by the individual ions. While $NaCl_{(aq)}$ and $KCl_{(aq)}$ do not absorb strongly in the visible range, there are some absorption features in the ultraviolet range that add to the water absorption (Chai *et al.*, 2008). Fluorescence in the visible range is present in aqueous samples with ultraviolet excitation but is very minimal for $NaCl_{(aq)}$ and $KCl_{(aq)}$ (Chai *et al.*, 2008).

Other effects that the dissolved ions have on the water absorption spectrum are related to the changes in structure, intermolecular interactions, and intramolecular interactions within the water molecule. The addition of a large quantity of salt to water causes a decrease in water molecule concentration. Though the concentration of water is not typically a variable of interest, the effect that the ions have on the water's molarity in solution cause changes in the number of water molecules in the absorption path length which causes a change in absorption. Intermolecular interactions with water are most strongly exhibited by the hydrogen bonding that occurs between the partial positive charge on the hydrogen and the partial negative charge on the oxygen. As discussed previously, hydrogen bonds between water molecules are less prominent in the presence of $NaCl_{(aq)}$ and $KCl_{(aq)}$. Na^+ and Cl^- ions decrease the average number of hydrogen bonds while K^+ ions increase the number of hydrogen bonds slightly (Hribar *et al.*, 2002). Overall, this causes the absorption due to hydrogen bonding to be reduced.

Intramolecular vibrations are also damped by the presence of $NaCl_{(aq)}$ and $KCl_{(aq)}$ in water. As the water forms a more structured arrangement, the H-O-H angle has less freedom and therefore the bending vibrations are reduced. Similarly, the length of the O-H bond is more rigid due to the interactions with the ions in solutions and both the symmetric and asymmetric vibrations are reduced. This damping of the vibrations causes the absorption bands to be reduced and, subsequently, the absorption harmonics present in the near infrared and visible range are reduced. This explains why transmission of light through a salt water sample increases as the salt

concentration increases (Hirschfeld, 1985). $NaCl_{(aq)}$ is classified as a kosmotrope as it causes a more structured arrangement of the water molecules (Berk, 2001). The classification of $KCl_{(aq)}$ is less clear as different authors support different findings as to its kosmotropic (Hribar *et al.*, 2002) or chaotropic (Berk, 2001) qualities. These differences are likely related to experimental set up and conditions as a particular molecule's ability to create or break structure can change based on experimental parameters (Ninham & Lo Nostro, 2010). Kosmotropic salts cause a shift towards longer wavelengths in the stretching vibrational absorption bands as more structure results in stronger (although fewer), better aligned hydrogen bonds (Nickolov & Miller, 2005), and more quadruple-bonded water molecules (Abe, 2004). These quadruple-bonded water molecules are not necessarily bonded to each other, but more likely bonded to four salt ions as the salt concentration increases. Taken as individual ions, Na^+ is a structure maker or a kosmotrope but K^+ is a structure breaker or a chaotrope (Amo & Tominaga, 1998).

These solute-induced changes in structure result in spectral absorption changes that may be correlated with concentration. Hirschefeld (1985) modeled the effect of salt concentration on water absorption in the near infrared range of the spectrum. He found a linear correlation between the $NaCl_{(aq)}$ concentration and the absorption of the solution at a variety of wavelengths between 1630 nm and 2170 nm. Di Noto and Mecozzi (1997) also found a linear correlation between salt concentration and absorption in the ultraviolet range.

2.4 Electrolyte Quantification Methods

Quantification of solutes is pervasive in analytical chemistry. Some current methods for quantifying electrolytes in solution include XRF, spectroscopy (UV, visible, and IR), mass spectrometry, density, refractive index, and laser-induced breakdown spectroscopy.

2.4.1 XRF

X-ray fluorescence is a method of determining NaCl and KCl concentrations and can be used with aqueous samples. XRF involves exposing samples to x-rays or gamma rays. This causes ionization among atoms in the sample. Electrons from higher orbitals then fall into the vacant space and the energy release produces a photon. Different elements produce photons at different wavelengths allowing for identification. However, the energy produced from elements with low atomic mass is much lower than for heavier elements making the detection of light elements difficult. This method requires an x-ray or gamma ray source which presents issues with human

exposure to radiation and requires that samples be analyzed in a lab. Portable handheld XRF devices are available but are primarily designed for solid sample applications and produce small amounts of radiation that could be hazardous over long periods of exposure.

2.4.2 UV Spectroscopy

Di Noto and Mecozzi (1997) observed the effect of temperature and overall ion concentration on the spectrum of seawater in the UV range and found a linear relationship capable of determining salinity using absorption between 25 and 30°C. This study only considered concentrations of single-salt solutions to a maximum of 0.585 $mol \cdot L^{-1}$, which is about 10% of the saturated concentration. Armstrong and Boalch (1961) also investigated the absorption of sea water in the UV range looking at the differences between sea water from different geographical locations as well as different water depths. Although this study did not investigate the correlation between UV spectral measurements and the chemical composition of water, it did mention the possibility of future research to this end.

2.4.3 Visible Spectroscopy

In the visible light range, water absorbs very little light, hence its transparent quality to the human eye. Around 750 nm, however, there is a small absorption peak which is temperature dependent and increases linearly between 5 and 20°C (Sullivan *et al.*, 2006). The absorbance of this peak is also linearly dependent on concentrations of $NaCl_{(aq)}$ between 10 and 100 g per kg of water. These concentrations are, again, nowhere near saturation. Ravisankar *et al.* (1988) investigated the effect of NaCl, $MgCl_2$, and Na_2SO_4 on the absorption of water between 400 and 630 nm. Their conclusion was that NaCl and Na_2SO_4 did not produce much effect on the absorbance of the water in this range, but $MgCl_2$ produced an increase in absorption in the visible range.

2.4.4 IR Spectroscopy

Hirschfeld (1985) investigated the effect of ion concentration on the water absorption bands in the near infrared region finding a linear correlation as well. Again, the concentrations under investigation were all under 0.651 $mol \cdot L^{-1}$ (10% of saturation) and extrapolation of these findings would be inappropriate. Lin *et al.* (1996) also used NIR spectroscopy to investigate various electrolytes in aqueous solutions. The focus of their research was identifying the species

present in the water for samples containing one, two, or three electrolytes. This study only considered a single concentration of 0.5 $mol \cdot L^{-1}$ for each solution and included many species other than NaCl and KCl, but it provides confirmation that different electrolytes provide qualitatively different changes to the water absorbance spectrum.

The spectra of $NaCl_{(aq)}$ and $KCl_{(aq)}$ have been described as being very similar in previous studies (Lin & Brown, 1993), (Max *et al.*, 2001). This is due, in part to their similar number of water molecules per solvated molecule (Max *et al.*, 2007). Some works have even classified KCl, along with other salts, into a subcategory of NaCl due to their similarities (Max & Chapados, 2001).

2.4.5 Other Quantification Methods

There are many other analytical techniques that can be used to determine concentrations in brine solutions but most of these techniques involve sample preparation and require the testing to be done in a lab. Mass spectrometry is a method that can analyze complex mixtures by sorting ions based on masses. This method requires a mass spectrometer which is expensive and testing can be time consuming. Atomic absorption spectroscopy and laser-induced breakdown spectroscopy are also effective for determining elements of mixtures, but still require lab work to analyze samples. Density, conductivity, and refractive index are three features that could be used to quickly determine concentrations of $NaCl_{(aq)}$ or $KCl_{(aq)}$ but these two methods only supply one point of data for each sample which could make determination of both $NaCl_{(aq)}$ and $KCl_{(aq)}$ concentration difficult. Ion selective electrodes provide useful data for single alkali metal ions in solution but often need frequent calibration especially in the presence of changing solution temperatures (Palmer & Civan, 1977). Another qualitative test includes a distinct taste difference between the two salts (with KCl tasting more bitter to most people). This test is quick and easy to perform but has a high degree of subjectivity and is obviously not suitable for monitoring solutions (for both logistic as well as safety reasons), especially on a large scale or in an in-line application.

2.5 Literature Review Summary

Stretching and bending vibrations between the hydrogen and oxygen atoms in water molecules cause absorption bands in the infrared range of the light spectrum. These absorption bands have harmonics which extend into the near infrared and visible range. The shape and

position of these harmonics are affected by temperature, pressure, salinity, and other impurities. These factors also affect the physical properties of the water including hydrogen bonding.

$NaCl_{(aq)}$ and $KCl_{(aq)}$ interact with the positive hydrogen and negative oxygen atoms in the water molecule to dissociate completely in water. This solubility has a limit for the NaCl and KCl that is affected by temperature, pressure, and the presence of other salts and impurities. At low concentrations each salt ion interacts with many water molecules, but as the concentration increases fewer water molecules are available and eventually the ions will remain attached in their solid crystal state. Adding salt to water also has effects on the physical properties of water such as increasing the boiling point and decreasing the melting point.

When NaCl and KCl are added to water, the absorbance spectrum of the solution is altered. These changes relate to the changes in structure of the water, the intermolecular interactions between water molecules, and the intramolecular interactions of the water. Hydrogen bonds are fewer in number but stronger in the presence of Na^+, K^+, and Cl^- and the bending and stretching vibrations are damped. These effects have been studied in the low concentration range throughout the absorbance spectrum but differentiation between these particular salts and modelling at high concentrations has not been investigated extensively. Other methods for differentiating between $NaCl_{(aq)}$ and $KCl_{(aq)}$ in solutions exist, but many are time consuming and present a safety risk.

3 OBJECTIVES

The objective of this project was to develop a method for determining concentration and speciation of brine samples using UV-Visible-NIR spectroscopy. This method should be capable of analyzing samples of $NaCl_{(aq)}$ and $KCl_{(aq)}$ in solution over the concentration range typically found in potash processing and along the NaCl-KCl saturation curve. Major goals included mitigating evaporation in high-temperature samples, collecting spectral data, and developing correlations between spectral data and sample parameters.

3.1 Developing a Method for Mitigating Evaporation in High-Temperature Samples

Evaporation in highly concentrated brine solutions can cause changes in concentration as well as precipitation of solutes. Mitigating this evaporation without increasing the pressure of the samples was necessary for determining accurate absorbance spectra at elevated temperatures.

3.2 Collecting Spectra

Spectral measurements were required to understand differences in $NaCl_{(aq)}$ and $KCl_{(aq)}$ absorbance as well as to determine the effects of temperature on samples of pure water. Single-salt $NaCl_{(aq)}$ and $KCl_{(aq)}$ samples were used to identify ranges where spectral differences are evident and mixed samples were used to determine if the two species had an additive effect on absorbance. Spectra of water over the temperature range were used for comparison between heat effects and salinity effects on the absorbance spectrum.

3.3 Model Development

The single-salt samples of $NaCl_{(aq)}$ and $KCl_{(aq)}$ were used to develop a model for differentiating between solutions containing only one salt. Na^+ and K^+ are similar ions but have a few key differences in their interaction with water molecules that were used to differentiate between salt species. Single-salt and dual-salt absorbance spectra were then used to develop two models for determining concentrations and speciation in dual-salt solutions. A model for determining temperature based on absorbance was also developed.

Analysis of the developed models provided information regarding the models specificity and accuracy. Testing was conducted over the range of solutions and temperatures typically found in potash processing to determine the applicability of the model in an industrial setting.

4 COLD FINGER APPARATUS: MITIGATING EVAPORATION IN HIGH-TEMPERATURE SAMPLES DURING SPECTRAL SCANNING

4.1 Introduction

In some laboratory practices, temperatures of aqueous solutions in a spectrophotometer can be higher than 100°C and can result in evaporation of the solvent used in the sample. When this occurs, the concentration of the sample can change and affect the accuracy of the scan over the full wavelength range used. Current methods reduce this evaporation but they require an increase in pressure, or for the solution to be pumped through a flow cell. In order to take high-temperature measurements at atmospheric pressure the system must mitigate evaporation while leaving the vessel open to environmental pressure. A simple condensing column made from a glass pipette was considered as a solution to this problem, but was found to retain significant amounts of water that did not return to the cuvette. A thermoelectrically-cooled cold-finger was developed and placed in a closed space above the heated cuvette. The hypothesis was that by reducing the available volume and condensing surface area above the cuvette, this environment could be closed and the active cooling would both condense the water vapor and maintain approximately atmospheric pressure.

In this chapter, the design of the cold-finger and associated apparatus is presented, and its ability to regulate the test solution concentration is compared to that of a cuvette open to the atmosphere, and a cuvette with a loose-fitting polytetrafluoroethylene (PTFE) lid.

4.2 Cold-Finger Design

The cold-finger was designed to fit with a Cary-5000 UV-Vis-NIR spectrophotometer (Agilent Technologies, Mississauga, Can.) and a 10 mm quartz cuvette. The purpose of the cold-finger apparatus was to provide a space above the cuvette in which evaporated water could be condensed quickly and easily be delivered back to the cuvette. The part of the apparatus that was in contact with water evaporate and condensate was made out of treated hydrophobic PTFE. This material allowed for formation of smaller water droplets that could be condensed back into the cuvette which provided a more consistent sample concentration over the scan time. A labelled cross section of the apparatus is shown in Figure 4-1.

Figure 4-1 shows the cuvette (1) placed in the spectrophotometer’s cuvette holder (2) with the cold-finger condensing apparatus sitting above. The first PTFE component above the cuvette

and holder (3) was designed to fit snugly over the quartz cuvette and provide a base for the rest of the apparatus. This component was secured to the second piece with two screws (4) with the first of two gaskets (5) between the two components. This gasket also provided a semi-seal between the top of the cuvette and the environment.

The second PTFE component (6) housed a cylindrical space above the cuvette (7) in which the water vapour would collect to be condensed back into the cuvette. This space continued through the entire component so that the cold-finger could be fit into the top of this component. This component was also designed for the incorporation of a thermocouple for monitoring sample temperature (not shown). This thermocouple was housed within a glass capillary tube to avoid corrosion exposure to samples. A portion of the PTFE extended into the uppermost empty space of the cuvette to provide a secondary route for water drops to fall back into solution (8). This portion was designed as a rectangular based pyramid with a cylindrical hole through the middle. Two screws (9) on the side of the second PTFE component (only one shown) were used to secure the whole apparatus to a bracket (10) that was attached to the spectrophotometer's cuvette holder. This was necessary as relying on gravity alone to secure the apparatus was insufficient and the cold-finger would not sit perfectly level above the cuvette.

The third PTFE section was comprised of the cold-finger (11), the peltier cooler used to cool the cold-finger (12), and the heat sink (not shown). The cold-finger was a cone with an extended cylindrical base made of copper and was coated (13) with the same PTFE as the rest of the apparatus. The cold-finger was designed to fit in the cylindrical space in the second component. The uncoated side of the cold-finger was in contact with the peltier cooler that cooled the copper to encourage condensation on the cone. A pin-fin heat sink (906 series, Wakefiled-Vette) was attached above the peltier cooler but is not shown in the diagram. As with the first and second sections, a gasket (5) was placed between this component and the second PTFE component. The combination of the friction fit of the cold-finger in the cylindrical space and the added weight of the heat sink provided enough support for this component to sit level on top of the other two components and it was not secured to the rest of the spectrophotometer. An image of the cold-finger with water condensing on it in Figure 4-2.

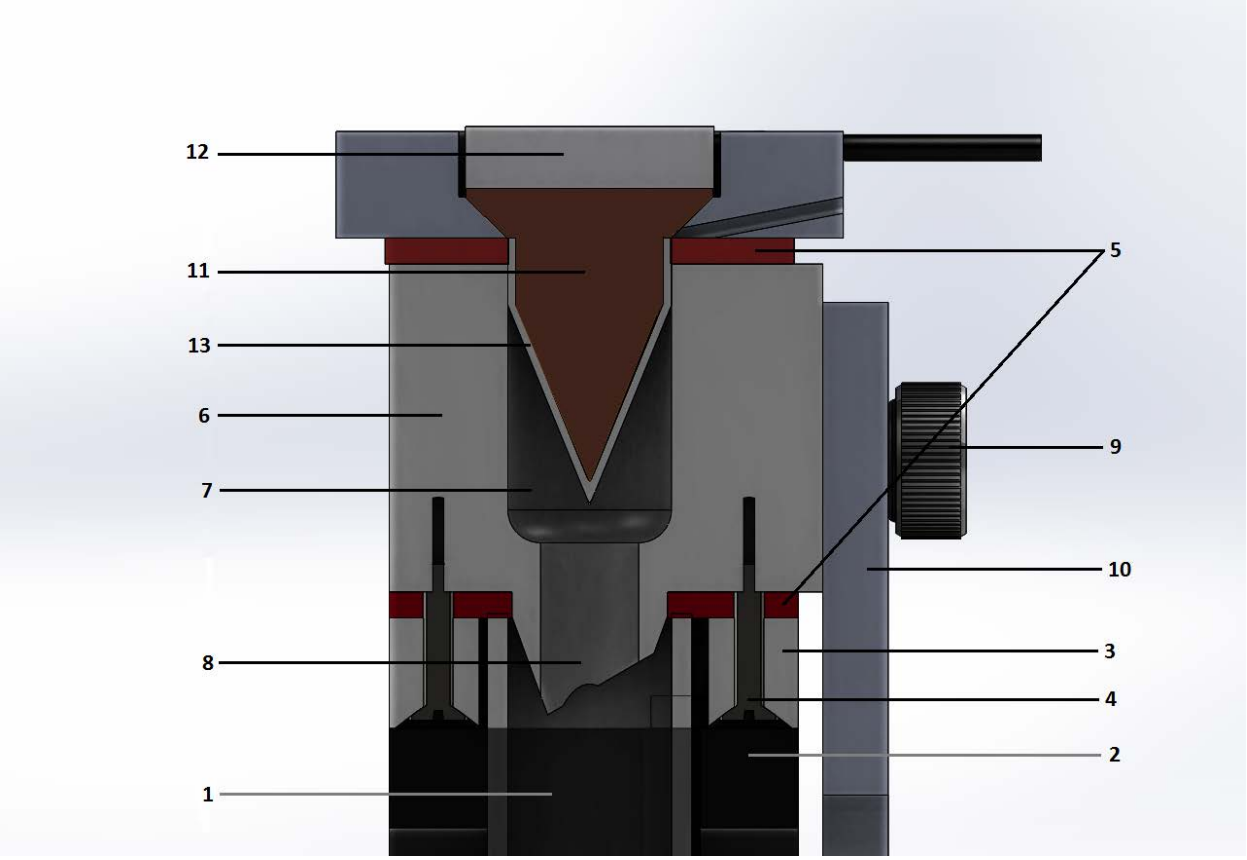

Figure 4-1: Cross section of the cold-finger apparatus. (1) cuvette, (2) cuvette holder, (3) first PTFE component, (4) screws, (5) gaskets, (6) second PTFE component, (7) condensing space, (8) secondary drop formation, (9) screw, (10) bracket, (11) cold-finger, (12) peltier cooler, (13) PTFE coating.

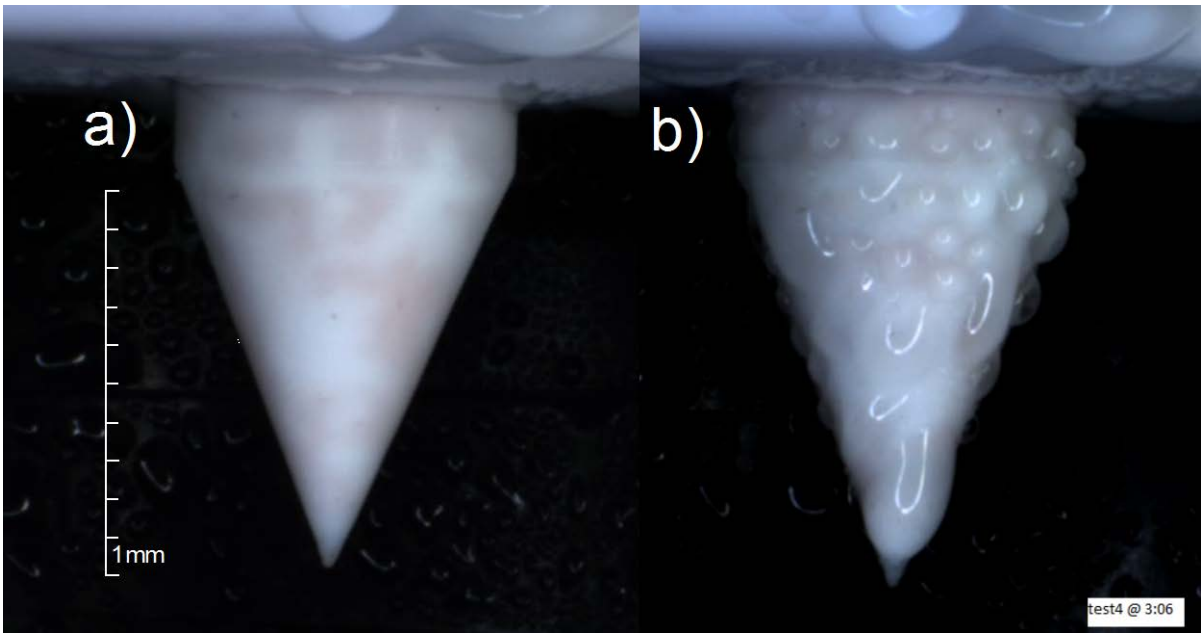

Figure 4-2: Image of (a) the dry cold-finger and of (b) water condensing on the cold-finger.

4.3 Materials and Methods

Cupric sulfate was dissolved in deionized water for testing the evaporation effect in a cuvette open to air, a cuvette fitted with a loose PTFE cap, and a cuvette with the cold-finger condensing apparatus. A 100 mL volumetric flask was used to mix 2.508 g of cupric sulfate and 99.520 g of water. This provided a stock solution with a 0.157 mole per liter and 24.6 gram per kilogram of solution.

Using this stock solution for all tests, approximately 3.5 mL of solution was transferred into a quartz cuvette containing a magnetic stirring bar and weighed prior to heating and scanning. Ideally a consistent starting mass would be used for each spectral measurement, so for each test the quantity of solution added to the cuvette was kept consistent within ± 0.01 g.

All spectral measurements were taken using a Cary-5000 UV-Vis-NIR spectrophotometer (Agilent Technologies, Mississauga, Can.) with an empty quartz cuvette used in the reference beam and as the zero reference prior to all scans. A kinetics scan, which measures absorbance at a single wavelength over time, was performed at the concentration-dependent wavelength of 810 nm. The sample was allowed to reach an equilibrium temperature of 25°C prior to each scan. Each kinetics scan was performed over the course of about one hour. The first minute monitored the sample at 25°C. After one minute had passed, the sample set point temperature was increased to

either 85°C or 95°C. The temperature of the thermostating cuvette holder was then monitored as a proxy for the sample temperature. Measurement of the actual sample temperature was only available when using the cold-finger apparatus. Once the cuvette holder had reached the higher equilibrium temperature, it was held for 20 minutes. After 20 minutes, the set temperature of the cuvette holder was reduced back to 25°C and the temperature was monitored until this value was reached. The temperature was then held at the 25°C equilibrium for at least 5 minutes. Three replicate trials were used for each apparatus configuration (open cuvette, lid, and cold-finger) and maximum sample temperature (85°C and 95°C), for a total of 18 trials. The order of these trials was randomized. Samples were not degassed but were visually inspected for bubbles after each scan. The absorbance values that were collected during the scans were also monitored for unexpected spikes that could indicate the formation or release of bubbles.

After each scan was complete, the cuvette, stir bar, and solution were weighed again to record any mass loss that occurred during the scan. All reductions in mass were assumed to be due solely to water evaporation. This change in mass, along with a density estimation (Ernst *et al.*, 1999), was then used to determine the post-scan molar concentration. The absorbance measured at the beginning of the kinetic scan and the end of the kinetic scan were also used to calculate the before and after molar concentration of the sample. The mass of the cold-finger apparatus was measured before and after each scan to determine the amount of water retained in the apparatus and the amount lost to the environment.

4.4 Calculations

The absorbance measured over the first minute (at 25°C) was averaged. This value used to determine the molar extinction coefficient at 810 nm and 25°C for $CuSO_4$ based on the known concentration using Equation 4-1.

$$\epsilon = \frac{A_{avg}}{Cl} \qquad 4\text{-}1$$

where ϵ is the molar extinction coefficient in $L \cdot mol^{-1} \cdot cm^{-1}$, A_{avg} is the average absorbance measurement over the first 60 seconds, C is the concentration in $mol \cdot L^{-1}$, and l is the path length (1 cm). This molar extinction coefficient was used for all future calculations for that test.

The final concentration of the sample was calculated in two different ways. First, the final absorbance measurement of each scan was used with the molar extinction coefficient from Equation 4-1.

The second method for calculating the final concentration used the change in mass observed from the beginning to the end of each scan. All mass lost during the scan was assumed to be from evaporation of water. Because the mass loss can only be applied to determine the mass-based concentration, a density correction was performed using the data presented by Ernst *et al.* (1999) to determine the molar concentration. The known mass of water and known mass of $CuSO_4$ were used to determine the density of $CuSO_4$ in solution and this value was used to calculate the molar concentration.

The change in concentration was compared for both final concentration measurements using a percent increase from original to final concentration. The calculation for this value in both final concentration cases is shown in Equation 4-2.

$$\Delta C = \frac{C_{final} - C_{initial}}{C_{initial}} * 100\% \qquad 4\text{-}2$$

4.5 Results and Discussion

The initial and final masses of the contents in the cuvette were recorded in order to determine the overall percentage of mass lost during each scan. Table 4-1 and Table 4-2 summarize the changes in mass for each test performed using an 85°C and 95°C set point temperature, respectively.

After observing significant disagreement between the loose-lid results at both 85°C and 95°C, a fourth trial was performed for this case at both temperatures. However, in the 95°C test the fourth measurement indicated that this case had a large amount of variability in its ability to mitigate evaporation. The amount of liquid lost due a single drop of water is large compared to the total volume in the cuvette, so this large variability is reasonable given the experimental parameters. All four tests were used in the calculations. The percentage lost is based on an overall mass lost during the heating and cooling process. The cold-finger was able to reduce the amount of mass lost due to evaporation to 3.29%. This value is considerably lower than the 9.96% loss for the open cuvette and 8.72% loss for the loose-lid cuvette.

The mass of the cold-finger apparatus before and after each trial was also collected to determine the amount of water that had collected inside the apparatus and could theoretically be returned to the cuvette if evaporation (and condensation) was allowed to continue. Adding these masses of water to the final cuvette mass decreased the average percent lost from 3.29% to 1.19%.

Table 4-1: Masses of solution before and after each scan at 85°C. All masses have uncertainties of ± 0.0002 g.

Trial	Open Cuvette			Loose-Lid			Cold-finger		
	Before (g)	After (g)	%Loss	Before (g)	After (g)	%Loss	Before (g)	After (g)	%Loss
1	3.6540	3.2876	10.027	3.6493	3.0971	15.132	3.6515	3.5208	3.579
2	3.6527	3.2888	9.962	3.6569	3.3448	8.535	3.6511	3.5427	2.969
3	3.6502	3.2891	9.893	3.6512	3.3992	6.902	3.6506	3.5292	3.325
4	---	---	---	3.6532	3.4897	4.476	---	---	---
Std. Dev.	0.0019	0.0008	0.067	0.0033	0.1681	4.563	0.0005	0.0110	0.307
Average			9.961			8.761			3.291

At 95°C the mass loss for the open cuvette was 18.50% and the loose-lid cuvette had an 11.77% mass loss. At 95°C the cold-finger was able to reduce the amount of mass lost due to evaporation 3.93%. Adding the masses of water found on the cold-finger apparatus to the final cuvette mass decreased the average percent lost from 3.93% to 1.55%.

Table 4-2: Masses of solution before and after each scan at 95°C. All masses have uncertainties of ± 0.0002 g.

Trial	Open Cuvette			Loose-Lid			Cold-finger		
	Before (g)	After (g)	%Loss	Before (g)	After (g)	%Loss	Before (g)	After (g)	%Loss
1	3.6565	2.9645	18.925	3.6573	3.0351	17.013	3.6503	3.4751	4.800
2	3.654	2.9879	18.229	3.6568	3.3501	8.387	3.6585	3.5175	3.854
3	3.6502	2.9811	18.331	3.6492	3.371	7.624	3.6544	3.5397	3.139
4	---	---	---	3.6517	3.1403	14.004	---	---	---
Std. Dev.	0.0032	0.0120	0.376	0.0040	0.1635	4.513	0.0041	0.0328	0.833
Average			18.495			11.757			3.931

Figure 4-3 and Figure 4-4 present the absorbance data of the $CuSO_4$ solution over the heating and cooling process. All of the trials for the open cuvette, loose-lid, or cold-finger apparatus were averaged at each temperature. The standard error of the estimates shown in Figure

4-3 were 0.032 for the open cuvette, 0.133 for the loose-lid, and 0.052 for the cold-finger. The standard error of the estimates shown in Figure 4-4 were 0.007 for the open cuvette, 0.034 for the loose-lid, and 0.009 for the cold-finger. The equation used for the standard error of the estimates can be found in Appendix A – Additional Calculations, Equation A-1.

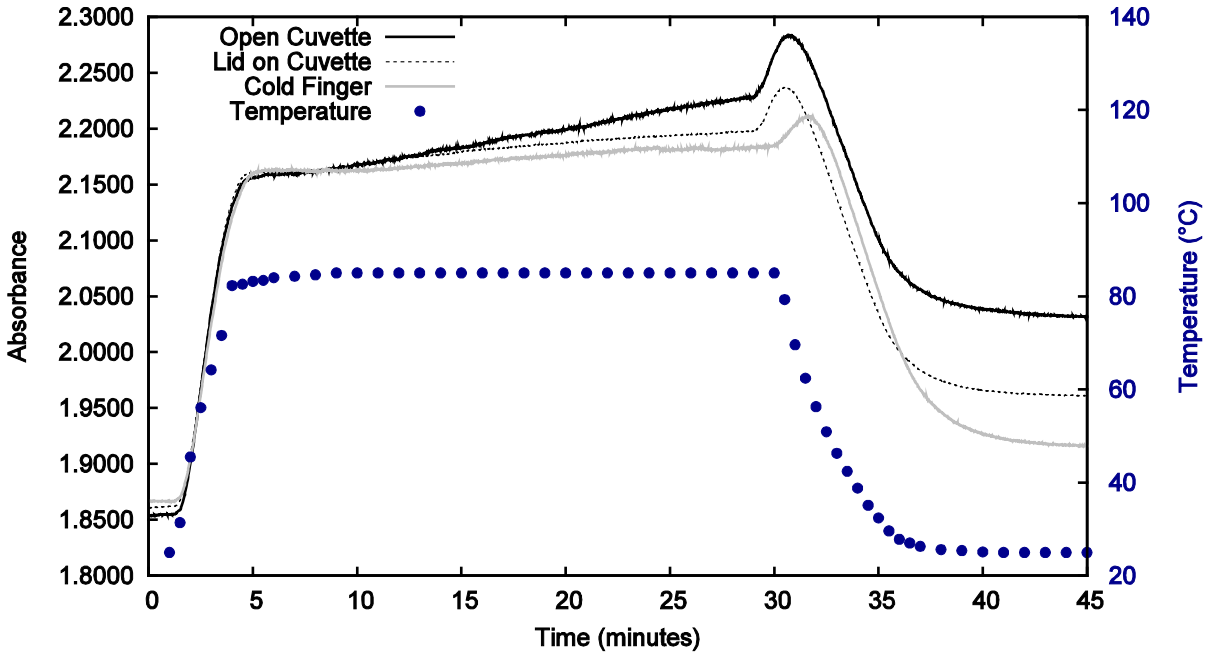

Figure 4-3: Absorbance (solid and dotted lines) at 810 nm over 45 minutes of the $CuSO_4$ solution during heating to 85°C and cooling. Temperature values are displayed with blue circles.

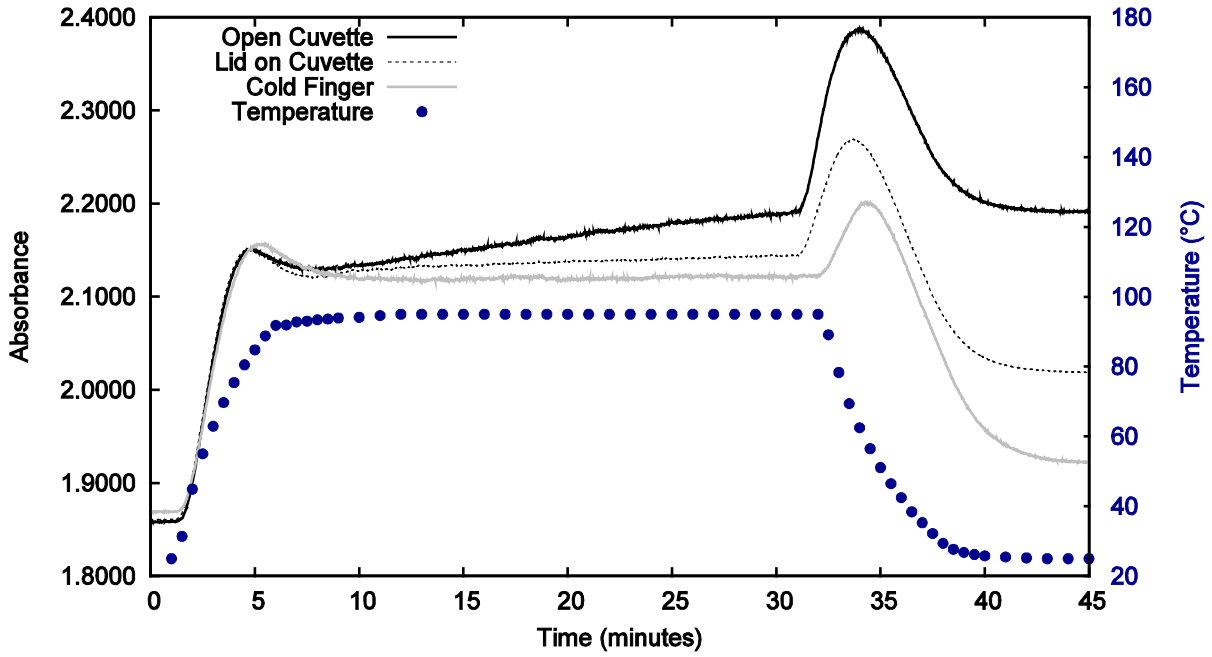

Figure 4-4: Absorbance (solid and dotted lines) at 810 nm over 45 minutes of the $CuSO_4$ solution during heating to 95°C and cooling. Temperature values are displayed with blue circles.

Through the initial heating phase there was a prominent absorbance increase. The concentration of the solution could not be changing so rapidly through the heating phase as evaporation is not be prominent in this temperature range and the density of the solution is not changing drastically. This change was likely due to a change in spectroscopic properties of the solution. It was unknown whether this increase is due to a change in physical or chemical properties of the solution. It was possible that the heating was generating a disruption in the cuvette and the stirring is causing refraction of more light, which would result in an apparent increased absorbance. It was also possible that the hydrogen bonds of the water are interacting with the dissolved ions changing the absorption harmonics typically produced by these bonds. Though the true cause of this increase of absorbance was not investigated in this work, a few possible causes were eliminated.

Figure 4-5 displays the change in absorbance of pure water from 10°C to 95°C at 810 nm. Over this temperature range, the absorbance of the water changed less than 2% when compared to the $CuSO_4$ solution over a similar temperature range. It was therefore concluded that the

temperature-dependent water absorption harmonics of pure water at this wavelength were not accounting for the absorbance changes that occur with heating.

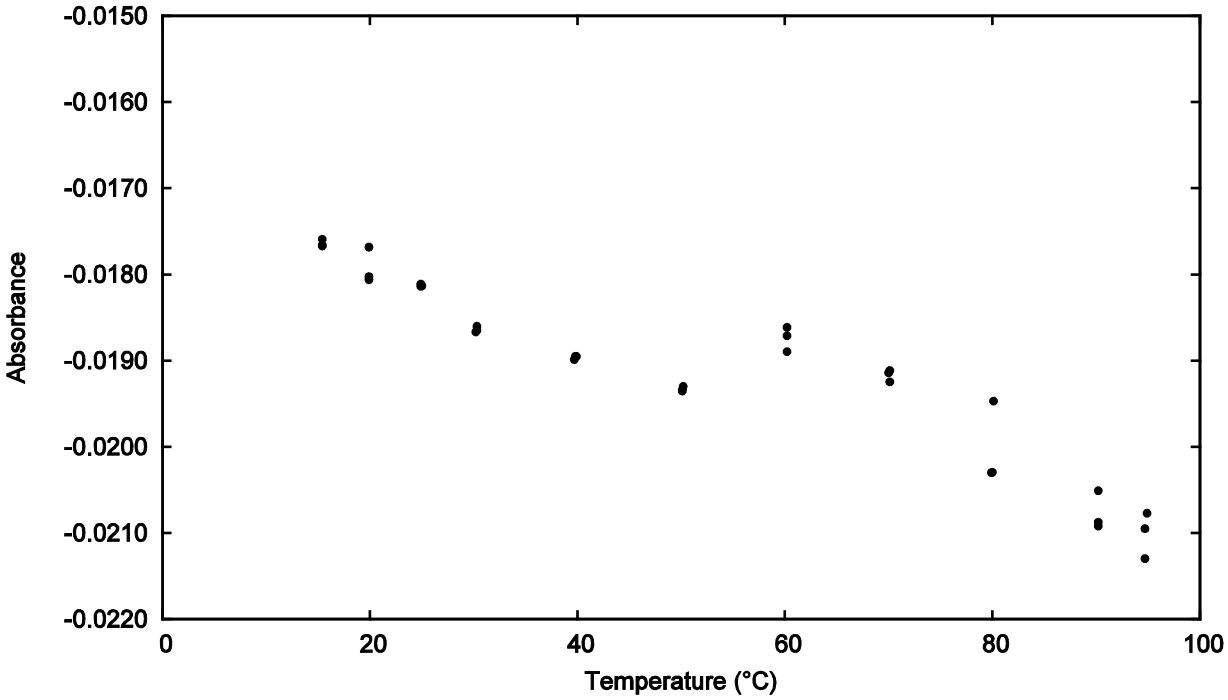

Figure 4-5: Absorbance of water referenced against air at 810 nm at temperatures between 15°C and 95°C.

When the heat was reduced during the scans, there was another increase in absorbance that was present in all of the scans. The cause of this absorbance increase was also unknown and was not investigated in this work.

The middle, linear portion of each scan represents the constant temperature phase. The slope of this line represents the rate at which the concentration of the sample was changing which is directly related to the rate at which water was evaporating. Compared qualitatively, the samples with the open lid cuvette were evaporating more quickly than the loose-lid cuvettes, and those with the cold-finger apparatus were evaporating more slowly than both. These results confirm that evaporation is an issue when taking scans at high temperatures as these scans can take more than 10 minutes over a wavelength range of 180 nm to 1800 nm. Using an open cuvette with a sample temperature of 95°C for a scan of this length would result in concentration gradient throughout the scan. As seen in Figure 4-3 and Figure 4-4, the loose-lid cuvette and the cold-finger reduced concentration gradients over the scan time. The absorbance at the end of each scan was used to

determine the final concentration for comparison with the concentration calculated by the final mass. Table 4-3 and Table 4-4 summarize this comparison.

Table 4-3: Final concentration comparison between absorbance and mass calculation at 85°C.

Trial	Open Cuvette			Loose-Lid			Cold-finger		
	Abs. Based (g/L)	Mass Based (g/L)	% diff	Abs. Based (g/L)	Mass Based (g/L)	% diff	Abs. Based (g/L)	Mass Based (g/L)	% diff
1	27.7	26.6	3.83	27.5	28.2	2.69	26.0	24.9	4.24
2	27.3	26.6	2.60	26.3	26.2	0.29	25.6	24.8	3.51
3	27.4	26.6	2.97	26.0	25.8	0.86	25.6	24.8	2.83
4				25.9	25.1	3.07			

Initial concentration was 25.1 $g \cdot L^{-1}$.

Table 4-4: Final concentration comparison between absorbance and mass calculation at 95°C.

Trial	Open Cuvette			Loose-Lid			Cold-finger		
	Abs. Based (g/L)	Mass Based (g/L)	% diff	Abs. Based (g/L)	Mass Based (g/L)	% diff	Abs. Based (g/L)	Mass Based (g/L)	% diff
1	29.6	29.5	0.27	27.8	28.8	3.68	25.9	25.2	2.69
2	29.9	29.2	2.12	26.6	26.2	1.43	25.7	25.0	3.03
3	29.6	29.3	0.98	26.5	26.0	1.94	25.8	24.8	3.78
4				28.1	27.8	0.79			

Initial concentration was 25.1 $g \cdot L^{-1}$.

The difference between the final concentration calculated by the mass of the cuvette and the absorbance in the cuvette was 3.68% or less for all samples. The final concentration calculated by mass and absorbance have sufficiently similar values to confirm that a decrease in evaporation accomplished with the cold-finger apparatus.

4.6 Conclusions

Evaporation from cuvettes with high-temperature solutions produces vapor that can interfere with light paths in the spectrophotometer chamber and decrease concentrations of samples. $CuSO_4$ dissolved in water was used to measure the effect of evaporation from a cuvette

in a spectrophotometer. Samples were heated to 85°C and 95°C for 20 minutes while scanning at 810 nm to determine the changes in absorbance due to evaporation.

Results were obtained using three different apparatuses to compare the amount of evaporation and test a cold-finger apparatus designed to mitigate evaporation. An open cuvette, a cuvette with a simple PTFE cap, and a cuvette with a thermoelectrically cooled cold-finger were compared to determine evaporation mitigation efficiency. At 85°C the cold-finger was able to reduce the evaporation to 3.29% loss compared to 9.96% loss with open cuvette and 8.72% loss with the loose-lid cuvette. In addition to these improvements, it was found that a portion of the evaporated water was collected on the cold-finger itself. Adding this water back into the system decreased the overall mass lost during the scan from 3.29% to 1.19%. At 95°C the cold-finger was able to reduce the evaporation to 3.93% loss compared to 18.50% loss with open cuvette and 11.77% loss with the loose-lid cuvette. Adding the water that was collected on the cold-finger back into the system decreased the overall mass lost during the scan from 3.93% to 1.55%.

This cold-finger apparatus effectively decreased the evaporation from a sample cuvette at high temperatures over long scan times. However, it was concluded that 3% change was too much to obtain accurate measurements of high-concentration samples. Ideally, less water would be trapped on the surface of the cold-finger and could more easily be reintroduced into the solution in the cuvette. Future designs will consider this preference and attempt to further reduce evaporation.

5 EXPERIMENT DESIGN

Solutions of single-salt solutions and well as dual-salt solution were prepared and measured to determine the spectral effect of adding NaCl and KCl to water. Sample concentrations were chosen based on typical potash processing conditions but were limited to samples that did not have suspended solids. Scans of deionized water at temperatures between 15°C and 95°C were also collected to compare the effects of salinity and solution temperature.

5.1 Mixing of Solutions

Samples of $NaCl_{(aq)}$ and $KCl_{(aq)}$ solutions were prepared using reagent-grade solutes and deionized water. Solutions were mixed in volumetric flasks and both salt and water masses in the mixture were recorded. This allowed for measurement of both molar and $g \cdot g_{water}^{-1}$ concentrations of the samples. In much of the literature, solubility of NaCl and KCl in water is given in grams of salt per 100 grams of water. Spectral absorbance, however, is based on moles per unit volume so both measurements are necessary. Table 5-1 and Table 5-2 describe the quantities of salt and water in each single-salt sample. The two lowest concentration samples for each salt species were made using 100 mL flasks as the quantities of salt were much smaller than the higher concentration samples. All uncertainties given for calculated variables were determined using error propagation as shown in Appendix A – Additional Calculations, Equation A-2 through A-5.

Table 5-1: Solution details for $NaCl_{(aq)}$ samples.

Water (g) ± 0.001g	NaCl (g) ± 0.001g	Volume of Solution (mL)	g NaCl/100g water	Concentration (mol/L)
95.585	8.676	98.7 ± 0.08	9.077 ± 0.001	1.504 ± 0.001
92.795	15.950	98.7 ± 0.08	17.188 ± 0.001	2.765 ± 0.002
45.566	11.802	50 ± 0.05	25.901 ± 0.002	4.039 ± 0.004
44.912	13.181	49.9 ± 0.05	29.349 ± 0.002	4.520 ± 0.005
44.440	14.335	49.9 ± 0.05	32.257 ± 0.002	4.916 ± 0.005
44.191	14.859	49.9 ± 0.05	33.624 ± 0.002	5.095 ± 0.005
44.113	15.094	49.9 ± 0.05	34.217 ± 0.002	5.176 ± 0.005
43.985	15.416	49.9 ± 0.05	35.048 ± 0.002	5.286 ± 0.005

Table 5-2: Solution details for $KCl_{(aq)}$ samples.

Water (g) ± 0.001g	KCl (g) ± 0.001g	Volume of Solution (mL)	g KCl/100g water	Concentration (mol/L)
95.214	8.599	98.7 ± 0.08	9.031 ± 0.001	1.169 ± 0.001
92.288	15.921	98.7 ± 0.08	17.251 ± 0.001	2.164 ± 0.002
44.855	11.835	49.9 ± 0.05	26.385 ± 0.002	3.181 ± 0.003
44.168	13.279	49.9 ± 0.05	30.065 ± 0.002	3.570 ± 0.004
43.825	14.084	49.9 ± 0.05	32.137 ± 0.002	3.786 ± 0.004
43.689	14.416	49.9 ± 0.05	32.997 ± 0.002	3.875 ± 0.004
43.383	14.838	49.9 ± 0.05	34.202 ± 0.002	3.989 ± 0.004
42.867	15.308	49.9 ± 0.05	35.710 ± 0.002	4.115 ± 0.004

To determine the effect of both types of salt in solution, samples containing a mixture of $NaCl_{(aq)}$ and $KCl_{(aq)}$ were prepared. Similar to the single-salt solutions, masses of both salt and water were recorded and the samples were mixed in a volumetric flask. When both $NaCl_{(aq)}$ and $KCl_{(aq)}$ are in solution, the solubility of each salt is affected by the other. Figure 5-1 shows the relationship between the solubility of the two salts. Samples were chosen along the saturation curve as well as at lower concentrations. This allowed for comparison of multiple concentration samples that were all at saturation. Typical potash processing concentrations as represented by the black box on this figure. Table 5-3 summarizes the details for each dual-salt sample.

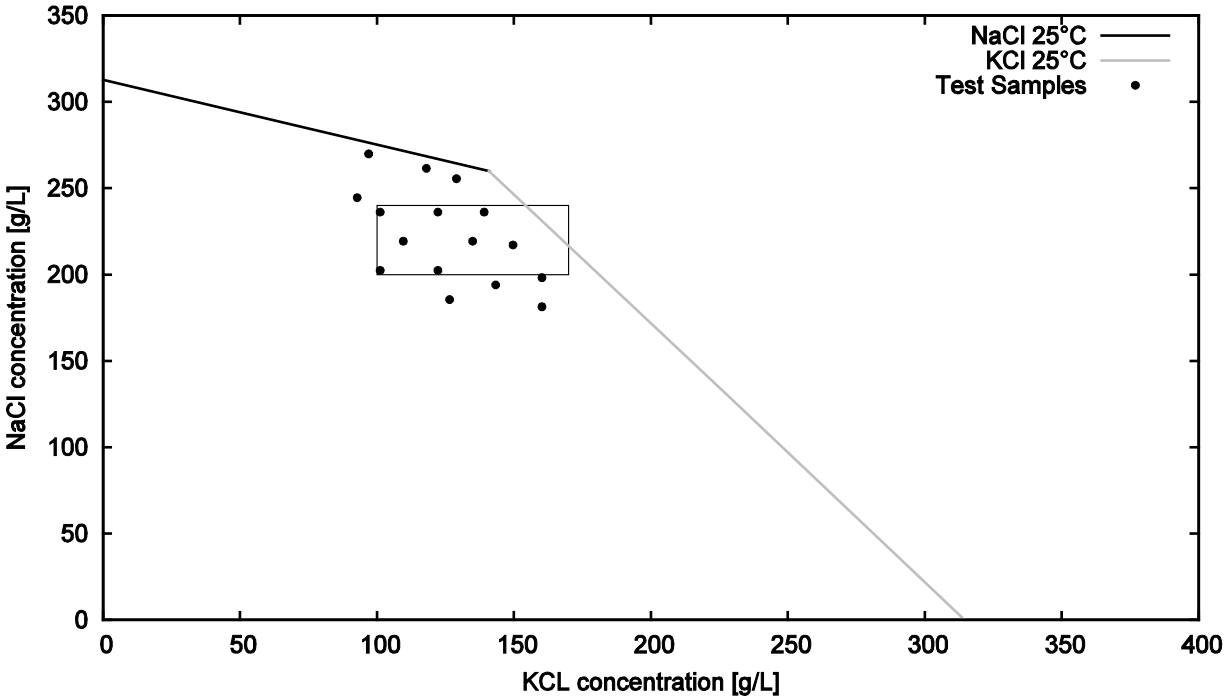

Figure 5-1: NaCl-KCl saturation curve at 25°C (Sterner *et. al*, 1988), the black box represents the concentrations of $NaCl_{(aq)}$ and $KCl_{(aq)}$ that are typically found in potash processing.

Table 5-3: Solution details for dual-salt samples.

Water (g) ± 0.001g	NaCl (g) ± 0.001g	KCl (g) ± 0.001g	Volume of Solution (mL)	g salt/ g water		Concentration (mol/L)	
				NaCl	KCl	NaCl	KCl
21.774	4.617	3.136	24.9 ± 0.08	0.212	0.144	3.17	1.69
21.285	5.876	3.048	24.9 ± 0.08	0.276	0.143	4.04	1.64
21.335	5.867	2.704	24.9 ± 0.08	0.275	0.127	4.03	1.46
21.567	5.440	2.735	24.9 ± 0.08	0.252	0.127	3.74	1.47
21.266	5.565	3.371	24.9 ± 0.08	0.262	0.159	3.82	1.82
21.627	5.032	3.032	24.9 ± 0.08	0.233	0.140	3.46	1.63
21.897	5.051	2.511	24.9 ± 0.08	0.231	0.115	3.47	1.35
21.554	6.074	2.321	24.9 ± 0.08	0.282	0.108	4.17	1.25
21.477	4.837	3.541	24.9 ± 0.08	0.225	0.165	3.32	1.91
21.406	4.534	3.969	24.9 ± 0.08	0.212	0.185	3.12	2.14
21.220	6.709	2.437	24.9 ± 0.08	0.316	0.115	4.61	1.31
21.098	6.506	2.935	24.9 ± 0.08	0.308	0.139	4.47	1.58
20.929	6.336	3.201	24.9 ± 0.08	0.303	0.153	4.35	1.72
21.060	5.838	3.450	24.9 ± 0.08	0.277	0.164	4.01	1.86
21.188	5.396	3.712	24.9 ± 0.08	0.255	0.175	3.71	2.00
21.227	4.943	3.961	24.9 ± 0.08	0.233	0.187	3.40	2.13

5.2 Water Spectra at High Temperatures

Samples of deionized water at 15, 20, 25, 30, 40, 50, 60, 70, 80, 90, and 95°C were used to determine the effect of temperature of the absorbance spectrum of water. The brine samples were not scanned at temperatures above 25°C as the current method for mitigating evaporation during scans (as developed in section 4) was deemed insufficient for collecting data that would be accurate for model development.

5.3 Spectral Measurements

All spectra were collected using a dual-beam spectrophotometer (Cary-5000, Agilent Technologies, Mississauga, Can.). Quartz cuvettes with a 10 mm path length were used for all measurements to allow for scanning into the ultraviolet wavelength range. No lids were used to

cover the cuvette. Solution temperature was moderated by a dual-cell temperature controller for both the sample and reference cuvettes when necessary. Samples were stirred during scans to help mitigate any crystallization on the cuvette wall for very-high-concentration samples.

A zero/baseline correction was applied to all scans using two matched empty cuvettes (i.e. filled with air) for 100% transmittance and an empty cuvette in the reference beam path with the sample beam blocked for 0% transmittance. All spectra were measured with an empty cuvette as reference. A scan of deionized water at room temperature was taken for all scanning sessions for reference. Water was not used in the reference cuvette because the concentration of water in the reference and the sample was not the same. Using water as the reference is especially problematic at high salt concentrations as the amount of pure water in the sample is very low and in fully saturated solutions the amount of unsolvated water (water molecules that are not interacting with any ions in solution) is theoretically zero. Using an empty cuvette as the reference allowed for any absorbance from the cuvette walls to be accounted for but provided a more flexible set of data that could be compared to the water scan taken with the sample in later processing if desired (Max *et al.*, 2007).

The Cary 5000 spectrophotometer used in this study has a photometric accuracy of 0.00025 absorbance units. Spectra were collected between 180 nm and 1800 nm at 1-nm intervals with a 2-nm bandwidth. A target signal to noise ratio of 5000 was used with a timeout of 0.5 seconds. For each sample, scans were taken in triplicate with sample replacement between scans. The cell temperature accessory was set to 25°C for all room temperature scans. Samples were given 5 minutes to reach an equilibrium temperature before the spectra were collected.

6 EXPERIMENTAL RESULTS AND ANALYSIS

The data collected spans a wavelength range that is too large to show the whole spectrum in one figure and preserve all the information that can be interpreted from the samples. The amplitude of the absorbance over the wavelength range also has high variability and it is better represented in shorter wavelength range portions. This is due in part to the water absorption band harmonics that have very strong absorbance is certain wavelength regions. The chosen wavelength ranges to be investigated separately include the ultraviolet range (180-400 nm), the visible range (400-800 nm), the near infrared-A range (800-1400 nm), and the near infrared-B range (1575-1775 nm). These ranges and names were chosen specifically for the case in this project. A gap in the data presentation is noted between 1400 nm and 1575 nm. In this wavelength range there is a strong water absorption band harmonic. With the path length chosen for data collection (10 mm) the absorbance was too high for the spectrophotometer to accurately measure. Therefore, the data in this range were not used for any subsequent analysis or calculations.

6.1 Water Spectrum between 15°C and 95°C

Spectral measurements of water between 15°C and 95°C demonstrate regions of linear absorbance differences with temperature throughout the collected range. These regions are highlighted and compared to literature values in the following sections.

6.1.1 Ultraviolet (180 nm – 400 nm)

In the UV range, water has a major absorbance peak at 185 nm as well as a minor absorbance peak at 280 nm. Both peaks are dependent on temperature as shown in Figure 6-1 and Figure 6-2. These peaks are both at the lower range limit of the spectrophotometer and both contain significant noise. Most of the water absorption spectra in the literature do not include data below 200 nm. Hale and Querry (1973) collected data for water at 25°C to 200 nm and found a similar increasing trend to the lower wavelengths. They did not note the peak seen near 280 nm, but their data were collected at 25 nm intervals in this range so it is possible that this feature was missed. Persichetti *et al.* (2013) studied the fluorescence of water in the UV range and found that with excitation at 266 nm, water produced fluorescence peaks near 270 and 290 nm. Due to the nature of the spectrophotometer used in this study, fluorescence produced by excitation at 266 nm would be read as additional transmission at 266 nm instead of the appropriate wavelengths. Increased

transmission would be interpreted as a valley in the absorbance spectra and could explain the apparent absorbance peak seen near 280 nm.

Negative absorbance readings are reported in Figure 6-1 and Figure 6-2. These negative values are due to the different refractive indices of water and air. Hecht (2002) reported a refractive index of 1.000293 for air, 1.330 for water, and 1.458 for quartz. All refractive indices were given at 589.29 nm and can have different values at different wavelengths (Hecht, 2002). Because the refractive index for quartz it closer to water than air the amount of light reflected at the cuvette interfaces was lower when water was in the cuvette. Using the refractive indices given at 589.29 nm, this difference resulted is an approximate -0.027 absorbance reading for water when air is used in the reference beam. Calculations for this value are shown in Appendix A – Additional Calculations, Equation A-6 through A-12. This value is not exact over the wavelength range used due to changes in refractive indices and the changing temperature of the sample solution.

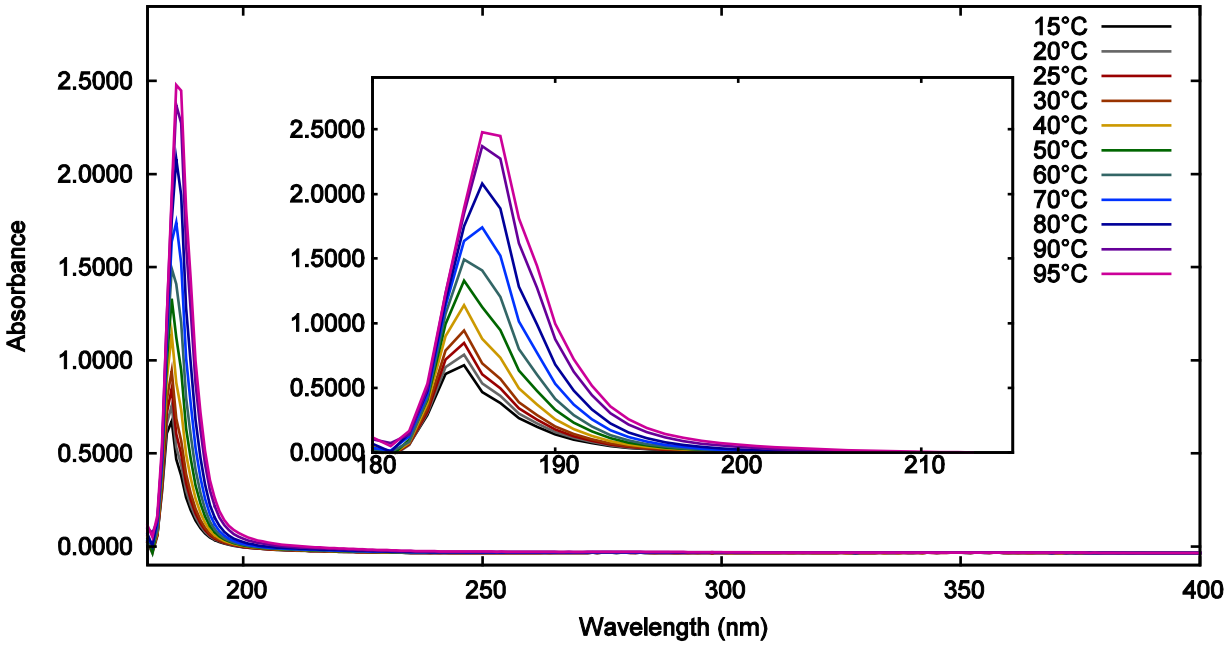

Figure 6-1: UV absorbance of water between 15°C and 95°C.

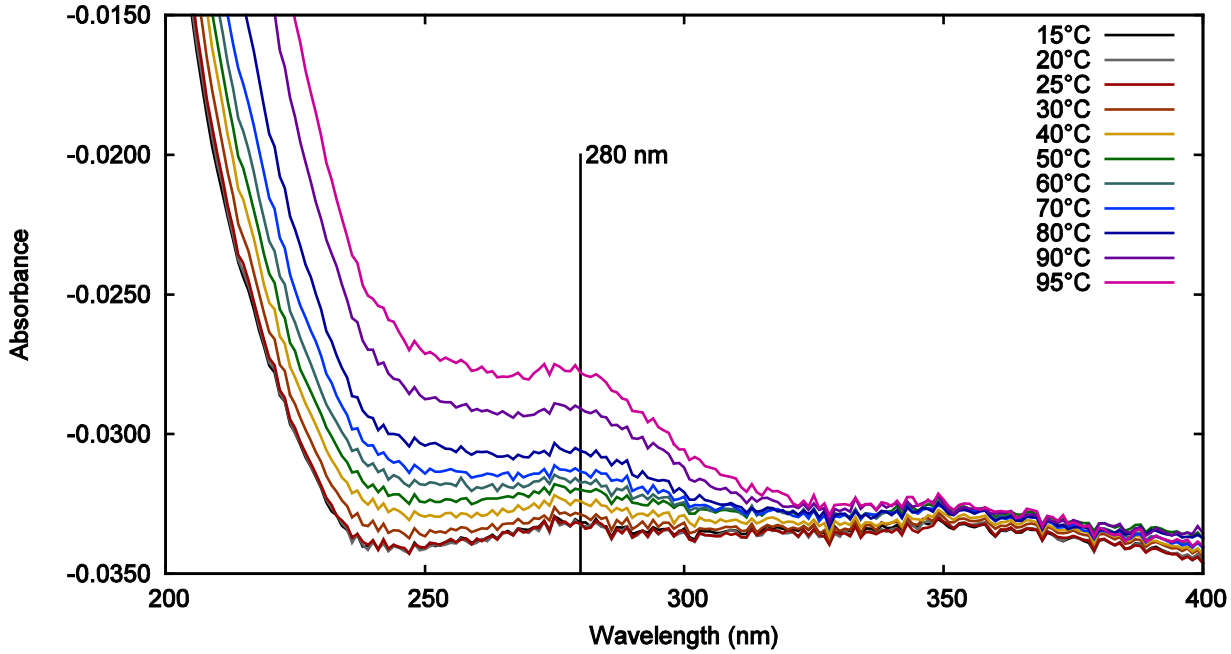

Figure 6-2: UV absorbance of water between 15°C and 95°C highlighting 280 nm peak.

6.1.2 Visible (400 nm – 800 nm)

The magnitude of absorbance of water in the visible range is low compared to the ultraviolet and near infrared regions. Negative absorbance values in this range are accounted for by the differences in refractive indices between water and air (Hecht, 2002). The main absorbance peak between 400 and 800 nm occurs around 740 nm and is dependent on temperature as shown in Figure 6-3. As temperature increases, this peak shifts to shorter wavelengths and increases in amplitude. This absorbance peak is associated with harmonics from the main absorption bands from the ν_1 and ν_2 stretching vibrations of the water molecules. Similar results were found by Langford *et al.* (2001) between 15°C and 60°C with the strongest absorbance changes with temperature observed around 740 nm. They also observed absorbance increases with temperature around 600 nm and 660 nm. There are observable differences in Figure 6-3 at these wavelengths, however they do not follow an increasing absorbance trend with temperature. This could be due to the low level of absorbance measured in this range. The decreasing absorbance with increase in temperature seen above 775 nm is consistent with the findings of Langford *et al.* (2001). Collins (1925) investigated the absorption band between 700 nm and 800 nm from 0.5°C to 90°C with very similar results in shape and position of the absorption bands over the temperature range.

Sullivan *et al.* (2006) considered the linear absorbance increase with temperature seen at 740 nm and compared this effect to an increase in absorbance with $NaCl_{(aq)}$ concentration at 755 nm. These findings indicate that the effects of temperature and the effects of salinity have overlapping features that need to be considered when modelling temperature of solutions.

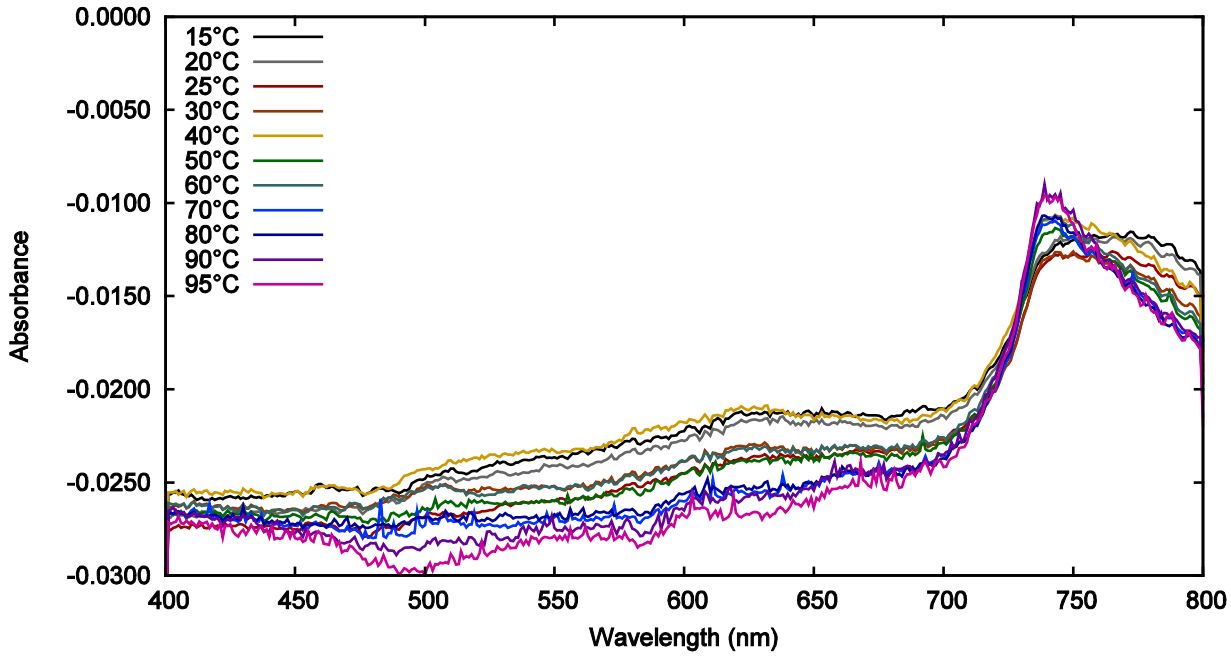

Figure 6-3: Visible absorbance of water between 15°C and 95°C.

6.1.3 Near Infrared-A (800 nm – 1400 nm)

The region denoted NIR-A contains two prominent absorption bands as shown in Figure 6-4. These bands result from the harmonics of the stretching vibrations and the bending vibration. As the temperature of the water increases, both bands experience a peak shift towards a shorter wavelength. Not only does this shift occur but absorbance at this lower wavelength also increases as temperature increases and the absorbance at higher wavelengths decreases. A similar trend is present above 1300 nm as an increase in absorbance is seen at the lower wavelength end of the next absorption band that is centered near 1470 nm.

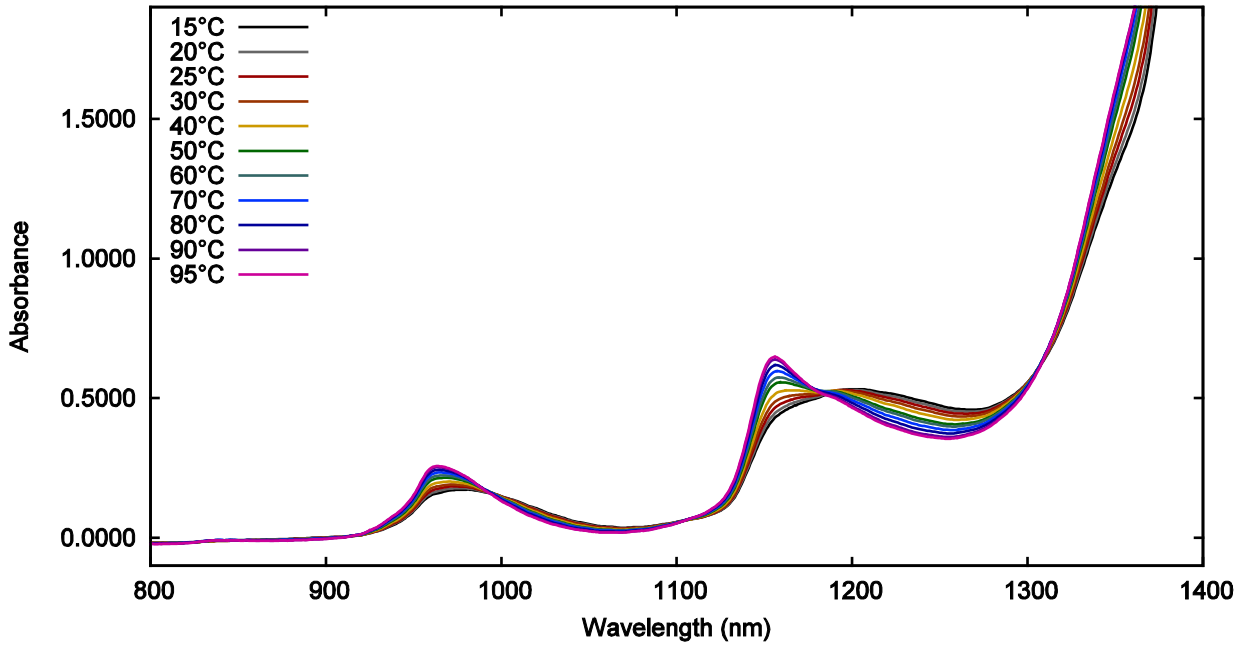

Figure 6-4: NIR-A absorbance of water between 15°C and 95°C

The bending vibration does not have a harmonic at 970 nm so the band centered around this wavelength only relies on the absorption from the two stretching vibrations (Walrafen & Pugh, 2004). A portion of the spectra between 900 and 1100 nm is shown in Figure 6-5 to highlight this band. The temperature variable peak is a result of the redistribution of water "species" in the sample, as described by Abe (2004). The stretching harmonic absorption (as seen near in the band near 970 nm) is the combination of the absorption from water in five states. As the temperature increases, the concentration of the water species with fewer hydrogen bonds increases. Water molecules without hydrogen bonds absorb at shorter wavelengths than water which has four (the maximum) hydrogen bonds. This causes the peak to shift to a shorter wavelength with temperature increases and also accounts for the increased and decreased absorbance to the left and the right of the peak, respectively. The isosbestic point likely indicates the interconverting of two water hydrogen bond states (Kim, & Swager, 2001).

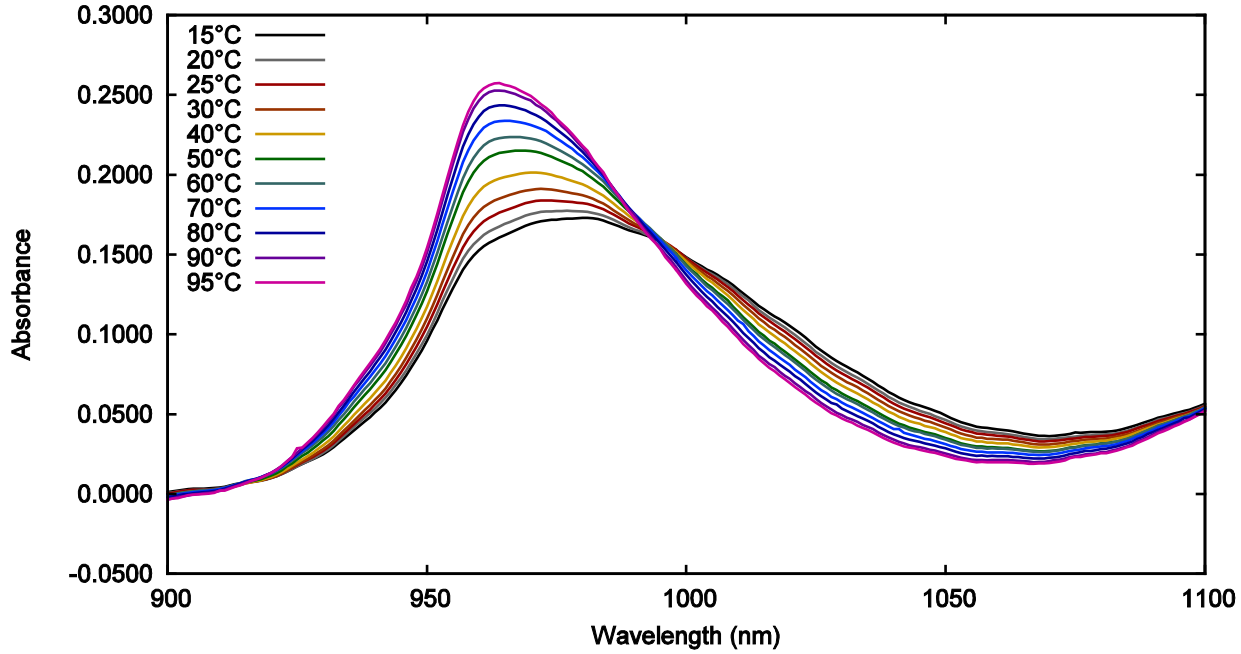

Figure 6-5: Absorption band near 970 nm of water between 15°C and 95°C.

The band centered around 1200 nm (at low temperatures) is a combination of the harmonics from both stretching vibrations and the bending vibration. The effect of temperature on this band is similar to the effect on the 970 nm band as shown in Figure 6-6. The decrease in absorbance at the longer wavelengths is more pronounced with this band and the shape of the peak has a more drastic shape change. The results from both bands investigated are similar to those results found by Collins between 0.5°C and 90°C (1925).

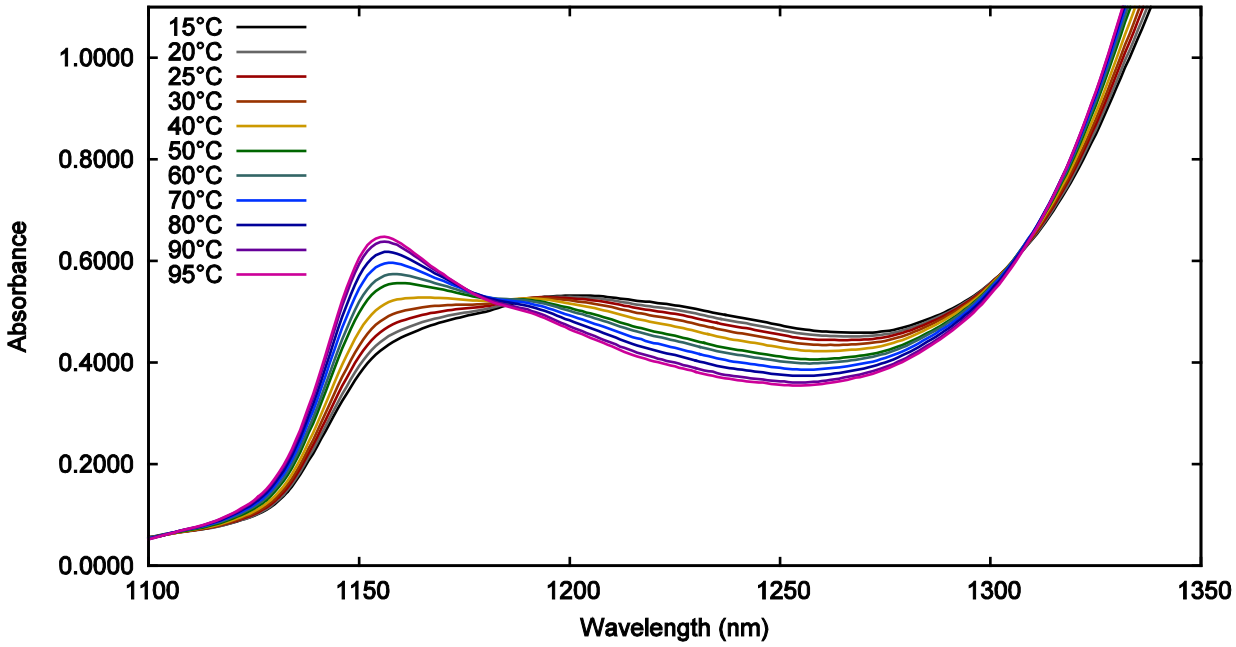

Figure 6-6: Absorption band near 1200 nm of water between 15°C and 95°C.

6.1.4 Near Infrared-B (1575 nm – 1775 nm)

The NIR-B region of the spectrum represents the region between two strong water absorption band harmonics (1470 nm and 1900 nm). Though this region does not include a peak absorbance, the absorbance from the tail ends of the two surrounding harmonics results in absorbance values that are temperature dependent throughout this wavelength range. At 1900 nm, the absorption is a combination of both the stretching vibrations and bending vibration in the water molecule while at 1470 nm, only the stretching vibrations contribute to the absorption. Similar to the peaks in the NIR-A range, in Figure 6-7 the region to the right of the 1470 peak exhibits a decrease in absorbance with increase in temperature. However, in Figure 6-4 the region leading up to 1400 nm has an increasing absorbance trend with temperature. It can be noted that the crossover that occurs near the 1200 nm band is also occurring near the 1470 nm band. Although an absorbance peak does not occur in this region, there is still a shift seen with a change in temperature. The minimum value of each spectrum in this region is shifting to shorter wavelengths as the temperature increases. This is expected as the peaks near 1470 and 1900 nm are also shifting to shorter wavelengths.

As the absorbance increases, more noise is visible in the spectrum. This is due to the nature of how these spectra are collected. The spectrophotometer measures the transmission of light through the sample and converts this to absorbance. At an absorbance reading of 4, the transmission through the sample is only 0.01% of light transmitting through the reference beam. At such low signal levels, small fluctuations in transmission result in large absorbance changes. The absorbance range in this figure was chosen to best show the feature in this wavelength range. At the lower temperatures, the absorbance would drastically increase to 10 and jump between an absorbance value of 5 and 10 below 1600 nm so this portion of the absorbance spectrum is not shown in Figure 6-7.

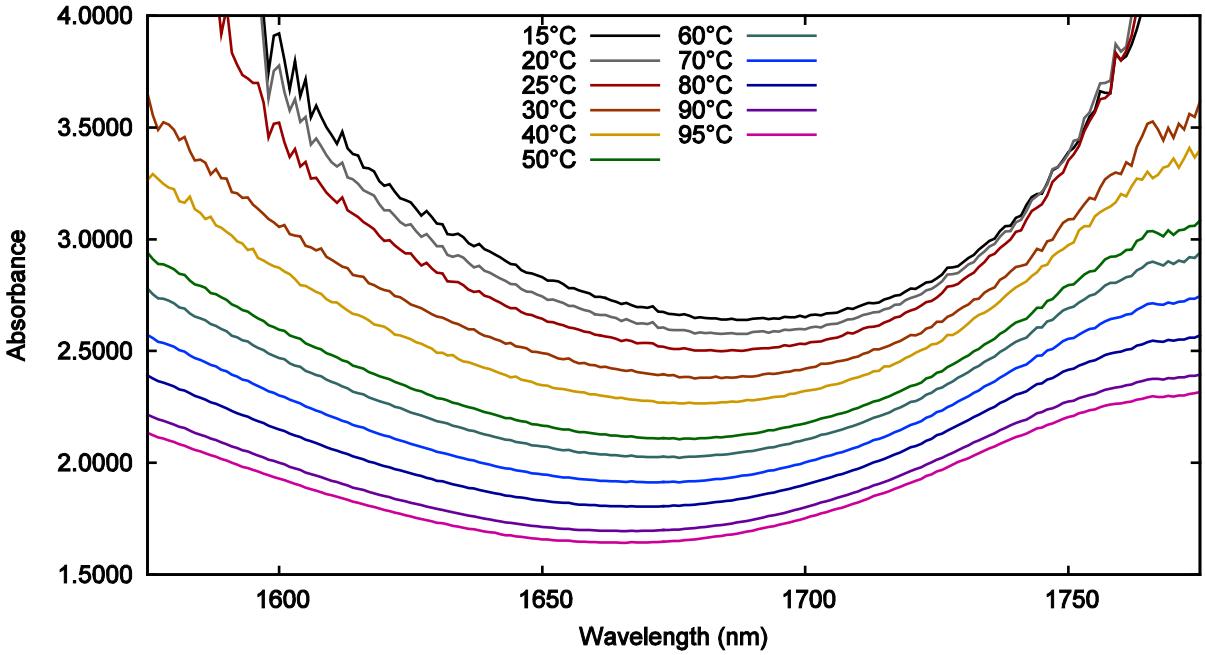

Figure 6-7: NIR-B absorbance of water between 15°C and 95°C.

Many individual wavelengths throughout the full scanned region have linear absorbance increase or decreases with temperature, though some regions are more easily exploited for this feature than others. The absorbance in the visible range has some linearity with temperature change but the data contain a large amount of noise making them less ideal for determination of temperature variation using spectral techniques. Both NIR regions show good absorbance linearity with temperature change and are at appropriate absorbance levels and sufficiently low noise to use for analysis. Regardless of the absorbance increase or decrease with temperature, many of the

wavelengths in the NIR range could be chosen for modelling purposes. The decision of which wavelength(s) would be most appropriate will be discussed further in the modelling sections after the absorbance effect of $NaCl_{(aq)}$ and $KCl_{(aq)}$ are presented.

6.2 Aqueous Potassium Chloride and Sodium Chloride Spectra

All spectra for $KCl_{(aq)}$ and $NaCl_{(aq)}$ in solution were taken with an empty cuvette in the reference beam. This results in the scans obtained for all samples representing the complete solution as opposed to the absorption of the dissolved ions by themselves. Two main types of spectra will be presented. The first type will be the scans as taken (with both the ions and the water absorbance represented) and the second type will show the scans with the spectrum of pure water subtracted from each measurement. This second type highlights the differences made to the water spectrum due to the presence of the salt ions. Consistent with previous research, $NaCl_{(aq)}$ and $KCl_{(aq)}$ were observed to have very similar absorbance spectra. However, a few regions where the shape and intensity diverges were observed that could be useful for species identification.

During data analysis and comparison with literature values, it was discovered that some regions of the spectra had absorbance levels that were too high or too low for good results. Better data for these regions could be collected by using different path lengths for the sample, however these regions were simply rejected for use in modelling for this project.

6.2.1 Ultraviolet Region

As noted by Di Noto and Mecozzi (1997), absorbance in the ultraviolet range is strongly affected by $NaCl_{(aq)}$ and $KCl_{(aq)}$, even at very low concentrations. This feature is consistent for many dissolved salt species, but the physical basis for this feature is unknown (Di Noto & Mecozzi, 1997). Figure 6-8 and Figure 6-9 combine all data from the single-salt scans ($NaCl_{(aq)}$ and $KCl_{(aq)}$ respectively) by taking the average of the three trials at each concentration and displaying the spectra over the entire concentration range. A water scan is also included although water does not have strong absorbance in this range (as shown in Figure 6-1). For both $NaCl_{(aq)}$ and $KCl_{(aq)}$ the main absorbance peak in this range shifts to longer wavelengths as the concentration increases. In comparison to Figure 6-1, the absorbance changes caused by the addition of $NaCl_{(aq)}$ and $KCl_{(aq)}$ are much greater than those cause by the studied temperature changes.

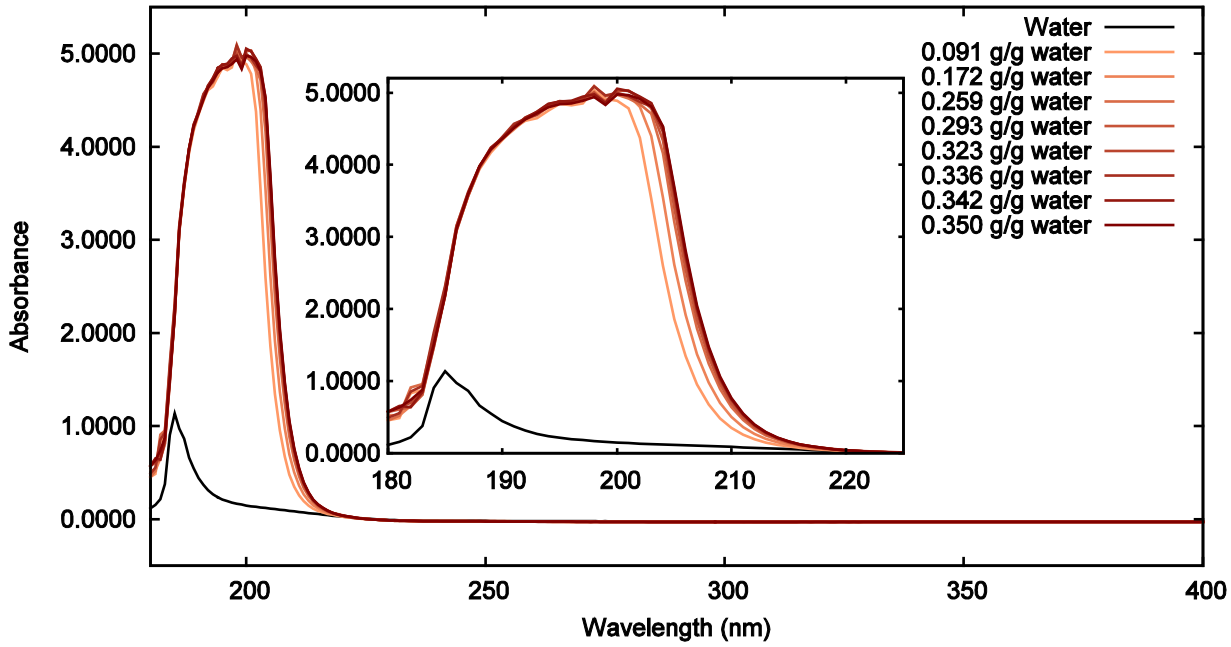

Figure 6-8: UV absorbance of $NaCl_{(aq)}$ at room temperature (180 – 400 nm).

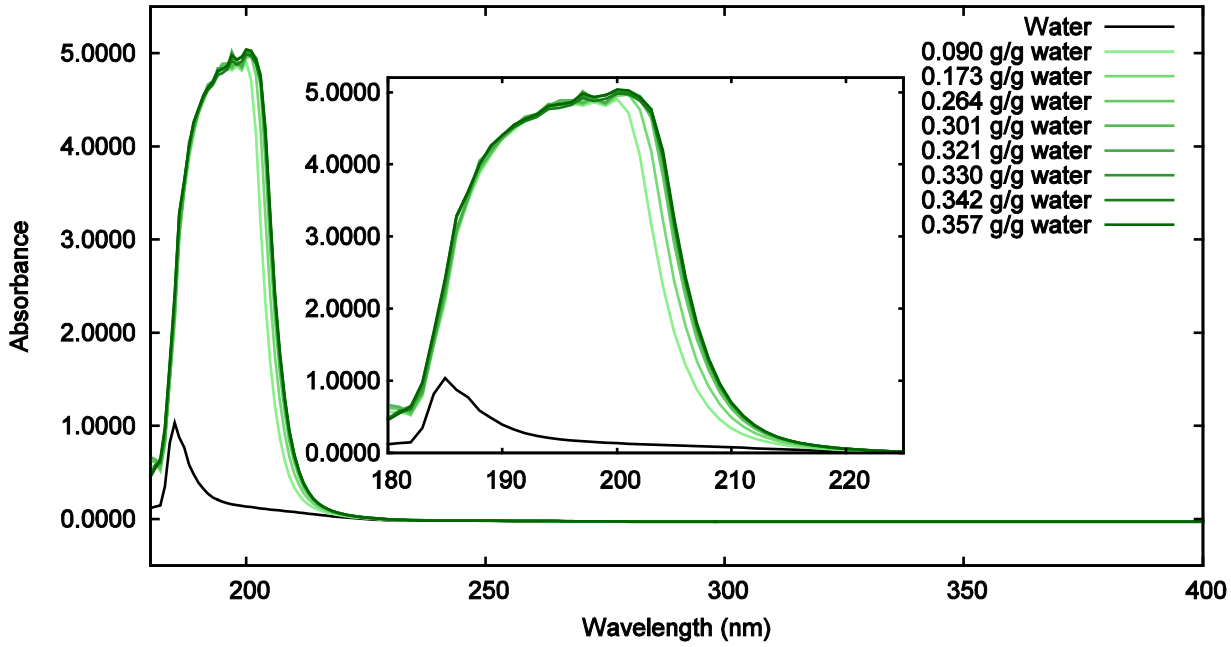

Figure 6-9: UV absorbance of $KCl_{(aq)}$ at room temperature (180 – 400 nm).

The spectra for the two salts are similar in a large portion of this range but there are a few points of divergence between the two species. Figure 6-10 displays the absorbance of both $NaCl_{(aq)}$

and $KCl_{(aq)}$ in the absorbance range where these differences are most noticeable. Between 230 nm and 280 nm a distinct gap in the absorbance of the two species is observed that is independent of concentration. The actual difference in absorbance value at these wavelengths is quite small making this a difficult point to use for species differentiation for this data set.

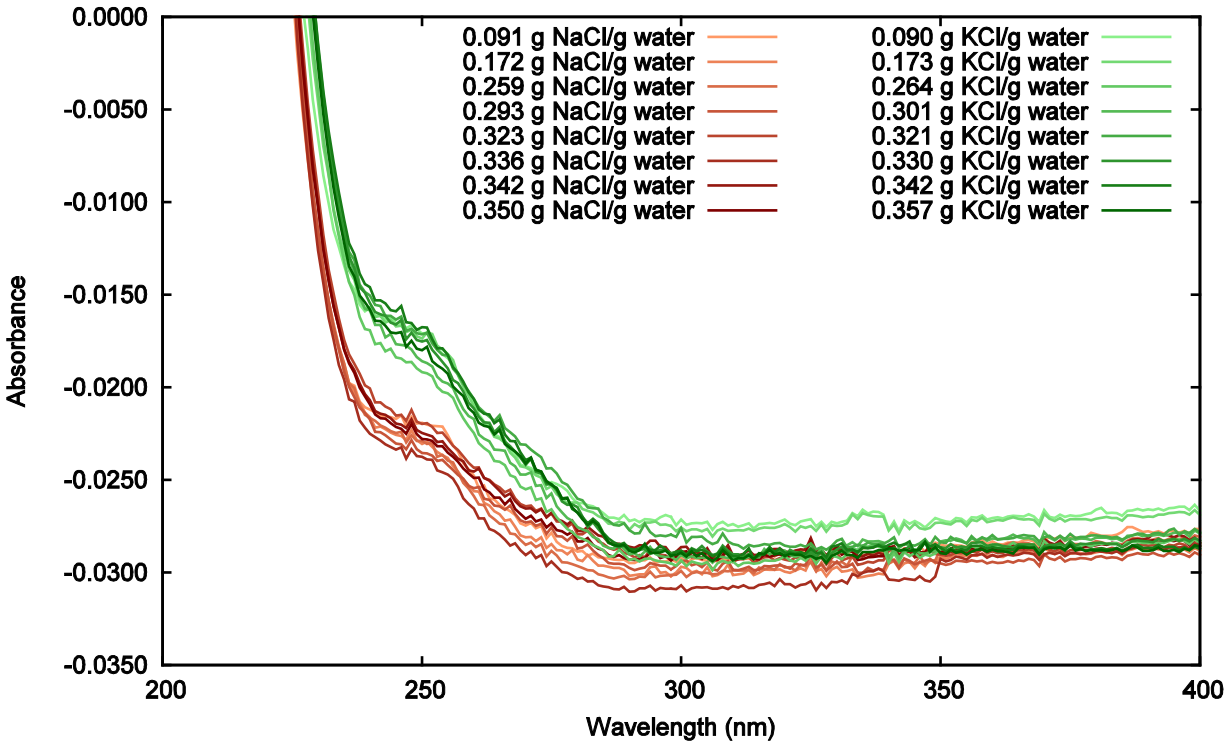

Figure 6-10: UV absorbance of $NaCl_{(aq)}$ and $KCl_{(aq)}$ at room temperature highlighting the differences between the salt species (200 – 400 nm).

6.2.2 Visible

Similar to the absorbance of pure water, absorbance of salt water in the visible range is very low. This is expected as salt water solutions appear transparent to the human eye. The most prominent peak in this region is observed at 750 nm and is similar in shape and magnitude to pure water at room temperature. Figure 6-11 and Figure 6-12 show the absorbance for $NaCl_{(aq)}$ and $KCl_{(aq)}$ respectively. When looking at the combined salt and water spectrum, there is no obvious trend of absorbance change with salt concentration in this region. To better visualize whether or not a linear trend is present the absorbance values at 625 nm and 760 nm were plotted against concentration. The results from this comparison are shown Figure 6-13 for both salts.

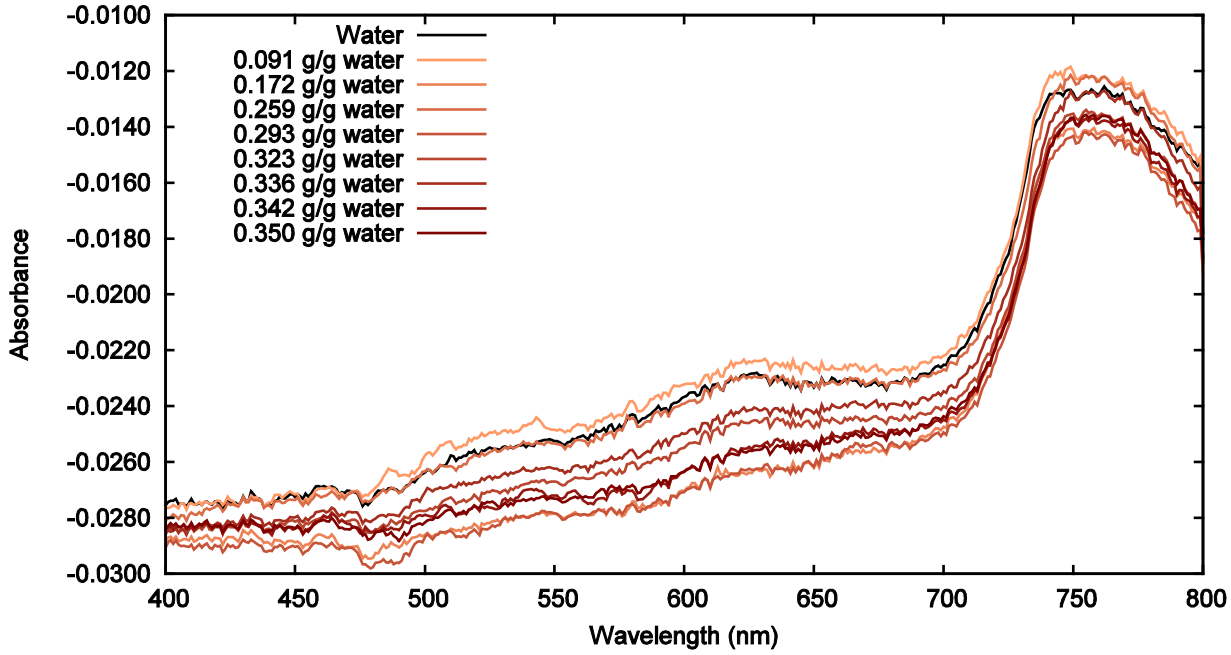

Figure 6-11: Visible range absorbance of $NaCl_{(aq)}$ at room temperature.

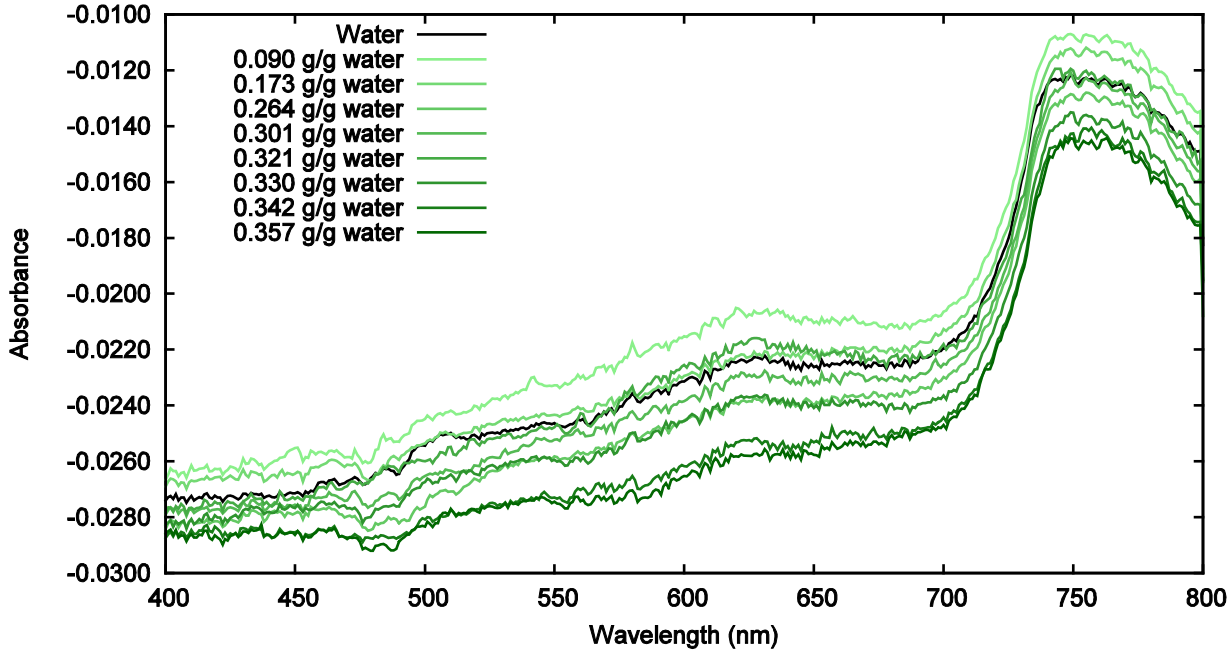

Figure 6-12: Visible range absorbance of $KCl_{(aq)}$ at room temperature.

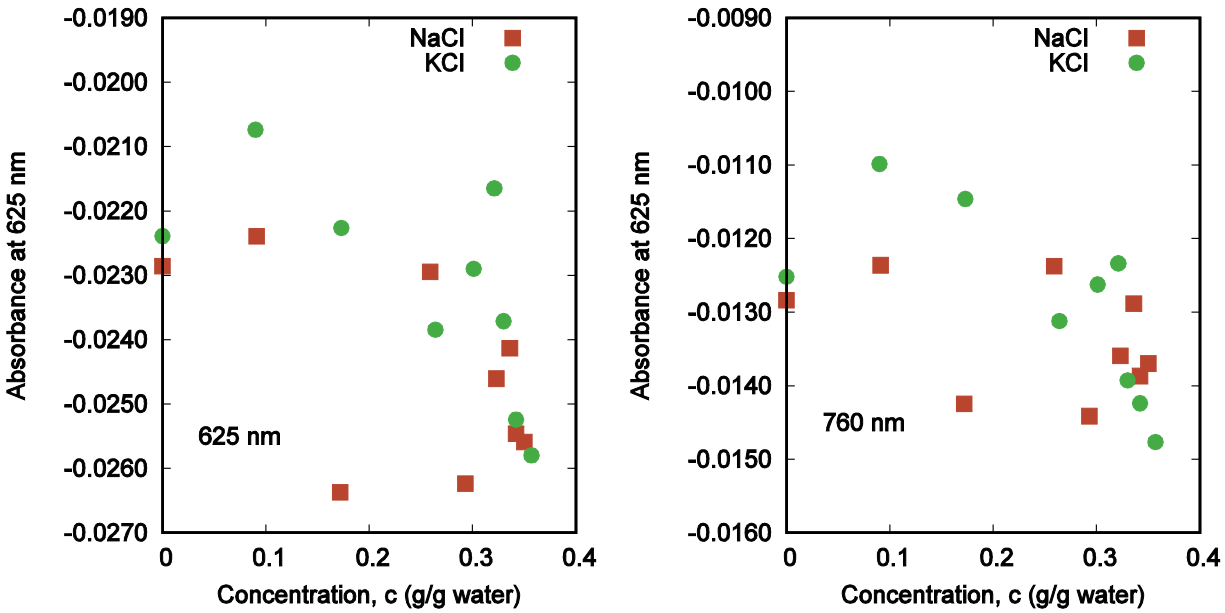

Figure 6-13: Absorbance values at 625 nm and 760 nm for $NaCl_{(aq)}$ and $KCl_{(aq)}$.

There does not appear to be a linear trend between concentration and absorbance for either salt at 625 nm or 760 nm. The spectra in this region differ from some literature findings as a correlation between salinity and absorbance is expected at 755 nm (Sullivan *et al.*, 2006). These differences are likely the result of low absorbance readings in this range. Sullivan *et al.* (2006) used a path length of 25 cm compared to the 1-cm path length used in Figure 6-13. Temperature dependence at 740 nm was discernable but salinity produces a less pronounced effect in the range and was not able to be detected using the shorter path length. The differences seen in Figure 6-13 are primarily attributed to noise and will not be used in modelling.

6.2.3 Near Infrared-A

The absorbance changes due to the addition of salt in the NIR-A region mimic some of the changes observed with a temperature increase of pure water but only when the increase in temperature causes a decrease in absorbance. Two major absorption band centers are seen in this wavelength range as shown in Figure 6-14 and Figure 6-15 for $NaCl_{(aq)}$ and $KCl_{(aq)}$ respectively. The changes for the two salt species are similar, but do exhibit differences in this region both in spectral shape and correlation between concentration and absorbance change. Each band will be presented and examined individually to provide better visualization.

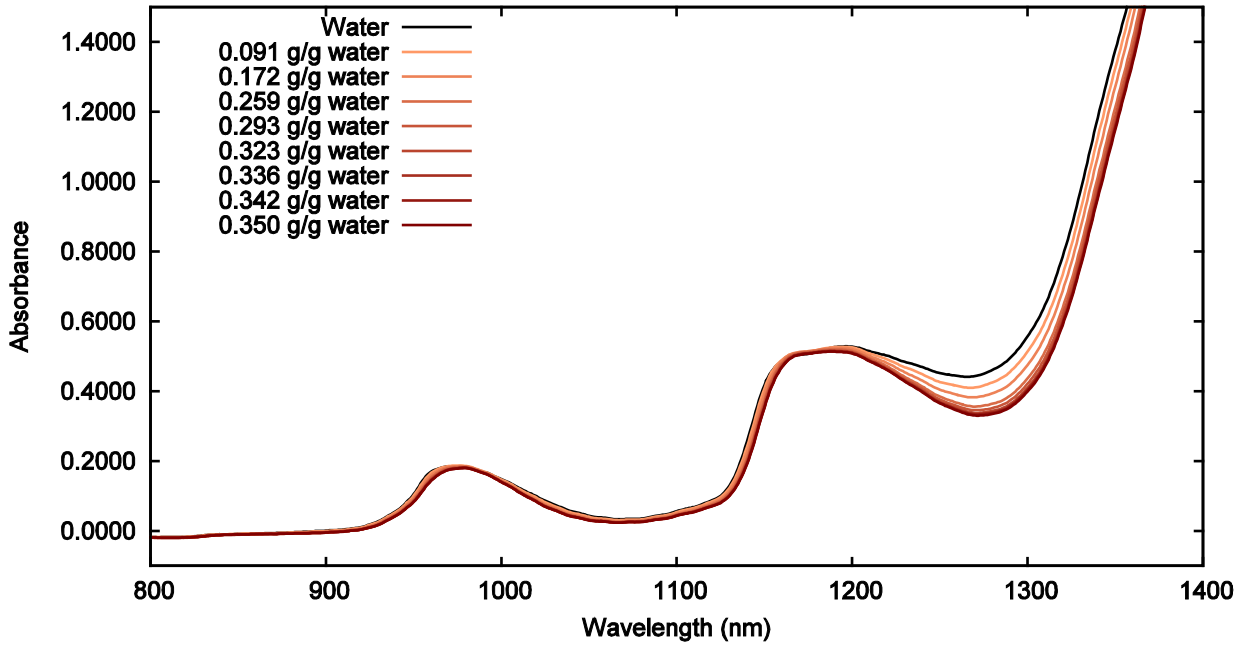

Figure 6-14: NIR-A range absorbance of $NaCl_{(aq)}$ at room temperature.

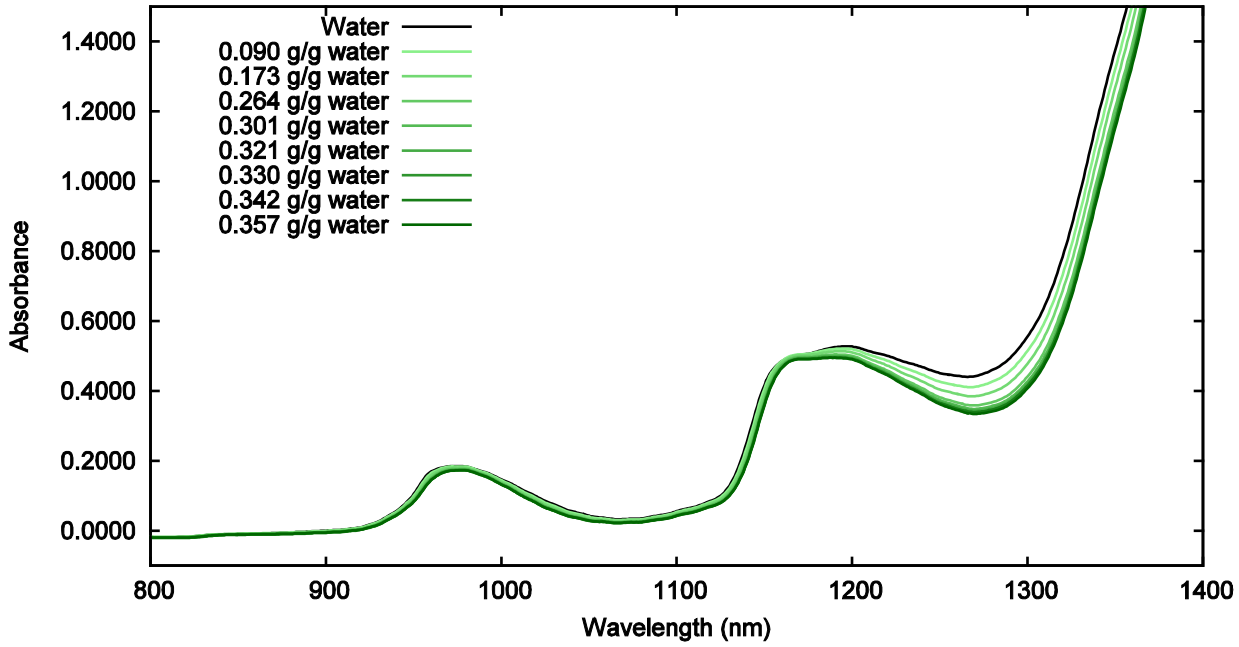

Figure 6-15: NIR-A range absorbance of $KCl_{(aq)}$ at room temperature.

The first band near 970 nm is shown in Figure 6-16 and Figure 6-17 for $NaCl_{(aq)}$ and $KCl_{(aq)}$ respectively. This band is dependent on both $NaCl_{(aq)}$ and $KCl_{(aq)}$ concentration and corresponds

to the water stretching vibration harmonics. As the salt concentration increases, the absorbance of this band decreases and shifts to a longer wavelength. This effect is similar to the effect observed during a decrease in the temperature of pure water. This could indicate a decrease in the number of water molecules with no hydrogen bonds according to Abe's analysis of the absorption decomposition at this band (Abe, 2004). A logical reasoning for this would be that water molecules that have no hydrogen bonding would more likely be attracted to the dissolved ions as they are not already paired with other water molecules. The decreased absorbance from both the 970 nm peak and the 1200 nm peak cause the region between the two peaks to decrease in absorbance as well. Between 1050 and 1100 nm, absorbance from the tail ends of both peaks is present. When the salt concentration is increased and the absorbance of the peak is decreased, the longer wavelength side of the 970 nm band decreases and the shorter wavelength side of the 1200 nm band decreases resulting in a relatively consistent decrease in absorbance at the wavelengths between the two bands. The overall concentration of water molecules in the path lengths is also decreasing as the salt concentration increases causing less overall absorbance due to the water absorption harmonics.

When comparing the absorbance features of $NaCl_{(aq)}$ and $KCl_{(aq)}$ near 970 nm, it can be noted that the solutions containing $NaCl_{(aq)}$ generate a greater shift toward longer wavelengths with increasing concentration than the solutions containing $KCl_{(aq)}$. This is likely due to the kosmotropic effects of Na^+ and Cl^- compared to the chaotropic effects of K^+. Both salts contain kosmotropic chloride ions which cause a more structured water arrangement resulting in better aligned, and therefore stronger, hydrogen bonds (Hribar *et al.*, 2002). These stronger hydrogen bonds create a shift towards longer wavelengths in the absorbance spectra (Nickolov & Miller, 2005). In solutions containing $NaCl_{(aq)}$, this effect is increased as sodium ions are also kosmotropes. However, in solutions containing KCl, the potassium ions break the structured water arrangement causing the hydrogen bonds to be weaker. This counteracts the shift induced by the chloride ions resulting in an absorbance band with its center closer to that of pure water.

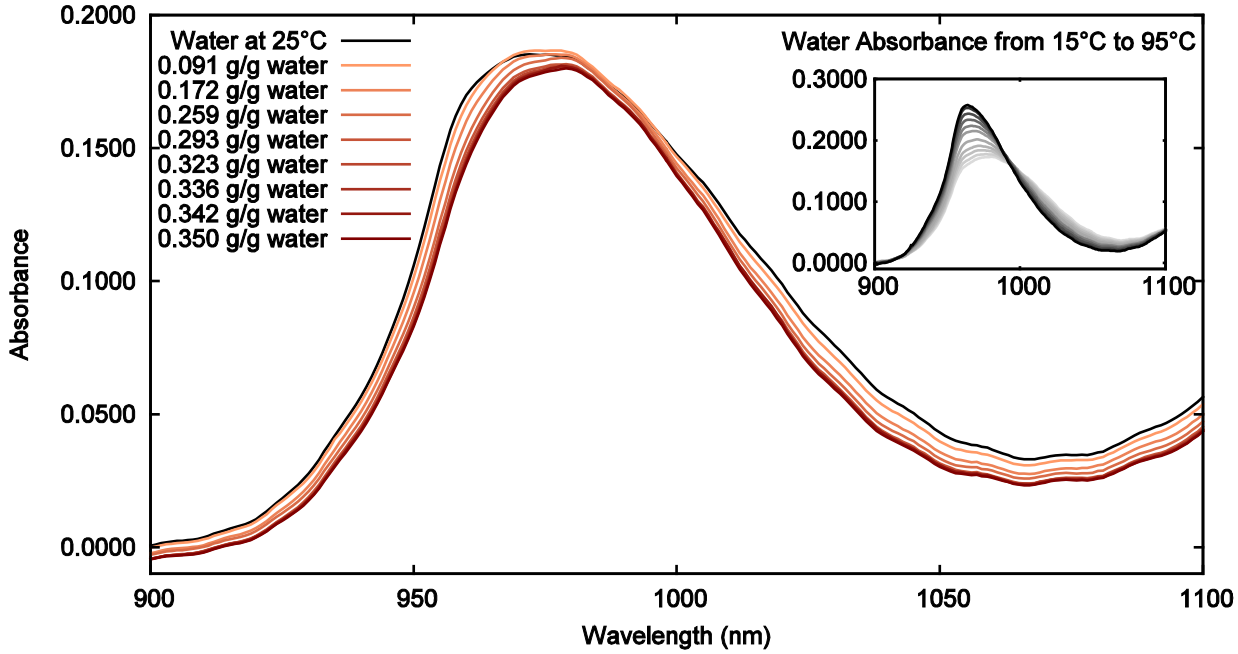

Figure 6-16: Absorbance band near 970 nm of $NaCl_{(aq)}$ at room temperature. Inset is taken from Figure 6-5.

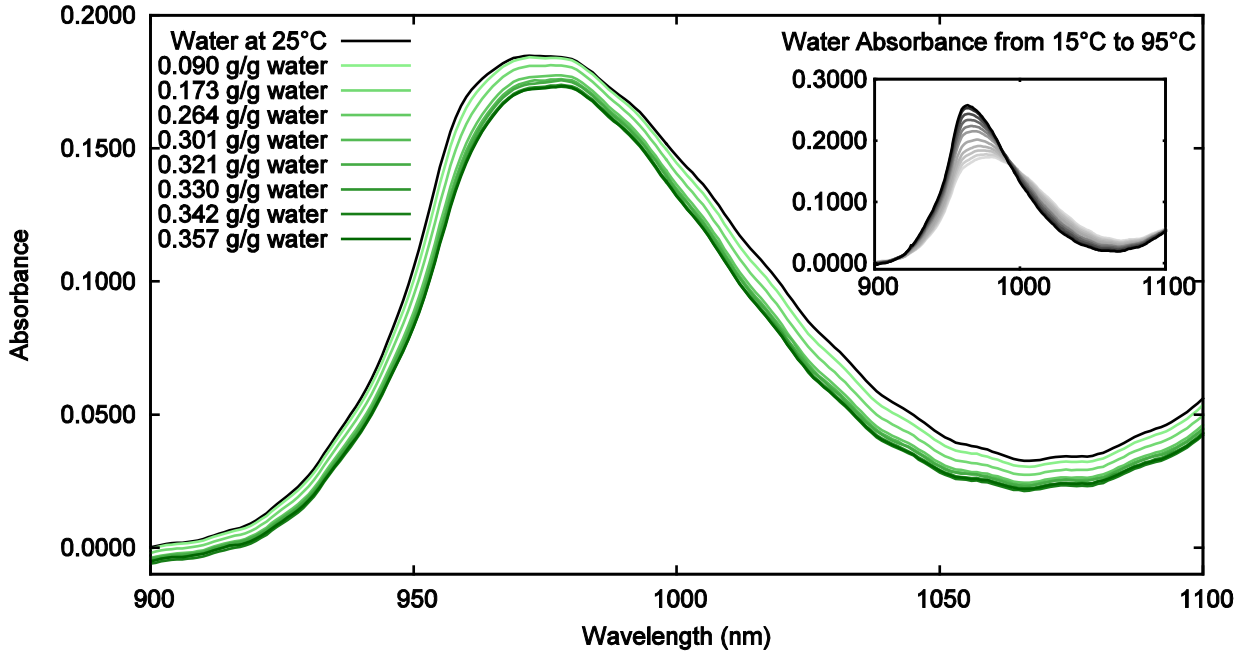

Figure 6-17: Absorbance band near 970 nm of $KCl_{(aq)}$ at room temperature. Inset is taken from Figure 6-5.

The second absorbance band observed in this region occurs near 1200 nm as shown in Figure 6-18 and Figure 6-19 for $NaCl_{(aq)}$ and $KCl_{(aq)}$ respectively. This band is also dependent on both $NaCl_{(aq)}$ and $KCl_{(aq)}$ concentration, but unlike the band at 970 nm this band corresponds to both the water stretching vibration harmonics and the bending vibration harmonic. Similar to the 970 nm band, absorbance decreases with an increase in salt concentration. The shift that is seen with the 970 nm band is less prominent with this band likely due to the combination of all three water vibrations. Temperature variation has opposing shifting effects on the stretching and bending vibrations (Praprotnik *et al.*, 2004) so it is likely that salt concentration also produces different effects on the different vibration types. As mentioned previously, Na^+ and Cl^- are structure-making ions or kosmotropes, but K^+ is a structure-breaking ion or chaotrope. This could account for the greater decrease in absorbance seen at 1200 nm with $KCl_{(aq)}$ than with $NaCl_{(aq)}$ solutions. The chaotropic K^+ ion could prevent the water molecules from forming as many quadruple-bonded water molecules due to a less structured arrangement. If this absorbance band behaves similarly to the band at 970 nm, fewer quadruple-bonded water molecules would decrease absorbance on the longer wavelength side of the absorption band harmonic (Abe, 2004).

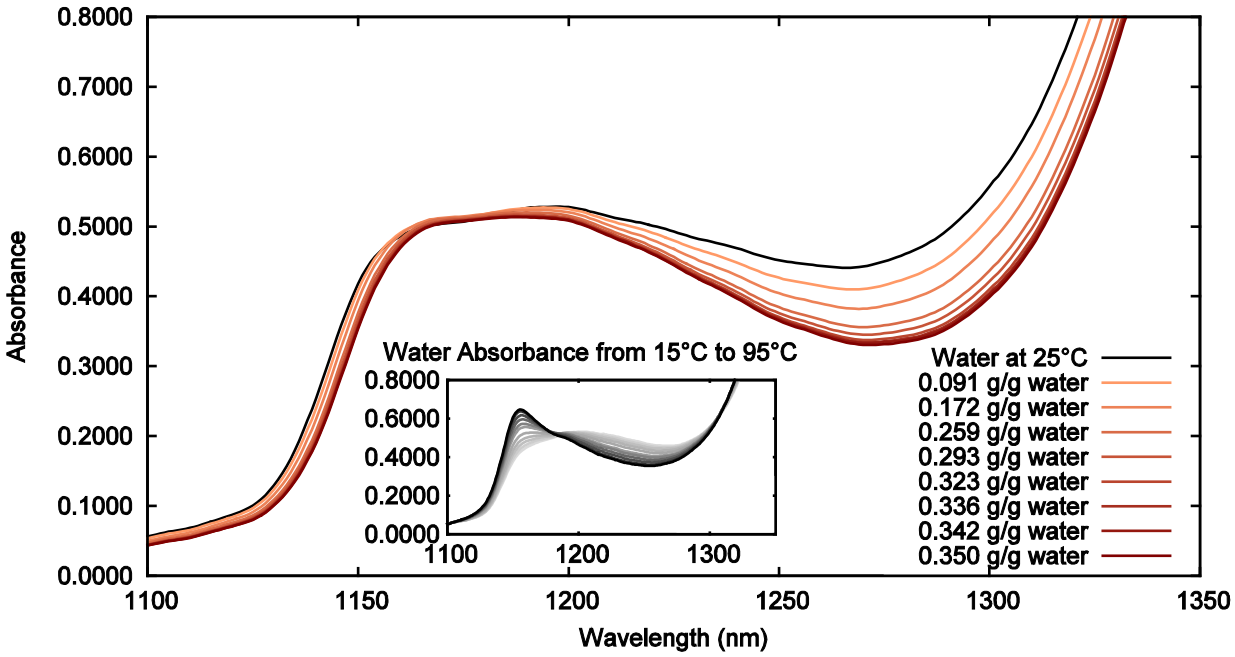

Figure 6-18: Absorbance band near 1200 nm of $NaCl_{(aq)}$ at room temperature. Inset is taken from Figure 6-6.

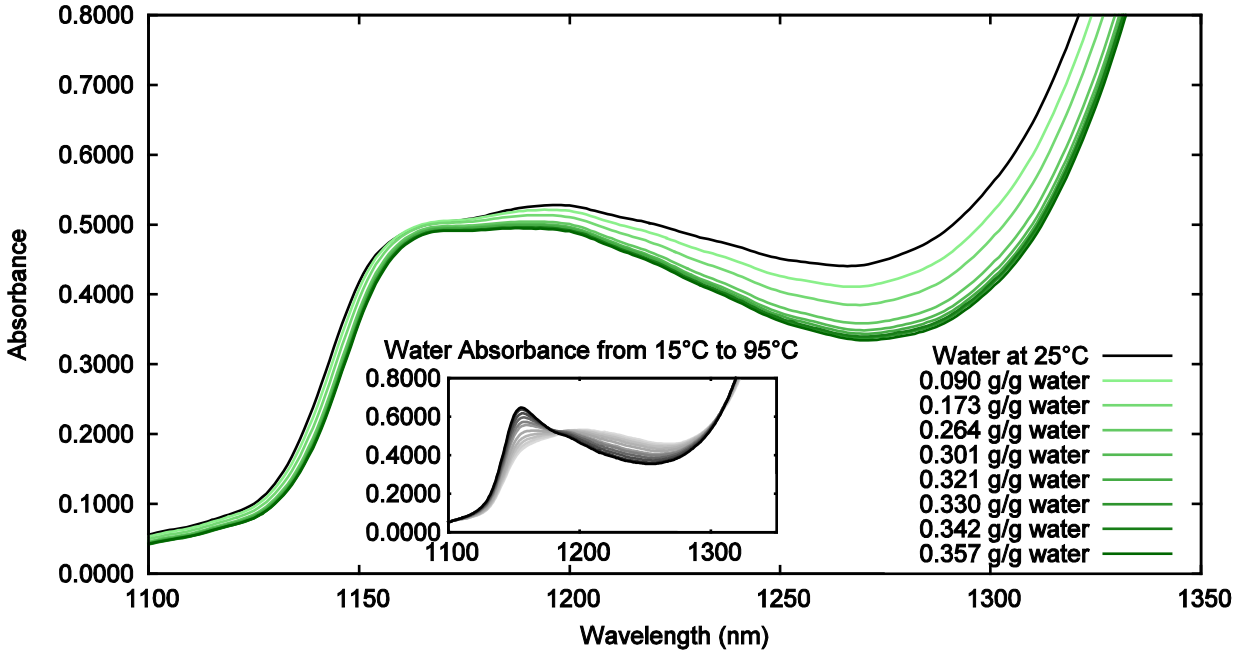

Figure 6-19: Absorbance band near 1200 nm of $KCl_{(aq)}$ at room temperature. Inset is taken from Figure 6-5.

The effects of the different salt species at the 970 nm band appears to have more similarities on the shorter wavelength side of the band peak and more differences on the longer wavelength side. The same can be noted for the band near 1200 nm as $KCl_{(aq)}$ causes a greater decrease in absorbance on the longer wavelength side of the peak. These differences are not easily visualized when comparing the spectra that includes water as the water absorption bands are more substantial than the changes induced by the salt. In order to provide a better comparison of these differences, the deionized water spectrum was removed by subtraction and the two salt species were displayed on the same graph as shown in Figure 6-20. In this figure there are a number of interesting features that are more evident than in the spectra that include the water absorbance. Congruent with the findings from the previous figures, $NaCl_{(aq)}$ and $KCl_{(aq)}$ appear to have the greatest absorbance differences on the longer wavelength side of each absorbance peak. These differences are noted near 975 nm and 1175 nm with $KCl_{(aq)}$ producing a greater decrease in absorbance. Another notable deviation between the two salt species occurs near 1350 nm. This feature appears on the edge of the high-absorbance harmonic that centers near 1470 nm so the full shape and explanation are difficult to ascertain. Many of the differences between the $NaCl_{(aq)}$ and $KCl_{(aq)}$ in this region

could potentially be used for discrimination between the two species as will be discussed further in the modelling section of this work.

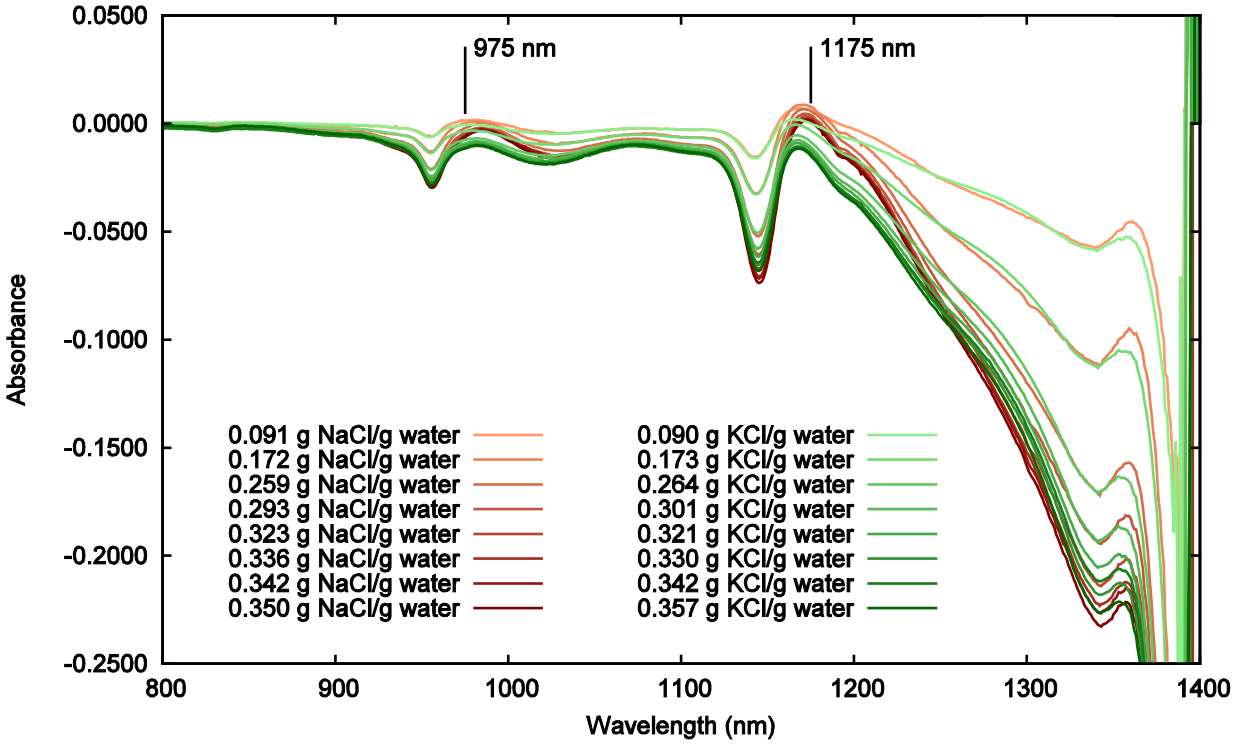

Figure 6-20: NIR-A range absorbance of $NaCl_{(aq)}$ and $KCl_{(aq)}$ with the water absorbance subtracted at room temperature.

6.2.4 Near Infrared-B

Similar to the absorbance changes with increasing temperature, increasing salt concentration decreases the absorbance throughout this range of the spectrum. As seen in Figure 6-21 and Figure 6-22, $NaCl_{(aq)}$ and $KCl_{(aq)}$ have a similar effect between 1575 and 1775 nm. As mentioned previously, this region does not include a water absorbance peak but accounts for the absorbance from the tail ends of two peaks at 1470 nm and 1900 nm.

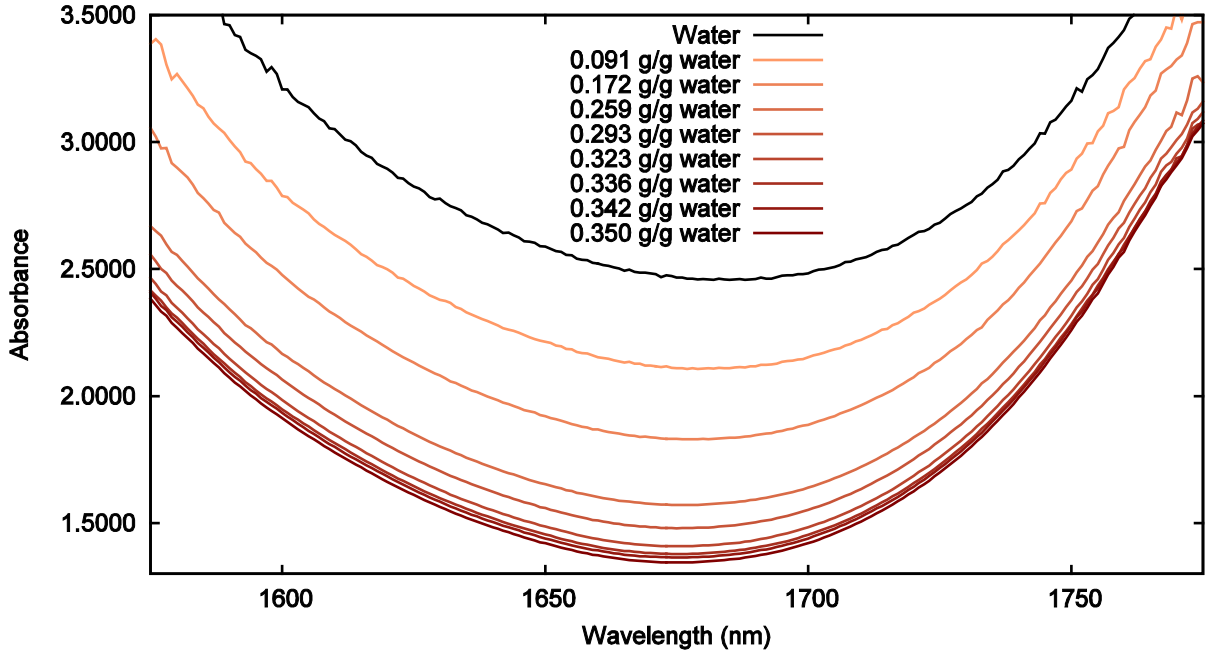

Figure 6-21: NIR-B range absorbance of $NaCl_{(aq)}$ at room temperature.

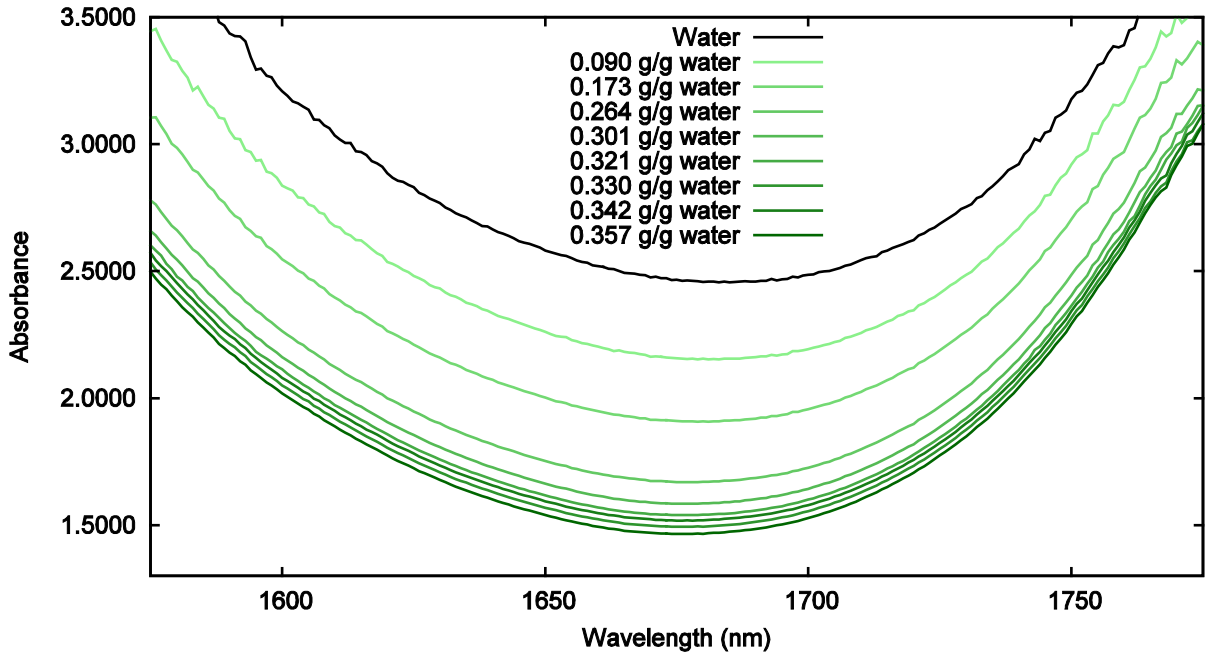

Figure 6-22: NIR-B range absorbance of $KCl_{(aq)}$ at room temperature.

The deionized water absorbance was removed from the spectra and both salts were displayed on the same graph to visualize any differences between the two species. This comparison

is shown in Figure 6-23. Both species have obvious absorbance decreases with increasing salinity but there are some spectral shape differences that can be noted in this comparison. As the absorbance approaches 1750 nm the relative absorbance changes of $NaCl_{(aq)}$ appear to diminish in comparison to $KCl_{(aq)}$. This is consistent for all measurements displayed in this figure as is seen in the two lines of similar $g \cdot g water^{-1}$ concentration in $KCl_{(aq)}$ and $NaCl_{(aq)}$. At higher wavelengths, the absorbance lines tend towards each and as the wavelength decreases $NaCl_{(aq)}$ has a greater effect on absorbance. The cause of these differences between $KCl_{(aq)}$ and $NaCl_{(aq)}$ are not obvious as a similar trend is not seen between the bands near 970 nm and 1200 nm. The general decrease in absorbance difference with increasing wavelength that is seen with both salts is explained by the redistribution of hydrogen bonding in the water molecules. The absorbance due to the water molecules with 4 hydrogen bonds is greatly reduced as bonds between the water molecules and salt ions are preferable. This causes greater absorbance changes at the longer wavelength tail of the 1470 nm band. The addition of salt has the greatest effect on absorbance at the lower wavelength range in Figure 6-23 due to these changes in the 1470 nm band.

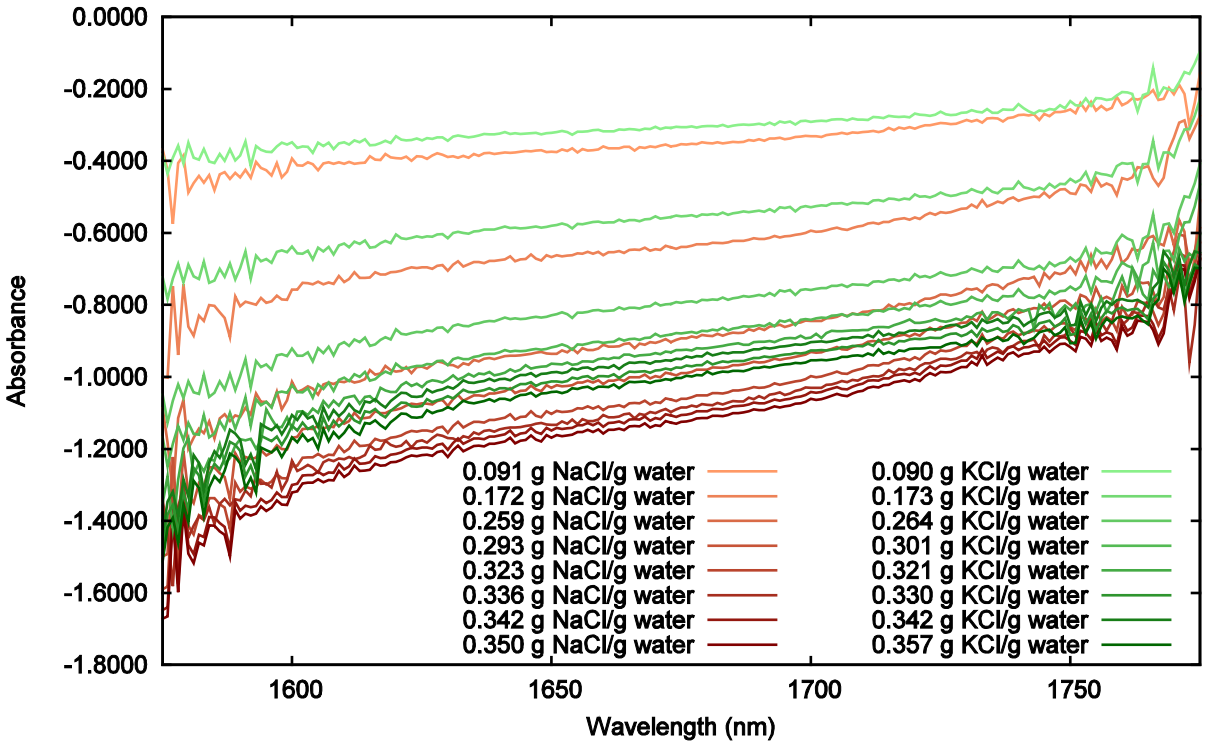

Figure 6-23: NIR-B range absorbance of $NaCl_{(aq)}$ and $KCl_{(aq)}$ with the water absorbance subtracted at room temperature.

7 MODELLING

The spectral data collected for $NaCl_{(aq)}$ and $KCl_{(aq)}$ solutions provided enough information to develop models for differentiating between $NaCl_{(aq)}$ and $KCl_{(aq)}$ and the spectral data of deionized water from 15°C to 95°C was sufficient for correlating temperature and absorbance. Four models were developed for three different purposes using the data collected and analyzed. First, a model for differentiating between single-salt samples at constant temperature provided important information about the differences between $NaCl_{(aq)}$ and $KCl_{(aq)}$ spectra and how those differences could be most effectively exploited. Next, a model for determining temperature of water samples using spectral measurements was designed based on known wavelengths that correlated with overall salinity and correlation values between temperature and absorbance. In determining which wavelengths would be most useful for temperature determination, limiting the number of degrees of freedom was important so information discovered through developing the first model was used. The third and fourth models both estimated concentrations in dual-salt samples at constant temperature. Similar to the temperature model, these models were developed based on information learned from the developing the first model.

7.1 Model Development: Single-Salt Solutions at Constant Temperature

Differentiation between single-salt solutions of $NaCl_{(aq)}$ and $KCl_{(aq)}$ involved exploiting differences in the spectra and using a closest-fit approach to species determination. As noted previously, there were a number of wavelength ranges that could be used for differentiating between $NaCl_{(aq)}$ and $KCl_{(aq)}$ in solution. To determine the best ranges for modelling, correlations between absorbance and concentration were calculated through the range of the spectrum.

Figure 7-1 summarizes the correlations between molarity and $g \cdot g_{water}^{-1}$ concentration for the entire wavelength range studied. This figure includes data from individual salts and combines the data to see the overall relationship between absorbance and salinity. This allows for visualization of wavelength regions that could be useful for overall salt concentration determination and regions that could be useful for species differentiation. When NaCl and KCl are considered separately, converting between $g \cdot g_{water}^{-1}$ concentration and molarity is nearly linear through the concentration range. However, when the data for NaCl and KCl are combined, the conversion from $g \cdot g_{water}^{-1}$ concentration to molarity cannot be described by a single linear trend across both salts because of their different molar masses. This non-linear conversion accounts for

the differences between the combined g·gwater^{-1} concentration and combined molarity shown in Figure 7-1.

Between 1230 nm and 1360 nm there was very high correlation between the g·gwater^{-1} concentration and absorbance for both species separately as well as combined. High correlation with both species combined indicates that this region could be effective for determining overall salt concentration regardless of speciation. In comparison, the regions between 1160 nm and 1230 nm show good correlation for individual salt species but poor correlation for the combined data. This indicates that the region between 1160 nm and 1230 nm could be useful for species differentiation or an overall salinity check with salt discrimination. There are also many regions that show poor correlation for both $NaCl_{(aq)}$ and $KCl_{(aq)}$. These poor correlations allowed for quick rejection of many wavelength regions when considering the optimum range to use for modelling.

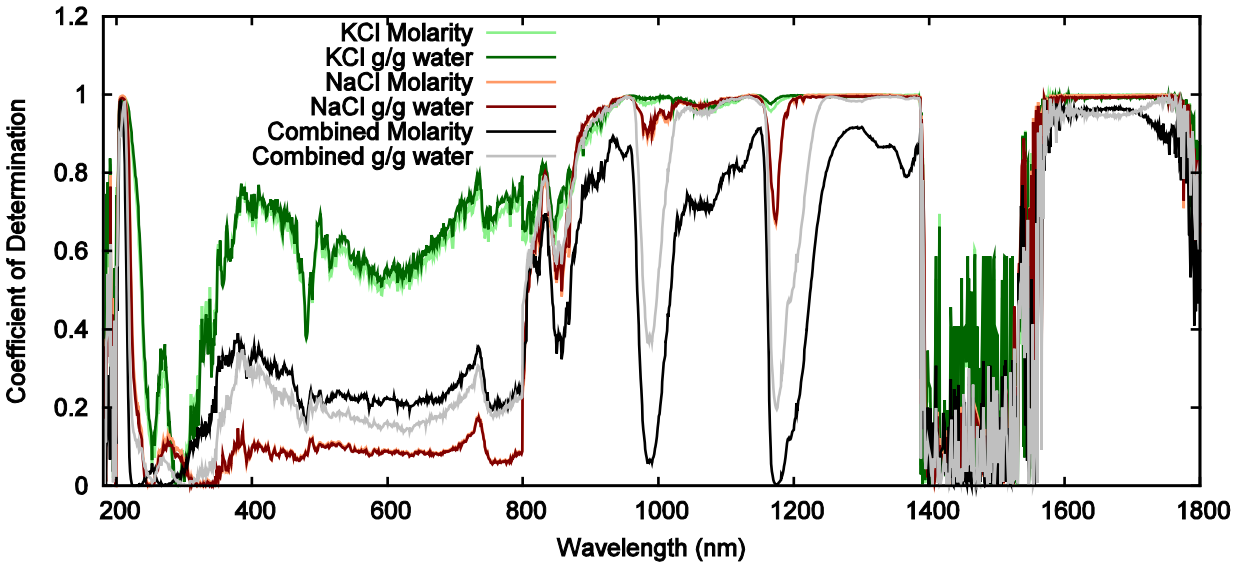

Figure 7-1: Correlation between molarity, g·gwater^{-1} concentration, and absorbance for both salt species.

All of the correlation values were sorted to determine the best regions for modelling. For both species together, the g·gwater^{-1} concentration provided better correlation with the absorbance than the molarity over the majority of the wavelength range. Through sorting these values, it was determined that many of the highest correlation values were present in the NIR-A range (800 nm – 1400 nm). In addition to determining the best correlation, it was important to consider absorbance sensitivity in determining the best wavelength range to be used in modelling. The three

wavelengths with the highest correlation were 1353 nm, 1265 nm, and 1135 nm. These three wavelengths along with 953 nm, another high correlation wavelength, were compared to evaluate their relative sensitivity.

Figure 7-2 shows the linear relationship between the $g \cdot gwater^{-1}$ concentration and absorbance that is present at the chosen wavelengths. Using the $g \cdot gwater^{-1}$ concentration of the solutions allows for a generic relationship between absorbance and concentration of $NaCl_{(aq)}$ or $KCl_{(aq)}$. These correlations are valuable for analysis of dual-salt solutions as the $g \cdot gwater^{-1}$ concentration and molarity of the two salts can be combined to easily estimate the overall salinity of the solution. The slope magnitude represents the relationship between the magnitude changes in absorbance and the salt concentration. This indicates that (among these wavelengths) the absorbance is most sensitive to changes in salt concentration at 1353 nm as this correlation has the highest slope magnitude.

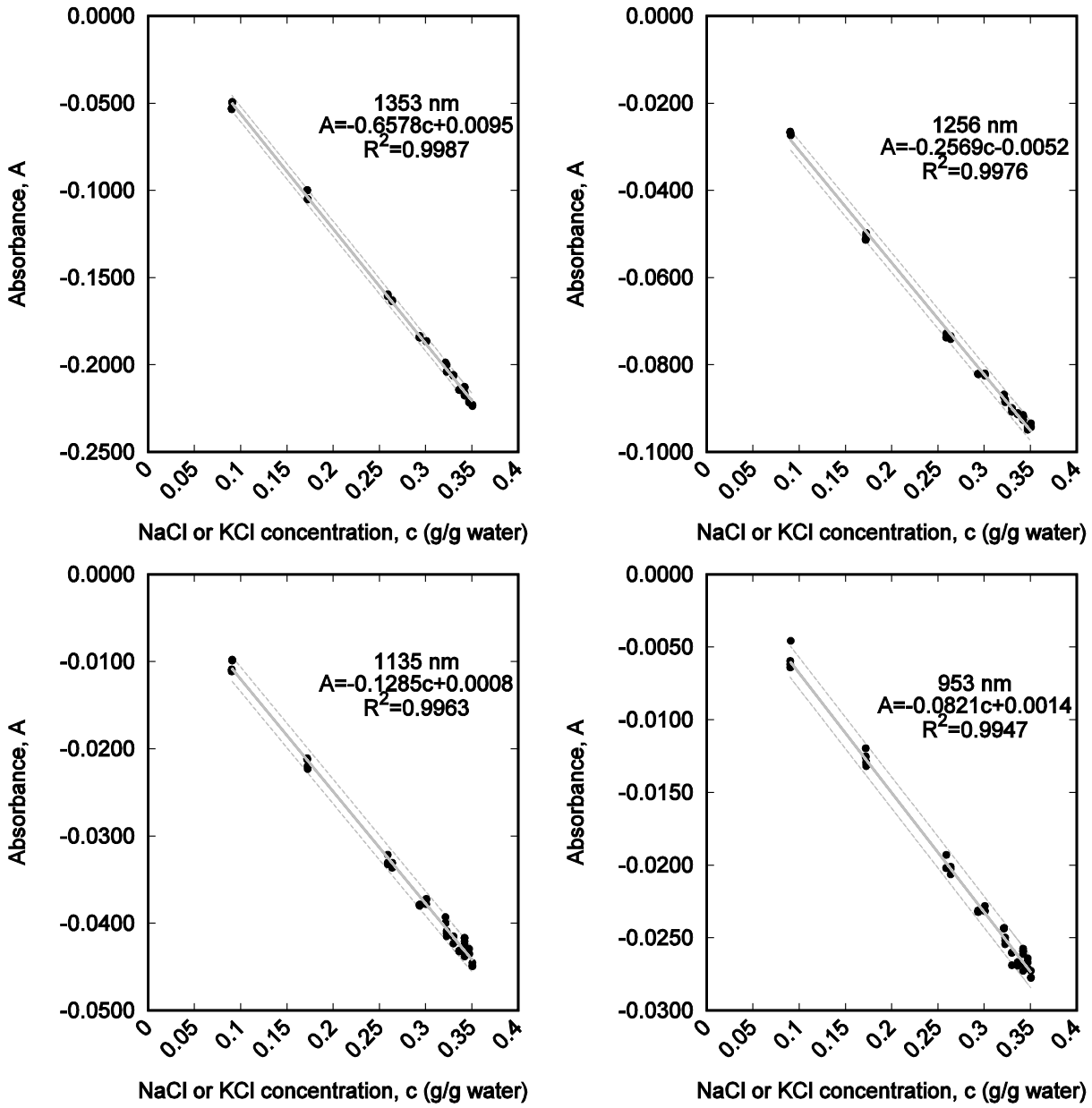

Figure 7-2: Linear relationship between g·gwater^{-1} concentration and absorbance for both $NaCl_{(aq)}$ and $KCl_{(aq)}$ at four wavelengths. Dotted lines represent 95% confidence intervals.

The molarity correlation values were also sorted to determine possible wavelengths of interest that could be used for modelling. The three best wavelengths that resulted from this sorting were 206 nm, 205 nm and 207 nm. Only the correlation for 206 nm is shown due to the similarities in these wavelengths. Other wavelengths with high correlation values included 1588 nm, 1768 nm, and 1674 nm. As with the g·gwater^{-1} concentration correlation, the sensitivities at these four wavelengths were compared.

Figure 7-3 summarizes the results for the molarity correlation at the chosen wavelengths. When comparing the magnitude of the slope, the UV wavelength shows the highest sensitivity. However, it is more difficult to obtain accurate measurements in this range (particularly for in-line applications) and the concentration-dependent wavelengths have absorbance values that are very high. These high values could decrease the accuracy and sensitivity of the model. At 1588 nm there is also high sensitivity, but this wavelength, along with 1768 nm, is at the edge of a strong water absorption band and has presented an issue with noise in the collected data. When comparing the two species as separate series, there is a clear (although minor) separation between the two salts at 1674 nm. The use of this wavelength is still possible as the correlation is high enough to get an estimate accurate enough for use in species differentiation. Once the salt is determined, a more accurate concentration could be back calculated using a linear relationship specific to the salt species.

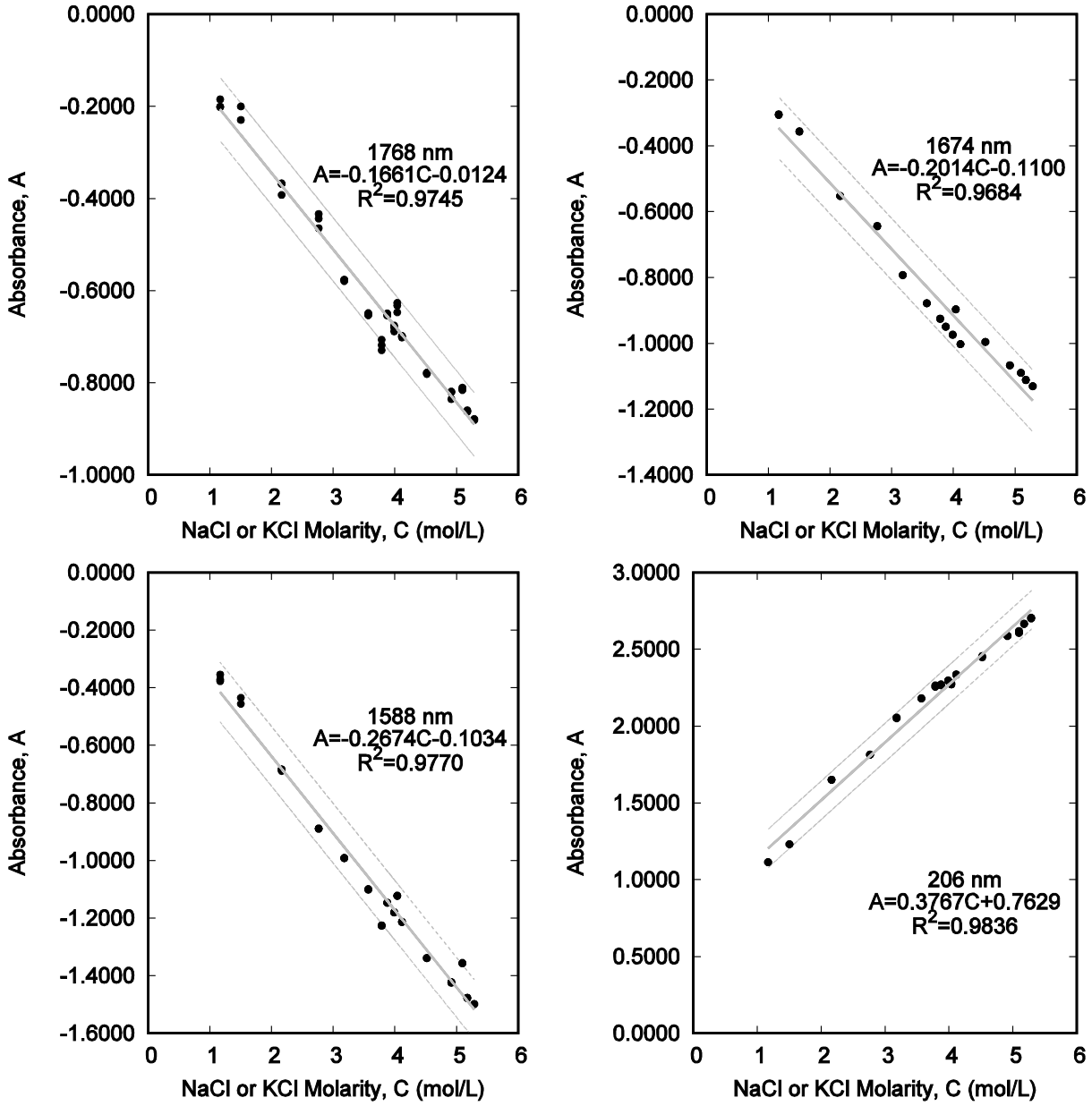

Figure 7-3: Linear relationship between molarity and absorbance for both $NaCl_{(aq)}$ and $KCl_{(aq)}$ at four wavelengths. Dotted lines represent 95% confidence intervals.

The sensitivities seen in Figure 7-2 and Figure 7-3 cannot be accurately compared using the slopes shown in the linear equations due to the differences in maximum molar and $g \cdot g water^{-1}$ concentrations. By observing absorbance range shown on each graph, it is clear that the wavelengths correlated with molarity have higher sensitivity to changes in concentration, but the sensitivity of 1353 nm was sufficient for modelling. Wavelengths that have a linear correlation with molarity do not necessarily have a linear correlation with $g \cdot g water^{-1}$ concentration and vice

versa. This is due to the different molar masses and maximum salinities of each salt. When comparing the absorbance at 1353 nm with molarity a linear trend is observed with individual salts. When the absorbance and molarities of both salts are used, however, the linear trend with molarity is not observed.

Regions which have good correlation between absorbance and concentration for individual salts but have poor correlation over both species may be good for species differentiation. The region between 1160 nm and 1230 nm fits these criteria. As with the overall salinity, the correlation values for $NaCl_{(aq)}$ and $KCl_{(aq)}$ were separately sorted to determine which wavelengths provided the best relationship between concentration and absorbance. Focus was placed on the 1160 nm to 1230 nm range to find wavelengths with good correlation that could be used for species determination. The wavelength that was found to have a high correlation between absorbance and $g \cdot gwater^{-1}$ concentration for both $NaCl_{(aq)}$ and $KCl_{(aq)}$ was 1210 nm. This wavelength provided a coefficient of determination of 0.9990 for $KCl_{(aq)}$ and 0.9966 for $NaCl_{(aq)}$ with only 0.7761 for both datasets. Using the molarity correlations, 1229 nm was found to have a coefficient of determination value of 0.9995 for $KCl_{(aq)}$ and 0.9993 for $NaCl_{(aq)}$. Due to the differences in maximum molar concentration between $NaCl_{(aq)}$ and $KCl_{(aq)}$, the intercept for line of best fit of the combined salts experienced an offset at 1229 nm. The zero-concentration intercept was set at the absorbance value for deionized water to correct this offset and a coefficient of determination of 0.7494 was found for both datasets. These results are summarized in Figure 7-4.

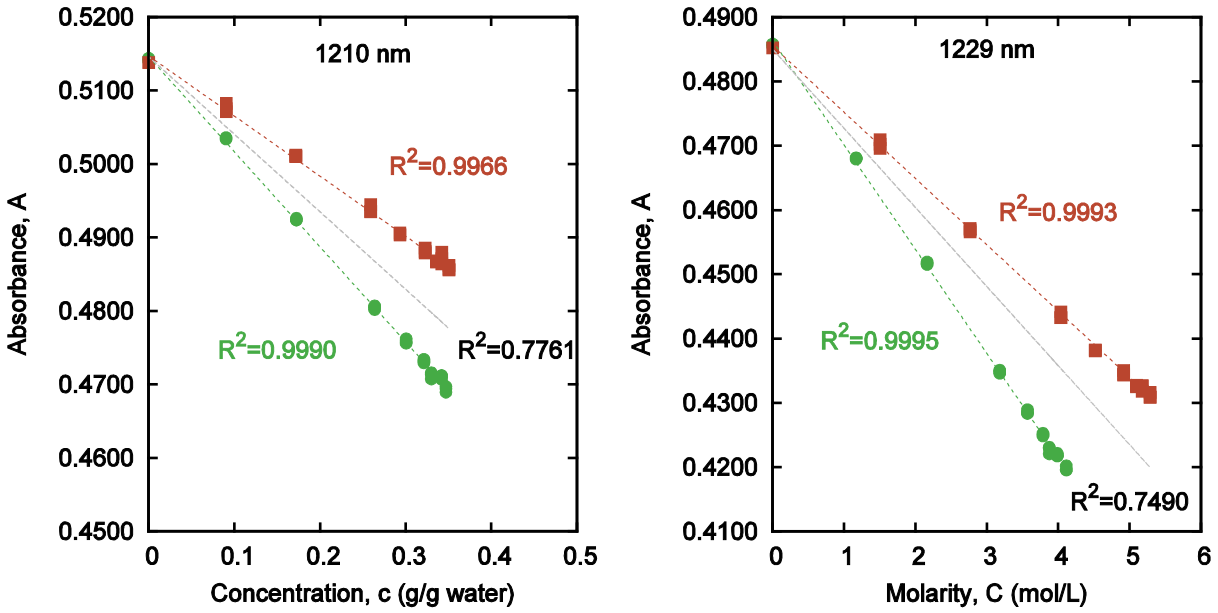

Figure 7-4: Correlations for single-salt samples and overall salinity: $NaCl_{(aq)}$ (orange squares), $KCl_{(aq)}$ (green circles), both series (grey line).

Comparing the eight wavelengths that were considered for overall salinity determination, the best correlation value was seen for 1353 nm with g·gwater^{-1} concentration. This wavelength also had the highest sensitivity and the absorbance at this point was within the reasonable measurement capability of most spectrophotometers (between 1 and 2 absorbance units). These three criteria made 1353 nm a good option for overall salinity determination in modelling. For discriminating between $NaCl_{(aq)}$ and $KCl_{(aq)}$, the absorbance at 1210 nm and the g·gwater^{-1} concentration was used. A separate calculation for determining molarity was used with 1229 nm.

Three spectral measurements were taken for each concentration of $KCl_{(aq)}$ and $NaCl_{(aq)}$. The first two measurements were used to develop the equations used for species and concentration determination and the third was used to test the model.

The first step performed by the model was to determine the overall salinity using Equation 7-1. The absorbance value at 1353 nm was used in this equation. Using this calculated concentration, Equations 7-2 and 7-3 were used to generate expected absorbance values for both $NaCl_{(aq)}$ and $KCl_{(aq)}$ at 1210 nm. The actual absorbance value of the sample at 1210 nm was then compared to these expected absorbance values to determine which species was in the solution. An example comparison of expected and measured absorbance values is shown in Figure 7-5. The

species was identified based on the expected absorbance value that was the closest fit to the measured absorbance value. Once the salt species was identified, Equation 7-4 or 7-5 (for NaCl or KCl respectively) was used to determine the molarity of the solution. The complete model with all calculations can be found in Appendix B – Modelling at Constant Temperature.

$$Molality_{Overall} = -1.5622 * Absorption_{1353} + 2.2400 \quad 7\text{-}1$$

$$Absorption_{1210}^{NaCl} = -0.0811 * Molality_{overall} + 0.5145 \quad 7\text{-}2$$

$$Absorption_{1210}^{KCl} = -0.1282 * Molality_{overall} + 0.5144 \quad 7\text{-}3$$

$$Molarity_{NaCl} = -96.525 * Absorption_{1229} + 46.869 \quad 7\text{-}4$$

$$Molarity_{KCl} = -62.150 * Absorption_{1229} + 30.209 \quad 7\text{-}5$$

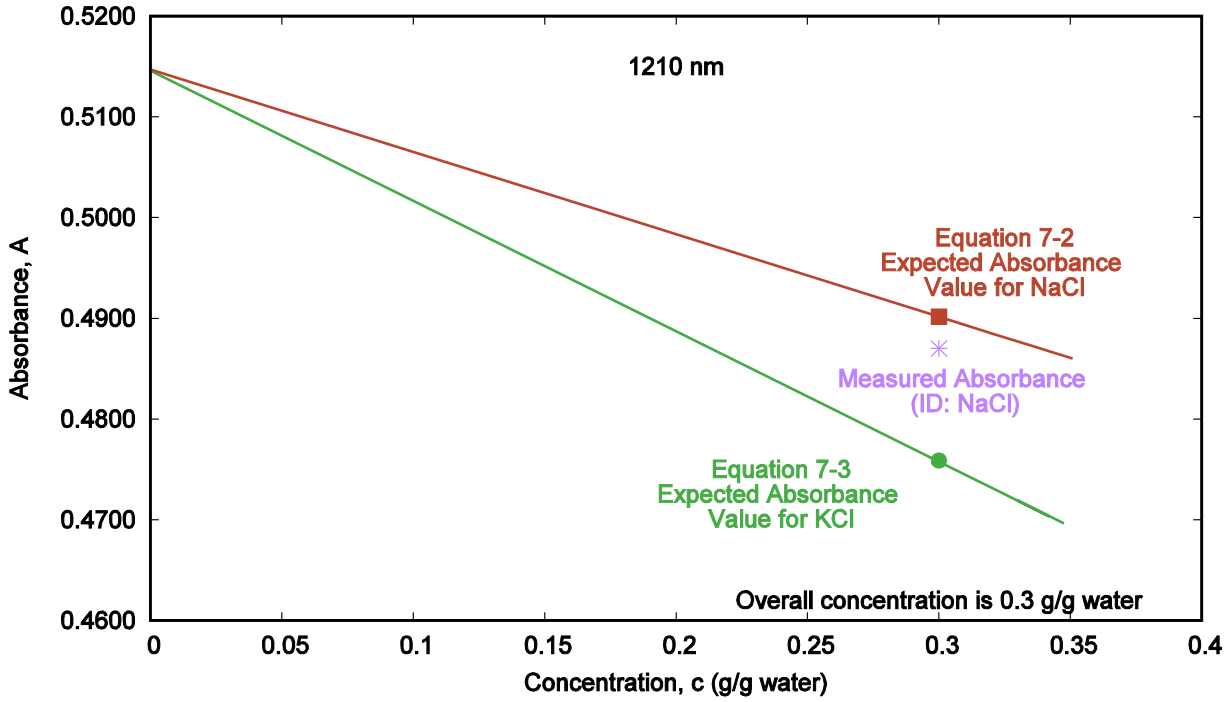

Figure 7-5: Sample comparison between measured absorbance value (purple star) and the expected absorbance values for $NaCl_{(aq)}$ (orange square) and $KCl_{(aq)}$ (green circle).

7.1.1 Model Testing: Single-Salt Solutions at Constant Temperature

Modelling single-salt solutions required a simple classification of speciation followed by a calculation to determine concentration of the resulting species. For the range of samples tested (between 25% of the maximum salinity and complete saturation) the model correctly identified the salt species in all cases. If the model found that the salinity of any given solution was less than 3%

of the maximum salinity, it would assume the sample to be pure water. This specification limited the sensitivity of the model to samples which had a salinity higher than 3% maximum saturation at 20°C or 0.16 mole per liter for $NaCl_{(aq)}$ and 0.13 mole per liter for $KCl_{(aq)}$. In the potash industry brine samples are almost always at or near saturation so for use in a potash process stream this level of sensitivity is sufficient.

The results from modelling at constant temperature are summarized in Table 7-1. Error values were calculated on a concentration range basis (excluding the water sample). The best average error between actual and modeled salinity achieved by the model was 0.9% for molarity at 1229 nm. The errors with the $g \cdot g_{water}^{-1}$ concentration were also low having an average of 1.7% and 1.4% for 1210 nm and 1353 nm (overall determination) respectively. The maximum errors in each category were 3.5%, 6.4%, and 3.1% for 1229 nm, 1210 nm, and 1353 nm respectively.

Table 7-1: Preliminary single-salt model results at constant temperature.

Sample Type	Model Type	Sample Molarity (mol/L)	Model Molarity (1229 nm) (mol/L)	%Error	Sample Concentration (g/100gwater)	Model Concentration (1210 nm) (g/100gwater)	%Error	Model Concentration[¥] (1353 nm) (g/100gwater)	%Error
Water	Water	0.000	0.035	1.0	0.000	0.930	3.6	0.772	3.0
Water	Water	0.000	-0.024	0.7	0.000	0.201	0.8	0.618	2.4
NaCl	NaCl	1.504 ± 0.001	1.479[‡]	0.7	9.077 ± 0.001	8.614[†]	1.8	8.526	2.1
NaCl	NaCl	2.765 ± 0.002	2.771[‡]	0.2	17.188 ± 0.001	16.389[†]	3.1	16.376	3.1
NaCl	NaCl	4.039 ± 0.004	4.082[‡]	1.1	25.901 ± 0.002	25.806[†]	0.4	25.780	0.5
NaCl	NaCl	4.520 ± 0.005	4.582[‡]	1.6	29.349 ± 0.002	29.336[†]	0.0	29.373	0.1
NaCl	NaCl	4.916 ± 0.005	4.881[‡]	0.9	32.257 ± 0.002	31.869[†]	1.5	32.544	1.1
NaCl	NaCl	5.095 ± 0.005	5.101[‡]	0.1	33.624 ± 0.002	34.102[†]	1.8	34.157	2.1
NaCl	NaCl	5.176 ± 0.005	5.111[‡]	1.7	34.217 ± 0.002	32.561[†]	6.4	34.546	1.3
NaCl	NaCl	1.504 ± 0.001	5.278[‡]	0.2	35.048 ± 0.002	35.440[†]	1.5	35.515	1.8
KCl	KCl	1.169 ± 0.001	1.128[§]	1.4	9.031 ± 0.001	8.607[◊]	1.7	9.048	0.1
KCl	KCl	2.164 ± 0.002	2.147[§]	0.6	17.251 ± 0.001	17.170[◊]	0.3	17.104	0.6
KCl	KCl	3.181 ± 0.003	3.198[§]	0.6	26.385 ± 0.002	26.648[◊]	1.0	26.192	0.8
KCl	KCl	3.570 ± 0.004	3.578[§]	0.3	30.065 ± 0.002	30.045[◊]	0.1	29.766	1.2
KCl	KCl	3.786 ± 0.004	3.778[§]	0.3	32.137 ± 0.002	31.923[◊]	0.8	31.778	1.4
KCl	KCl	3.875 ± 0.004	3.978[§]	3.5	32.997 ± 0.002	33.993[◊]	3.9	32.728	1.0
KCl	KCl	3.989 ± 0.004	3.999[§]	0.4	34.202 ± 0.002	34.011[◊]	0.7	33.764	1.7
KCl	KCl	4.115 ± 0.004	4.131[§]	0.5	35.710 ± 0.002	35.015[◊]	1.2	35.097	1.5
Avg.	Err.			0.9%			1.7%		1.4%

[¥]From Equation 7-1
[†]From Equation 7-2
[◊]From Equation 7-3
[‡]From Equation 7-4
[§]From Equation 7-5

A scatter plot comparing actual and modeled values was generated for each wavelength of these three wavelengths as shown in Figure 7-6. All three scatter plots shown in Figure 7-6 indicate that the model is capable of predicting the salinity of $NaCl_{(aq)}$ and $KCl_{(aq)}$ solutions. Consistent with the average error values found for each wavelength, 1229 nm produces the best estimation with a coefficient of determination of 1.0000. Both 1353 nm and 1210 nm have good coefficients of determination as well with values of 0.9999 and 0.9998 respectively. The plot at 1210 nm indicates that samples with higher concentrations are more difficult to model accurately using this wavelength as there is greater deviation at this end. This reduction in accuracy does not appear to be present to the same degree when using 1229 nm or 1353 nm for concentration estimation. Although using 1210 nm to estimate concentration does not produce results that are as accurate as when using 1229 nm or 1353 nm, this wavelength still provides very important information regarding speciation of the sample.

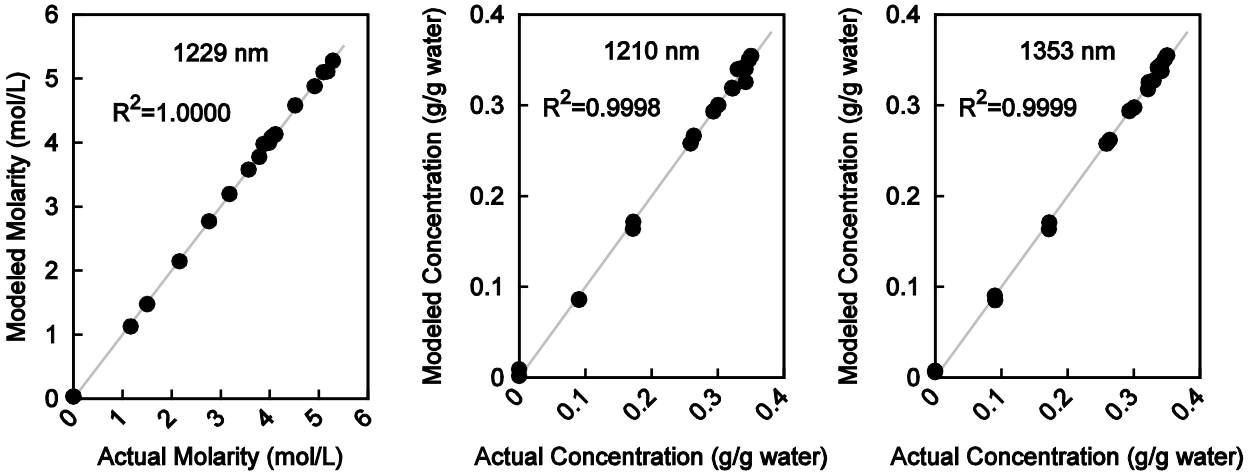

Figure 7-6: Scatter plot summary of single-salt model at 1229, 1210, and 1353 nm.

7.2 Model Development: Spectral Variation in Water with Temperature

Absorbance variations with temperature are different for pure water and salt water samples. Ideally, wavelengths that are dependent on temperature but independent of salinity could be used for modelling temperature effects. However, there is a large amount of overlap between the spectral effects of salinity and temperature and there were no suitable wavelengths between 180 nm and 1800 nm that fit this criterion. In order to limit the number of variables affecting the absorbance at the wavelengths chosen for temperature estimation, wavelengths that correlate with

overall salinity were examined. This reduced the number of degrees of freedom as both salts could be treated as one substance for the purposes of temperature variability. Table 7-2 summarizes the coefficients of determination and the absorbance sensitivity to changes in temperature at the eight wavelengths discussed for overall salinity at constant temperature. As denoted in the table with bold text, the correlations at 206 nm, 1588 nm, and 1768 nm are relatively low. These wavelengths were immediately rejected for use in temperature determination. The correlation values at 953 nm are high but the sensitivity at this wavelength is low. At 1135 nm and 1256 nm the sensitivity is improved slightly and the correlation values are high. The wavelength that provided the best correlation with $NaCl_{(aq)}$ and $KCl_{(aq)}$ g·g$water^{-1}$ concentration was 1353 nm. This wavelength had good temperature sensitivity, but the correlation values with temperature are lower than for some of the other wavelengths. The sensitivity at 1674 nm is high (in comparison to the other wavelengths) but as noted previously, there is some minor differences between $KCl_{(aq)}$ and $NaCl_{(aq)}$ at this wavelength.

Table 7-2: Coefficients of determination and sensitivity to changes in sample temperature for species-independent wavelengths. Correlations that were very low are denoted with bold text.

Wavelength	Water		50% $NaCl_{(aq)}$		50% $KCl_{(aq)}$	
	R^2	Sensitivity (Abs/°C)	R^2	Sensitivity (Abs/°C)	R^2	Sensitivity (Abs/°C)
206	**0.722**	0.00237	**0.885**	0.05648	0.915	0.05980
953	0.993	0.00089	0.996	0.00061	0.995	0.00065
1135	0.997	0.00102	1.000	0.00068	0.999	0.00072
1256	0.993	0.00134	0.999	0.00102	1.000	0.00104
1353	0.954	0.00421	0.982	0.00316	0.977	0.00328
1588	**0.514**	0.06453	0.998	0.01265	0.997	0.01415
1674	0.989	0.01259	1.000	0.00660	0.999	0.00769
1768	**0.441**	0.04446	0.988	0.01254	0.990	0.01331

The temperature variation for water was determined using the 1256 nm wavelength as this produced good correlation across both salts in solution and pure water, and had similar sensitivity with pure water and salt solutions. The linear relationship between temperature and absorbance at

1256 nm is described in Equation 7-6. Values were also calculated using 953 nm, 1135 nm, and 1674 nm for comparison.

$$Temperature_{water}(°C) = -794.87 * Absorption_{1256} + 379.06 \quad 7\text{-}6$$

As with the $NaCl_{(aq)}$ and $KCl_{(aq)}$ samples at constant temperature, three measurements were taken for each temperature of water (within +/-0.2°C). The first two measurements were used to develop Equation 7-6 and the third was used to test the model. This equation is only applicable for samples of water that do not contain salt. Similar equations could be developed for samples which contain $NaCl_{(aq)}$ and $KCl_{(aq)}$ as good correlation between temperature and absorbance at 1256 nm was also found for salt solutions as shown in Table 7-2. However, a single linear equation would not be effective for all salt concentrations as the absorbance at 1256 nm is also dependent on salt concentration as shown in Figure 6-18 and Figure 6-19. Developing a model to account for both salinity and temperature was out of the scope of this project but is a possible topic for future model development. The complete model for temperature determination of water samples with all calculations can be in Appendix C – Modelling Water between 15°C and 95°C.

7.2.1 Model Testing: Temperature Variation in Water

Four wavelengths were used in the temperature variation model. The actual and modeled temperature values are summarized in Table 7-3. Using the maximum +/- error values as comparison, the modeled temperatures using 1135 nm as reference produced the most accurate results with a maximum deviation of 1.4°C for all samples. The other wavelengths all produced results that were reasonably close to the measured values with maximum +/- error values of 1.7°C for 1256 nm, 2.4°C for 1674 nm and 3.0°C for 953 nm. Using an average of all estimated temperature values was considered, however the results were not accurate as using 1135 nm exclusively. The equation used for the standard error of the estimates is shown in Appendix A – Additional Calculations, Equation A-15.

Table 7-3: Preliminary model results for temperature variation in deionized water.

Actual Temperature	Modeled Temperatures at Wavelengths (°C)			
(°C)	1256 nm	1674 nm	953 nm	1135 nm
15.6	14.3	14.1	13.7	14.6
20.4	19.9	19.8	19.4	19.9
25.5	23.8	25.1	24.9	26.9
30.1	30.8	30.9	30.8	30.1
40.0	41.1	41.2	41.6	39.9
50.0	51.5	51.4	52.0	50.1
60.2	61.5	61.4	62.6	60.5
70.2	71.1	70.7	72.5	70.6
81.4	79.9	79.0	81.7	80.2
90.4	90.0	91.0	88.9	90.9
95.1	93.8	94.6	92.1	94.9
Max +/- Error (°C)	1.7	2.4	3.0	1.4
Std. Error of Est. (°C)	1.3	1.3	2.0	0.8

Figure 7-7 shows the differences between actual temperature of the water and that which the model has estimated. All of the measurements follow a trend where the lower temperature samples and the higher temperature samples are all estimated lower than the actual temperature and the samples in the middle of the sample range are all estimated higher than the actual temperature. This would indicate that the relationship between temperature and the absorbance used in the model is not perfectly linear. Despite this finding, the model was able to predict the temperature of the sample using absorbance values to within +/- 1.4°C at 1135 nm between 15°C and 95°C.

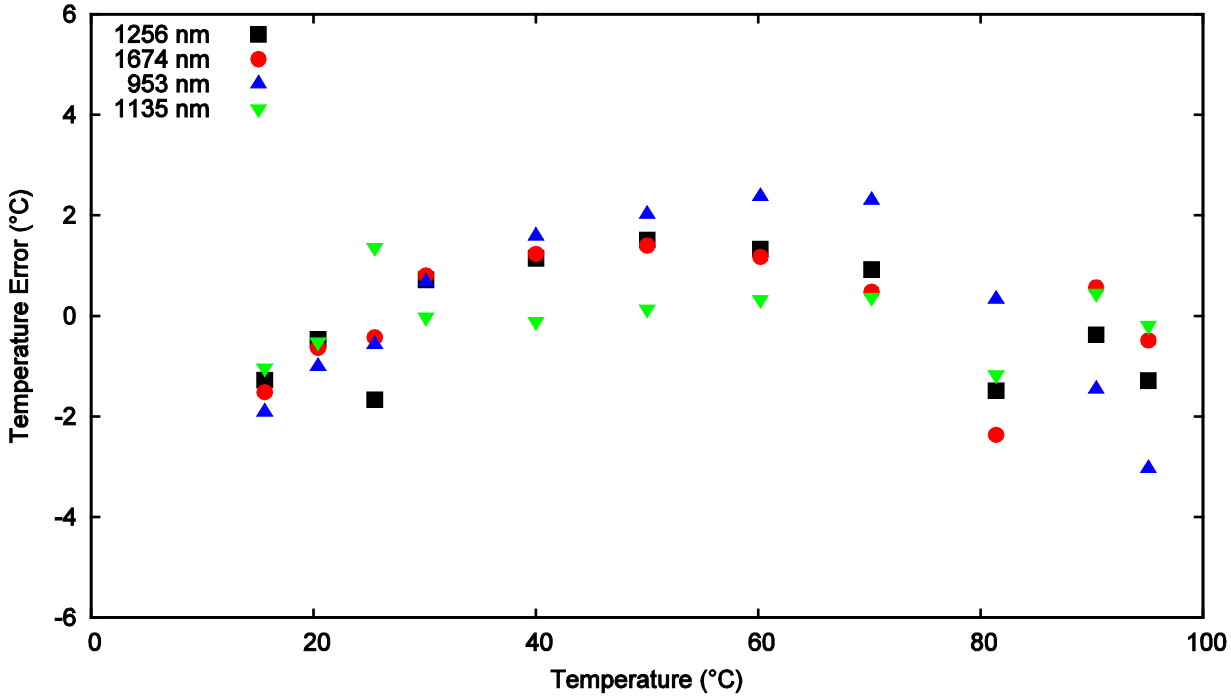

Figure 7-7: Difference error in modelling temperature variation.

7.3 Model Development: Two-Salt Solutions at Constant Temperature

When $NaCl_{(aq)}$ and $KCl_{(aq)}$ are both in solution, the chloride ions from both species have a summative effect on the absorbance for the wavelengths sensitive to chloride concentration. This allows for the overall molarity and $g \cdot g_{water}^{-1}$ concentration calculations that were developed for single-salt solutions to be used effectively for mixtures as well. Figure 7-8 and Figure 7-9 show the $g \cdot g_{water}^{-1}$ concentration and molarity trends at 1353 nm and 1674 nm respectively with both single-salt solutions and dual-salt solutions.

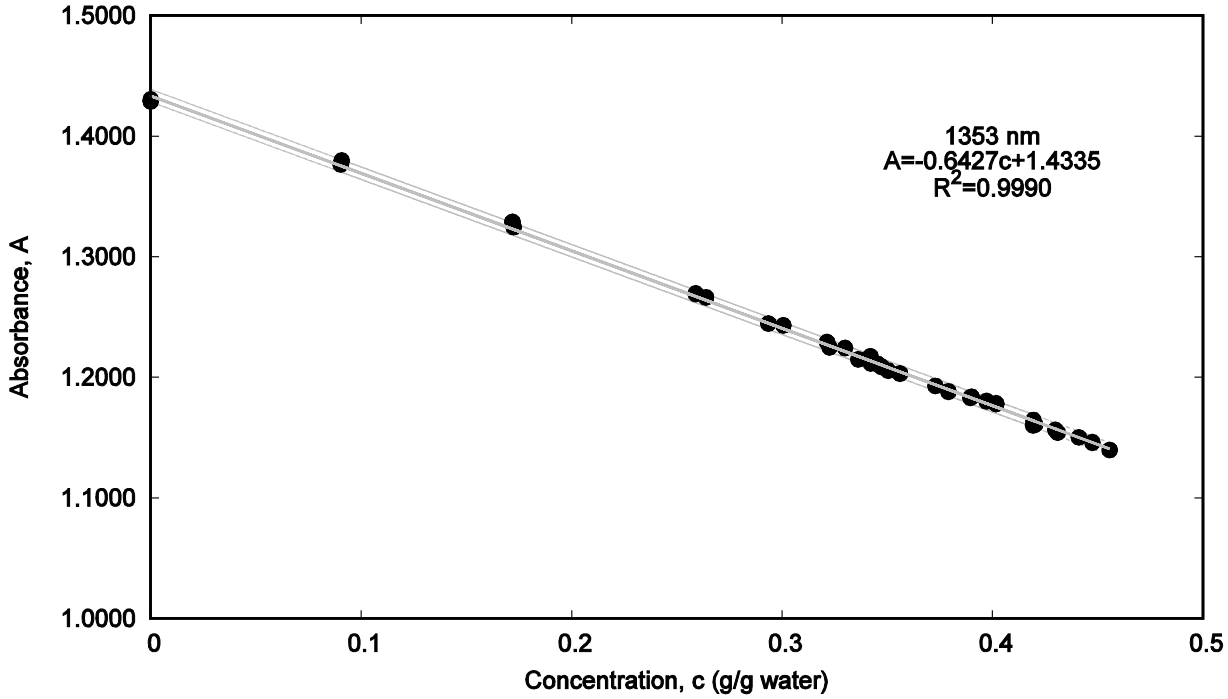

Figure 7-8: Concentration ($g \cdot g_{water}^{-1}$) with dual-salt samples and single-salt samples at 1353 nm. Dotted lines represent 95% confidence intervals.

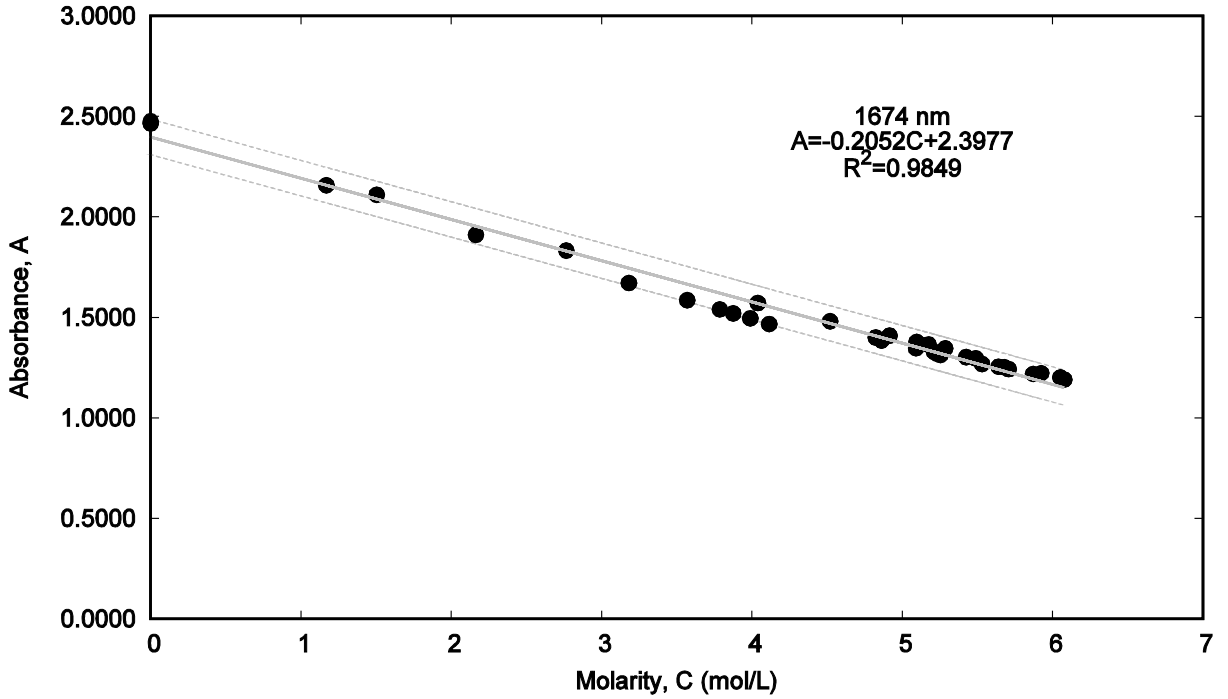

Figure 7-9: Molarity with dual-salt samples and single-salt samples at 1674 nm. Dotted lines represent 95% confidence intervals.

Similarly, the wavelengths that were effective for differentiating between $NaCl_{(aq)}$ and $KCl_{(aq)}$ in single-salt solutions can be effective in determining concentration of each salt in dual-salt solutions. Figure 7-10 shows the linear trend between absorbance and concentration for $NaCl_{(aq)}$ and $KCl_{(aq)}$ separately at 1210 nm.

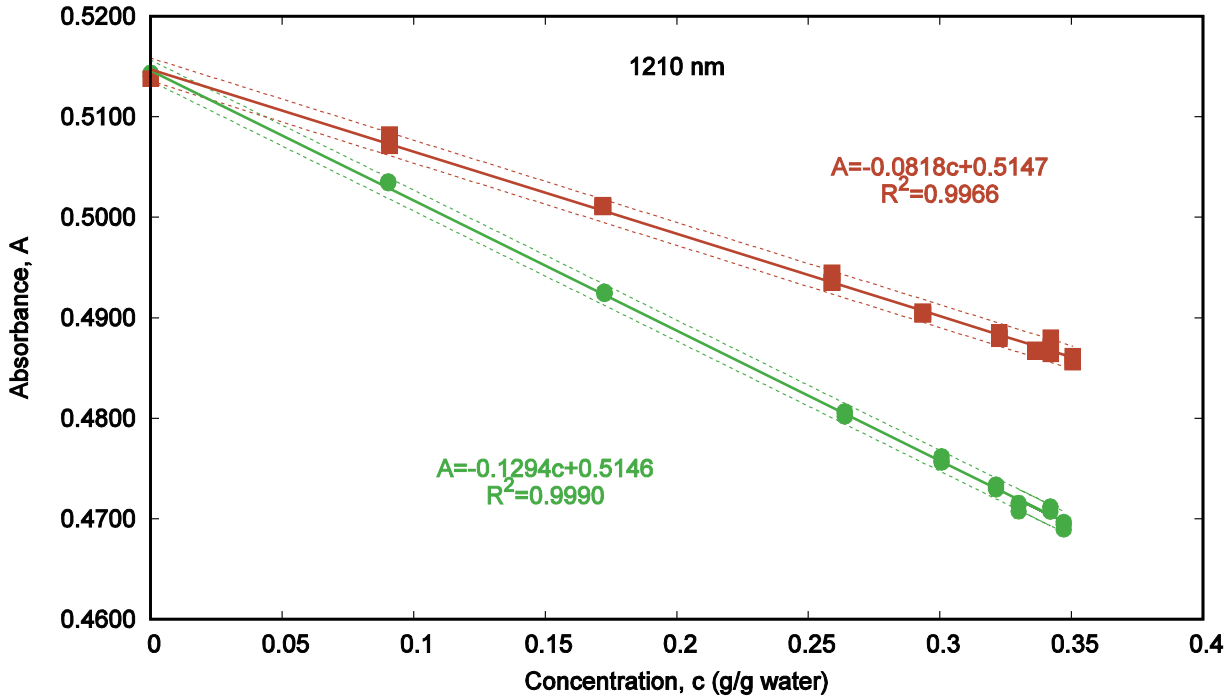

Figure 7-10: Absorbance trend differences for $NaCl_{(aq)}$ (orange squares) and $KCl_{(aq)}$ (green circles) at 1210 nm. Dotted lines represent 95% confidence intervals.

Two models were developed for determining the concentrations of $NaCl_{(aq)}$ and $KCl_{(aq)}$ in mixed-salt solutions. One used a single-wavelength comparison and the other used a dual-wavelength comparison.

7.3.1 Single-Wavelength Comparison

The first model developed for determining concentrations of $NaCl_{(aq)}$ and $KCl_{(aq)}$ mixtures used two wavelengths for overall salinity determination and six different wavelengths for species differentiation. Half of these wavelengths were correlated with the $g \cdot g_{water}^{-1}$ concentration and half were correlated with molarity. Overall $g \cdot g_{water}^{-1}$ concentration was determined using the linear relationship at 1353 nm and the $g \cdot g_{water}^{-1}$ concentration of individual species was calculated using 1210 nm, 1218 nm, and 1203 nm. For overall molarity, 1674 nm was used and 1229 nm, 1322 nm, and 1748 nm were used to determine the molarity of individual salt species. The species

specific wavelengths were chosen based on their high correlations with individual species and relative low correlations with overall salinity. Similar to the single-salt model, this model was calibrated using two of the three measurements taken for each single-salt sample as well as the dual-salt samples.

This model worked in a similar way to the single-salt model. Equation 7-1 was used to determine the overall g·gwater^{-1} concentration of the sample and Equation 7-7 was used to determine the overall molarity of the sample.

$$Molarity_{Overall} = -4.8742 * Absorption_{1674} + 11.6869 \quad 7\text{-}7$$

Once this value was determined, expected absorbance values at each of the species differentiation wavelengths were calculated. These expected absorbance values were determined based on the correlations for single-salt solutions so for each wavelength, two expected absorbance values were calculated as shown in Equation 7-2 for $NaCl_{(aq)}$ and Equation 7-3 for $KCl_{(aq)}$ at 1210 nm. The measured absorbance value at each of the specified wavelengths was then compared to the two expected values. A linear gradient was used to determine the concentration of both $NaCl_{(aq)}$ and $KCl_{(aq)}$ in the solution by comparing the measured absorbance value to the two expected values. A sample equation is shown in Equation 7-8 and Equation 7-9 for $NaCl_{(aq)}$ and $KCl_{(aq)}$ respectively. Separate estimates were performed for each of the six wavelengths.

$$Molality^{NaCl} = \frac{\left|Absorption_{1210}^{Sample} - Absorption_{1210}^{KCl}\right|}{\left|Absorption_{1210}^{NaCl} - Absorption_{1210}^{KCl}\right|} * Molality^{overall} \quad 7\text{-}8$$

$$Molality^{KCl} = \frac{\left|Absorption_{1210}^{Sample} - Absorption_{1210}^{NaCl}\right|}{\left|Absorption_{1210}^{NaCl} - Absorption_{1210}^{KCl}\right|} * Molality^{overall} \quad 7\text{-}9$$

Once the model had determined three molarity and three g·gwater^{-1} values, each value was converted from molarity to g·gwater^{-1} and vice versa using Equation 7-10 and Equation 7-11 for $NaCl_{(aq)}$ and $KCl_{(aq)}$ respectively. This conversion's linear correlation is shown in Figure 7-11.

$$Molality^{NaCl} = 0.0672 * Molarity^{NaCl} + 0.0004 \quad 7\text{-}10$$

$$Molality^{KCl} = 0.0849 * Molarity^{KCl} + 0.0009 \quad 7\text{-}11$$

With each value converted, six values for molarity and six values for g·gwater^{-1} were obtained. These values were then averaged and sorted based on their relative similarities. The five values that were closest to the average were then used to calculate a new average allowing for an outlying estimate to be excluded from the final calculation. The full model can be found in Appendix D – Modelling Mixed Salts Using Single-Wavelength Comparisons.

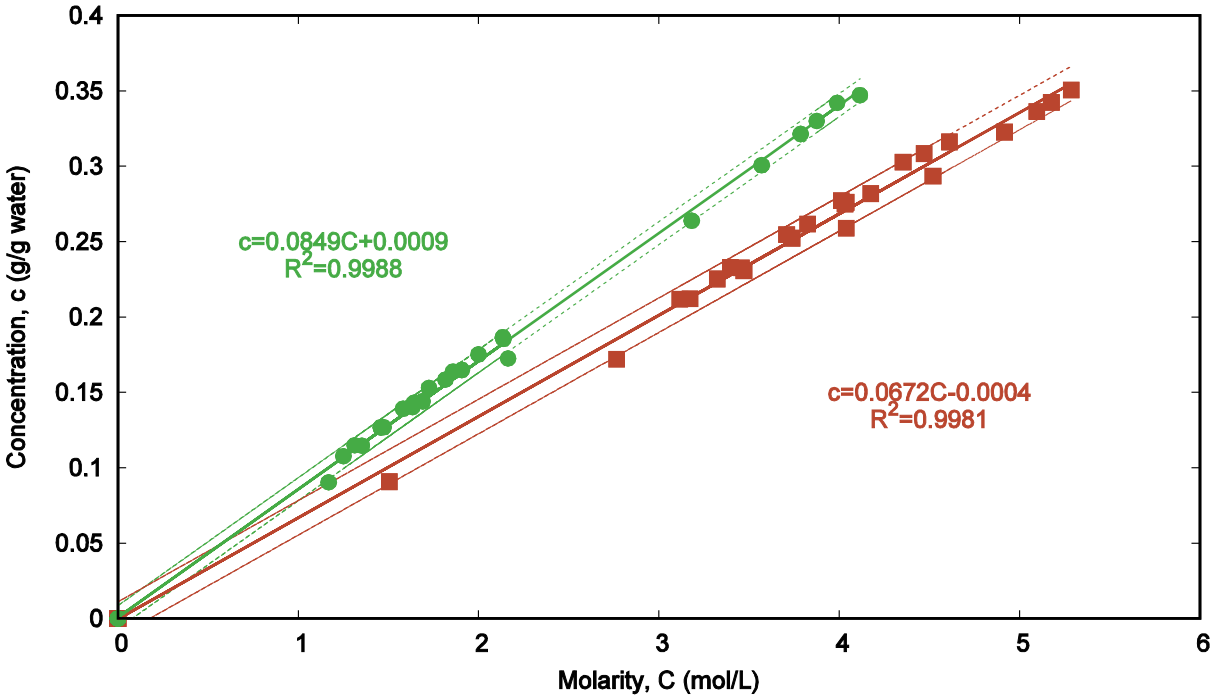

Figure 7-11: Conversion between molarity and g·gwater^{-1} for $NaCl_{(aq)}$ (orange squares) and $KCl_{(aq)}$ (green circles). Dotted lines represent 95% confidence intervals.

This model outputs six variables. The total and individual species molarities and the total and individual species concentrations in g·gwater^{-1} are all determined. Preliminary results for this model are summarized in Table 7-4. Percent errors were calculated based on the range of concentrations of all samples. The equation used for the standard error of estimate can be found in Appendix A – Additional Calculations, Equation A-16. The average errors indicate that this model can provide a rough estimate for $NaCl_{(aq)}$ and $KCl_{(aq)}$ concentrations. The capabilities of this model will be further investigated in section 7.4 Model Testing: Two-Salt Solutions at Constant Temperature.

Table 7-4: Preliminary mixed-salt model results for the single-wavelength comparison model.

Feature	Average Error %	Standard Error of Estimate
NaCl Molarity	7.0	0.375 mol/L
KCl Molarity	6.2	0.227 mol/L
Total Molarity	3.0	0.206 mol/L
NaCl $g \cdot g_{water}^{-1}$	6.4	2.468 g/100 g water
KCl $g \cdot g_{water}^{-1}$	5.8	1.834 g/100 g water
Total $g \cdot g_{water}^{-1}$	0.8	0.363 g/100 g water

7.3.2 Dual-Wavelength Comparison

The second model developed for determining $KCl_{(aq)}$ and $NaCl_{(aq)}$ concentrations in solution used one wavelength for overall $g \cdot g_{water}^{-1}$ determination and two wavelengths for species differentiation, one for NaCl, and one for KCl. This model used spectra with the water absorbance removed by subtraction. For overall salinity determination, the linear trend with $g \cdot g_{water}^{-1}$ concentration at 1353 was used as shown in Equation 7-12. This linear trend was developed using only single-salt solutions with the water spectrum subtracted to fit with the data sent to the model.

$$Molality_{Overall} = -1.5189 * Absorption_{1353} + 0.0146 \quad 7\text{-}12$$

Once the total salt content was determined, the entire spectra were normalized by the absorbance value at 1353 nm. This step highlights the wavelengths that are linearly dependent on individual salt concentrations. Figure 7-12 shows the differences between $NaCl_{(aq)}$ and $KCl_{(aq)}$ samples when this step is performed. Because 1353 nm is a concentration dependent wavelength, all other concentration dependent wavelengths are normalized to values which are similar across all of the spectra. This step also reduces any measurement offset present in the spectrum.

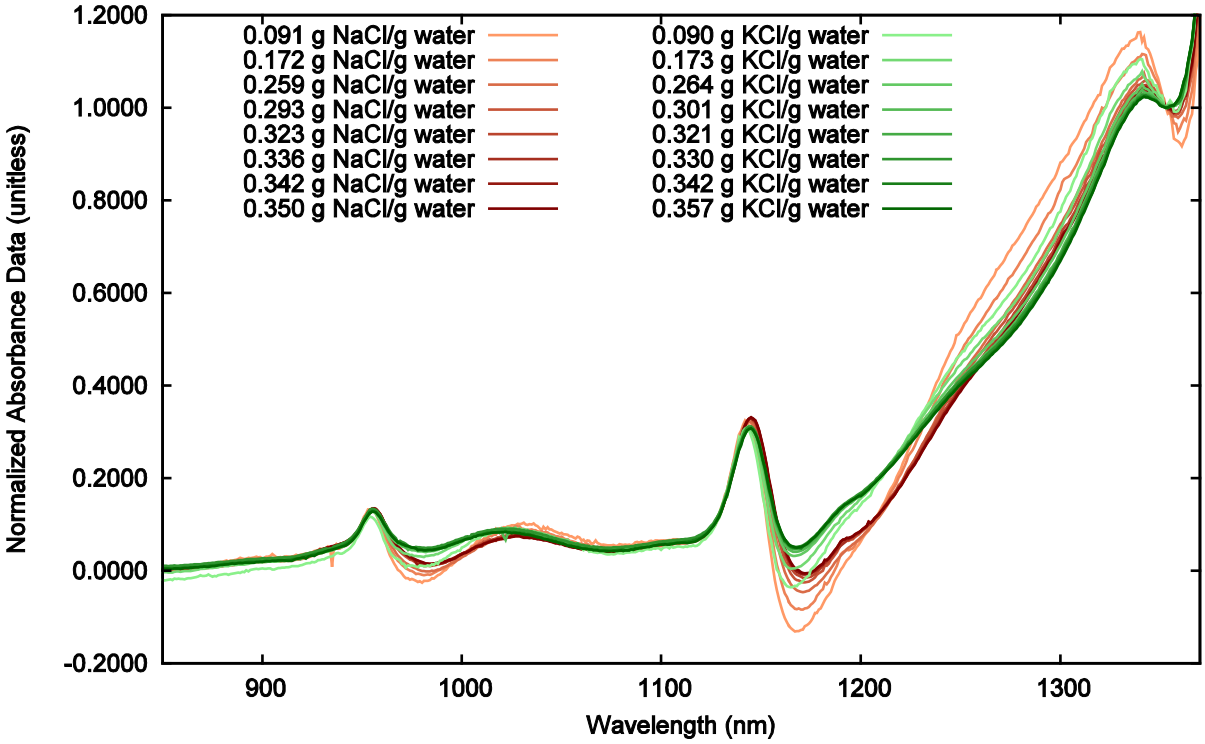

Figure 7-12: Pure $NaCl_{(aq)}$ and $KCl_{(aq)}$ spectra normalized at 1353 nm through the concentration range after subtraction of the water spectrum.

For species determination the wavelengths that had the least deviation in the normalized spectra were selected as shown in Figure 7-13. For NaCl, 1209 nm was chosen and for KCl, 1213 nm was chosen. The average absorbance values at these points for all single-salt calibration spectra were used in the dual-wavelength model. All pure $NaCl_{(aq)}$ samples had an average value of 0.12058 ± 0.00025 at 1209 nm and all pure $KCl_{(aq)}$ samples had an average value of 0.21988 ± 0.00025 at 1213 nm in the normalized spectra.

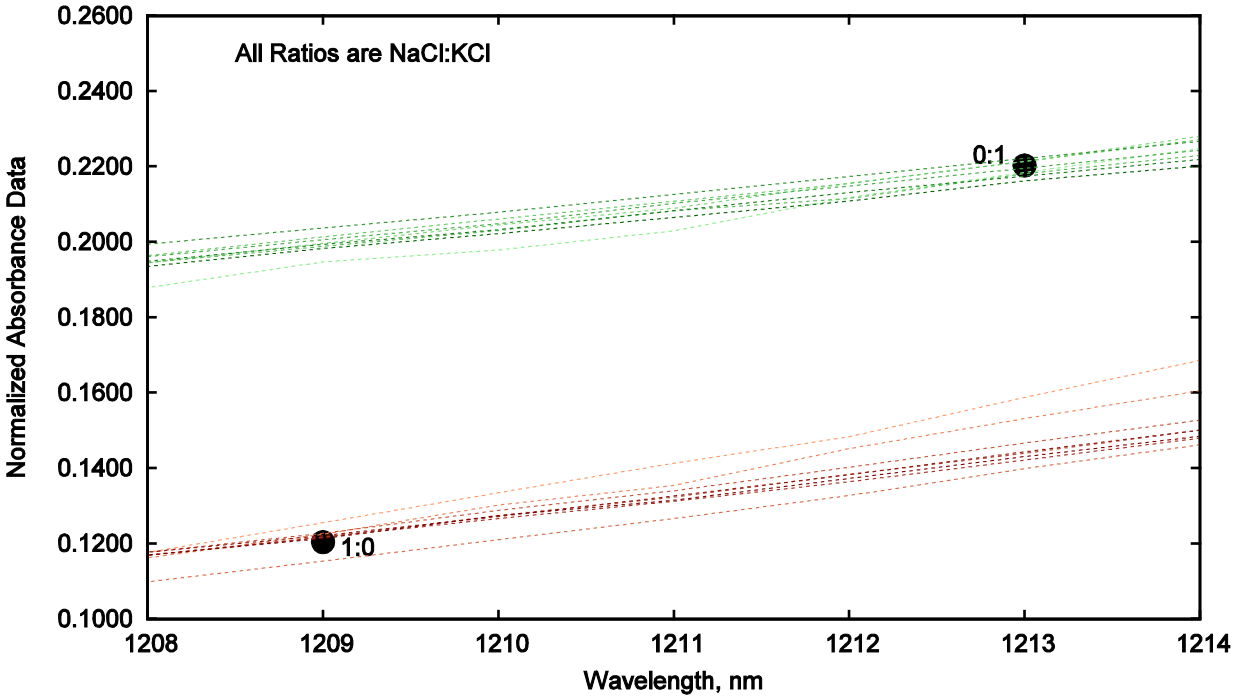

Figure 7-13: All single-salt species used for model calibration in dual-wavelength model. All ratios are NaCl:KCl. Dotted lines represent normalized (at 1353 nm) spectra.

Using the average absorbance at 1209 nm for NaCl and the average absorbance at 1213 nm for KCl, as endpoints a model calibration line was developed. This calibration line is shown as the grey line in Figure 7-14. For each sample of unknown composition (shown as the purple line in Figure 7-14), the equation of the sample line between 1209 and 1213 nm was calculated. The point of intersection of the calibration line and the sample line indicated the ratio of $NaCl_{(aq)}$ and $KCl_{(aq)}$ in the sample. This ratio was used with the overall g·gwater^{-1} concentration to determine individual $NaCl_{(aq)}$ and $KCl_{(aq)}$ concentrations. In the case that the sample was a single-salt solution, one of the points used to develop the sample line would lie at the 100% NaCl or 100% KCl point causing the lines to intersect at that point. Once the g·gwater^{-1} concentration of the individual salts was determined, their concentrations were converted to molarity using the relationships described in Equation 7-10 and Equation 7-11 and the total molarity was found by summing these values. On a few occasions during testing, the model returned a negative concentration value for one of the salt species. If this was the case, the model would set the concentration of the negative value salt to zero and read the overall g·gwater^{-1} equal to the g·gwater^{-1} of the non-zero salt. The full model

with all calculations can be found in Appendix E – Modelling Mixed Salts Using Dual-Wavelength Comparisons.

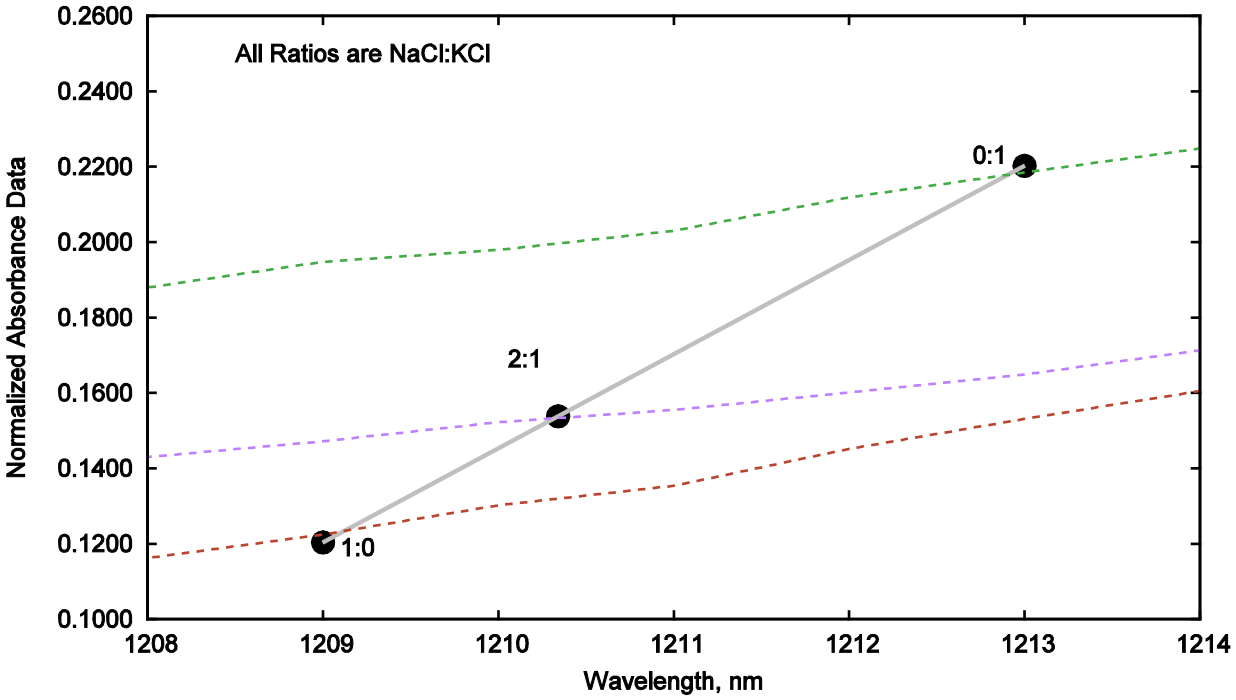

Figure 7-14: Dual-wavelength comparison for species determination. All ratios are NaCl:KCl. The grey solid line indicates the calibration line. Dotted lines represent normalized (at 1353 nm) spectra for various samples.

For the testing set, one measurement from each single-salt sample spectrum was used and all three sets of scans for the mixtures were available. None of the mixture spectra were used in model calibration so they could all effectively be used to test the model. However, for comparison with the single-wavelength model, the same test set was used to generate preliminary results. These results for this model are summarized in Table 7-5. The equation used for the standard error of estimate can be found in Appendix A – Additional Calculations, Equation A-16. Compared to the single-wavelength model, this model performed better on average for all six features.

Table 7-5: Preliminary mixed-salt model results for the dual-wavelength comparison model.

Feature	Average Error %	Standard Error of Estimate
NaCl Molarity	3.0	0.151 mol/L
KCl Molarity	3.4	0.136 mol/L
Total Molarity	2.4	0.156 mol/L
NaCl g·gwater^{-1}	2.1	0.768 g/100 g water
KCl g·gwater^{-1}	2.2	0.779 g/100 g water
Total g·gwater^{-1}	0.5	0.280 g/100 g water

7.4 Model Testing: Two-Salt Solutions at Constant Temperature

Modelling dual-salt solutions resulted in six output variables: NaCl molarity, KCl molarity, overall molarity, NaCl g·gwater^{-1}, KCl g·gwater^{-1}, and overall g·gwater^{-1}. Due to the different methods of development for the two-salt models, the testing data sets available to each model were different. For comparison purposes, a set of 32 samples was chosen that could be used by both models for testing. Further testing was done on the dual-wavelength model to include an additional 32 samples.

7.4.1 Single-Wavelength Comparison

The single-wavelength comparison model produced average error percentages between 0.8% and 7.0% for the six output variable. Separate scatter plots showing actual and estimated values for each variable are shown in Figure 7-15. For all output variables the coefficient of determination ranges between 0.9615 and 0.9986. The model was able to determine the overall g·gwater^{-1} concentration of the sample with the greatest accuracy and the scatter plot for this variable shows very good agreement between modeled and actual values.

In the KCl and NaCl plots, some modeled values are sitting along the y-axis. This is due to samples which only had one salt. In these cases, the model was not able to identify that only one salt was present in the solution so some of the estimated total salt content was attributed to the absent salt. This misidentification of salt was worse for samples which only contained KCl. The large variation in modeled molarity and g·gwater^{-1} concentration of $NaCl_{(aq)}$ in the $KCl_{(aq)}$-only samples also affect the estimation of the $KCl_{(aq)}$ in solution as the distribution is based on the overall g·gwater^{-1} concentration of the sample. For KCl molarity and g·gwater^{-1} concentration,

larger errors are noted at the high-concentration range. These errors correspond with the $KCl_{(aq)}$-only samples and are the result of the misidentification of $NaCl_{(aq)}$ in solution.

By inspecting the overall molarity scatter plot, there are a few samples that show noticeable deviation from the trend line but appear to be following their own linear path. These samples are also the KCl-only samples. This indicates that $KCl_{(aq)}$ may be presenting a non-additive absorbance feature at 1674 nm (used for overall molarity estimation) that was overlooked during modelling. The sensitivity of this model was the same as the single-salt model with a minimum value of 0.16 mole per liter for $NaCl_{(aq)}$ and 0.13 mole per liter for $KCl_{(aq)}$.

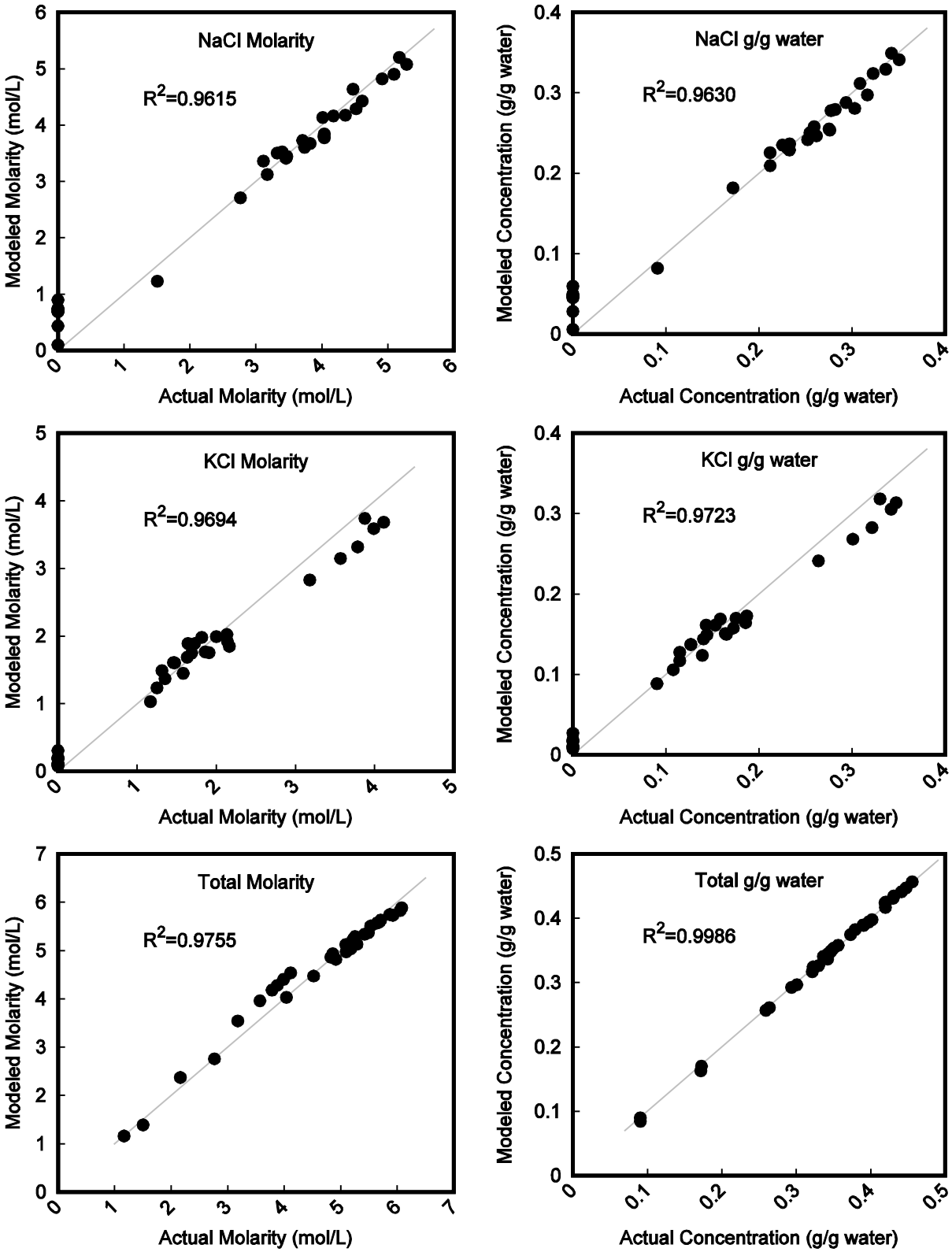

Figure 7-15: Scatter plots of the outputs from the single-wavelength comparison model. The grey line indicates the 1:1 line between actual and modeled values.

7.4.2 Dual-Wavelength Comparison

The dual-wavelength comparison model produced average error percentages between 0.5% and 3.4% for the six output variables. Similar to the results from the single-wavelength comparison model, separate scatter plots were produced for each variable as shown in Figure 7-16. These scatter plots were generated using the same 32 samples used for testing the single-wavelength model as well as an additional 32 samples of dual-salt solutions. For this model, the coefficients of determination were between 0.9790 and 0.9988 for all variables. The dual-wavelength model was best able to estimate the overall $g \cdot gwater^{-1}$ concentration.

A noticeable difference between the scatter plots generated from the dual-wavelength model and the single-wavelength model relates to the points found along the y-axis in the individual salt plots. With the single-wavelength model, there were a number of samples with high errors in $NaCl_{(aq)}$ and $KCl_{(aq)}$ estimations for single-salt samples. These errors are less prominent in the dual-wavelength model and the scatter plot shows this with the consistent grouping of modeled $g \cdot gwater^{-1}$ concentration and molarity values found along the y-axis. The ability of the dual-wavelength model to better identify single-salt solutions provides a major source of the improvement seen in this model. Correctly identifying these single-salt solutions also has a domino effect on the other variables as is seen in the high-concentration samples of $NaCl_{(aq)}$ and $KCl_{(aq)}$. With the single-wavelength model, a larger offset is seen in the scatter plots when the concentration of $KCl_{(aq)}$ is high. This increased error is not as prominent in the dual-wavelength model as the high-concentration points of $KCl_{(aq)}$ better follow the 1:1 trend shown in the plots.

The total molarity estimations found by the dual-wavelength model are result of the summation of the individual molarities for each salt. This method eliminates the possibility of incorrectly accounting for non-additive features that may be present between the two salt species. Although there are still samples with offsets that are similar to those found in the single-wavelength model, there does not appear to be a trend with a specific sample type in the dual-wavelength model.

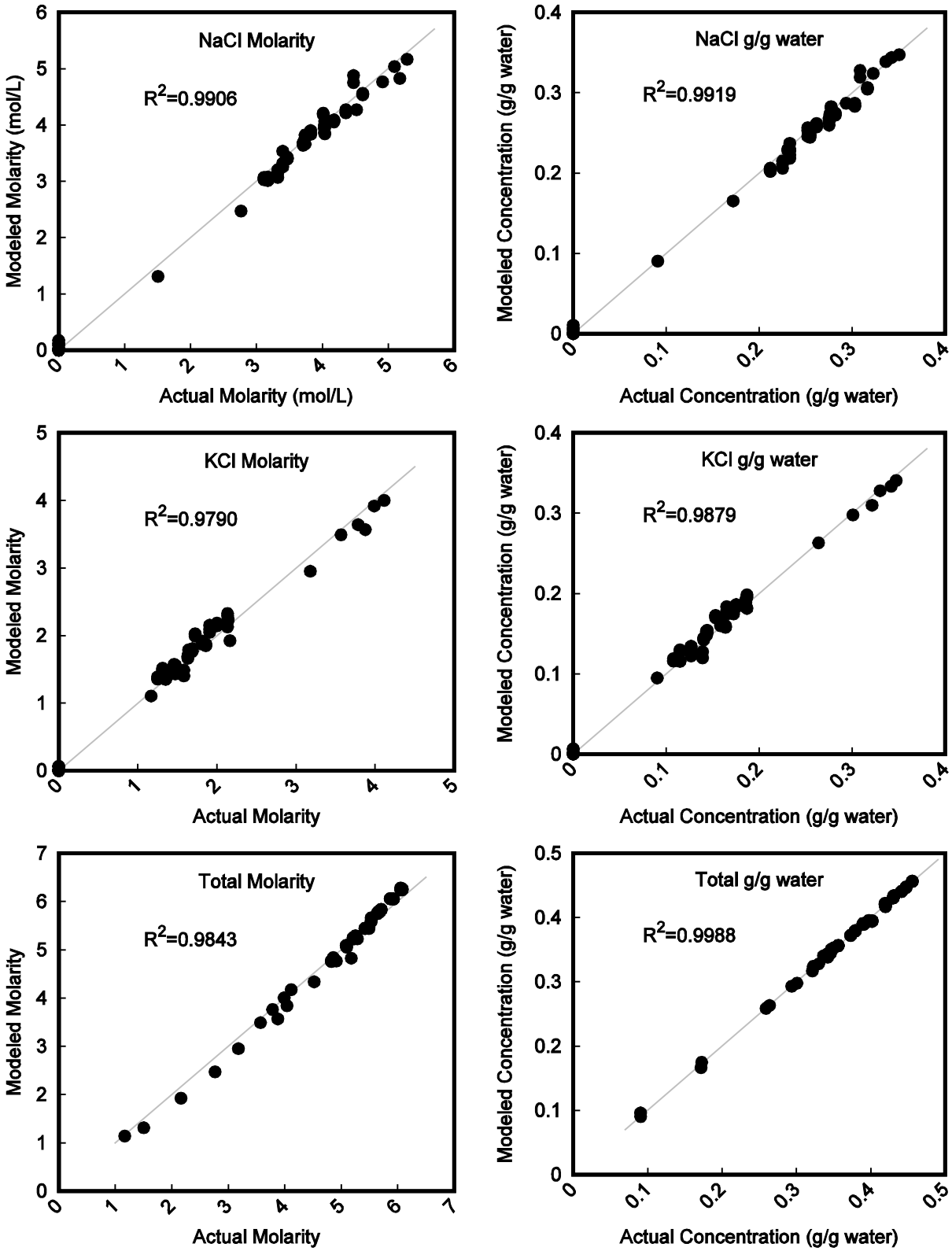

Figure 7-16: Scatter plots of the outputs from the dual-wavelength comparison model. The grey line indicates the 1:1 line between actual and modeled values.

7.4.3 Comparison of Single-Wavelength and Dual-Wavelength Models

Both dual-salt models were able to determine the concentrations of $NaCl_{(aq)}$ and $KCl_{(aq)}$ in solution with less than 7% average error. The dual-wavelength model performed better for all molarity and $g \cdot g_{water}^{-1}$ concentration measurements in metrics of average error and coefficients of determination. Using the same 32 samples as a test set, the single-wavelength model had an overall average error of 4.9% for all six output variables and the dual-wavelength model had an overall average error of 2.3%. A large portion of this improvement was due to the single-salt samples. The dual-wavelength model was better at differentiating between dual-salt and single-salt solutions and was able to better estimate the concentration of a single-salt solution as a result. Table 7-6 compares the results for both models using the same 32 samples for each model. In these 32 samples, 16 samples contained both $NaCl_{(aq)}$ and $KCl_{(aq)}$, 8 of the samples contained only $NaCl_{(aq)}$ and 8 of the samples contained only $KCl_{(aq)}$.

Table 7-6: Single-salt and dual-salt solution comparison for the single-wavelength and dual-wavelength models.

	Dual-Salt Solutions Error %		Single-Salt Solutions Error %	
Feature	Single-Wavelength Model	Dual-Wavelength Model	Single-Wavelength Model	Dual-Wavelength Model
NaCl Molarity	3.6	2.8	10.4	3.3
KCl Molarity	4.0	3.8	8.4	2.9
Total Molarity	1.8	1.6	4.2	3.1
NaCl $g \cdot g_{water}^{-1}$	3.7	3.2	9.1	1.1
KCl $g \cdot g_{water}^{-1}$	4.1	3.1	7.5	1.3
Total $g \cdot g_{water}^{-1}$	0.6	0.4	1.0	0.7

The dual-wavelength model performed better for both dual-salt solutions and single-salt solutions. However, the degree of improvement was much higher for samples that only contained one type of salt. The results summarized in Table 7-6 confirm that the dual-wavelength model performs better for dual-salt solutions and single-salt solutions. The dual-wavelength model also only requires measurement from three wavelengths in the absorbance spectrum between 1209 nm

and 1353 nm while the single-wavelength model requires measurements from eight wavelengths between 1203 nm to 1748 nm.

8 CONCLUSIONS

The use of spectroscopy for analyzing $NaCl_{(aq)}$ and $KCl_{(aq)}$ in solutions has been studied previously in the low concentration range, but extension to saturation and differentiation between the two species in solution has not been investigated extensively. The research presented in this work developed models for determining temperature of deionized water, differentiating between $NaCl_{(aq)}$ and $KCl_{(aq)}$ in single-salt solutions, and determining concentration of $NaCl_{(aq)}$ and $KCl_{(aq)}$ in dual-salt solutions all using spectral measurements in the near infrared range. A method for mitigating evaporation to obtain high-temperature absorbance data for salt solutions was also developed.

Modelling temperature of water solutions was performed using the absorbance of the sample at 1135 nm with maximum error values of +/-1.4°C between 15°C and 95°C. Differentiating between single-salt solutions resulted in 100% correct species identification that was sensitive to 0.16 mole per liter for $NaCl_{(aq)}$ and 0.13 mole per liter for $KCl_{(aq)}$. This model was able to determine the concentration of single-salt solutions with and average error of 0.9%. Mixed-salt samples were analyzed using two different models. The first model used single-wavelength comparisons at six different wavelengths to determine the speciation and concentration of the samples. This model was able to accurately estimate molarity and $g \cdot g_{water}^{-1}$ concentration for $NaCl_{(aq)}$, $KCl_{(aq)}$, and the overall salinity of the sample with an average of 7.0% error for the least accurate variable. The second model used a dual-wavelength comparison to determine speciation in the samples. This model was able to accurately estimate molarity and $g \cdot g_{water}^{-1}$ concentration for $NaCl_{(aq)}$, $KCl_{(aq)}$, and the overall salinity of the sample with an average of 3.4% error for the least accurate variable. When these two models were compared using the same test set, the single-wavelength model had an average error of 4.9% for all variables and the dual-wavelength model had an average error of 2.3% for all variables.

These models would be useful in estimating $NaCl_{(aq)}$ and $KCl_{(aq)}$ content for industrial purposes but only if the solutions do not contain other impurities. The effects of magnesium chloride are of particular interest for future work as this salt shares an ion with $NaCl_{(aq)}$ and $KCl_{(aq)}$ and will likely result in summative absorbance in some of the regions of interest discovered through this work. Other impurities such as iron and suspended particulates will also have effects on the absorbance spectrum and will have to be accounted for in future models.

Another limitation of these models is their inability to predict the temperature effect on salt-water samples. Determining the effect of temperature on samples with a wide variety of $NaCl_{(aq)}$ and $KCl_{(aq)}$ concentrations will be required if temperature control is not a possibility for in-line measurements. These temperature effect will also likely depend on the other impurities in the sample. In order to develop a model for determining these effects, the method of evaporation mitigation will need improvement so that implementation in saturated samples is feasible. Future work will focus on developing this method and subsequently collecting the required data for model development account for all of these interdependent variables. A final task that will be required before spectral measurements can successfully be used in an industrial setting for brine monitoring will include designing and testing an in-line apparatus.

9 REFERENCES

Abe, H. (2004). Estimation of heat capacity and properties of water by spectrum decomposition of the second overtone band of OH stretching vibration. *Journal of Near Infrared Spectroscopy, 12*(1), 45-54.

Amo, Y., & Tominaga, Y. (1998). Dynamical structure of water in aqueous solutions of LiCl, NaCl, and KCl by low-frequency Raman scattering: Comparison between the multiple random telegraph model and Cole-Cole relaxation. *Physical Review E, 58*(6), 7553-7560.

Armstrong, D. L. (ed.) (1998). Production and use of potassium. In *Better Crops with Plant Food Potassium for agriculture* (Vol. 82 No. 3, pp. 6-8). Published by Potash & Phosphate Institue. Retrieved June 14, 2016, from http://www.ipni.net/publication/bettercrops.nsf/0/E90E04A957EA624285257980007CD63C/$FILE/Better%20Crops%201998-3%20(lo%20res).pdf

Armstrong, F. A., & Boalch, G. T. (1961). The ultra-violet absorption of sea water. *Journal of Marine Biology Association of the United Kingdom, 41*(03), 591-597.

Berk, Z. (2001). *Water Science for Food Health*. CRC Press.

Carey, D. M., & Korenowski, G. M. (1998). Measurement of the Raman spectrum of liquid water. *The Journal of Chemical Physics, 108*(7), 2669-2675.

Chai, B.-h., Zheng, J.-m., Zhao, Q., & Pollack, G. H. (2008). Spectroscopic studies of solutes in aqueous solution. *The Journal of Physical Chemistry A, 112*(11), 2242-2247.

Collins, J. R. (1925). Change in the infra-red absorption spectrum of water with temeprature. *Physical Review, 26*(6), 771-779.

Collins, K. D., Neilson, G. W., & Enderby, J. E. (2007). Ions in water: Characterizing the forces that control chemical processes and biological structure. *Biophysical Chemistry, 128*(2), 95-104.

Di Noto, V., & Mecozzi, M. (1997). Determination of seawater salinity by ultraviolet spectroscopic measurements. *Applied Spectroscopy, 51*(9), 1294-1302.

Dougherty, R. C. (1998). Temperature and pressure dependence of hydrogen bond strength: A perturbation molecular orbital approach. *The Journal of Chemical Physics, 109*(17), 7372-7378.

Ernst, S., Gepert, M., & Manikowski, R. (1999). Apparent molar compressibilities of aqueous solutions of $Cu(NO_3)_2$, $CuSO_4$, and $CuCl_2$ from 288.15 K to 313.15 K. *Journal of Chemical & Engineering Data, 44*(6), 1199-1203.

Geissler, P. L., Dellago, C., Chandler, D., Hutter, J., & Parrinello, M. (2001). Autoionization in liquid water. *Science, 291*(5511), 2121-2124.

Government of Saskatchewan. (2015). *Economy*. Retrieved June 14, 2016, from http://www.economy.gov.sk.ca/Potash

Hale, G. M., & Querry, M. R. (1973). Optical constant of water in the 200 nm to 200 μm wavelength region. *Applied Optics., 12*(3), 555-563.

Hecht, E. (2002). *Optics*. Reading, MA: Addison-Wesley.

Hirschfeld, T. (1985). Salinity determination using NIRA. *Applied Spectroscopy, 39*(4), 740-741.

Hribar, B., Southall, N. T., Vlachy, V., & Dill, K. A. (2002). How ions affect the structure of water. *Journal of the American Chemical Society, 124*(42), 12302-12311.

Isaacs, E. D., Shukla, A., Platzman, P. M., Hamann, D. R., Barbiellini, B., & Tulk, C. A. (2000). Compton scattering evidence for covalency of the hydrogen bond in ice. *Journal of Physics and Chemistry of Solids, 61*(3), 403-406.

Jacobson, K. (2012). Details about potash processing. *Personal Communication*. May 7, 2012.

Kim, J., & Swager, T. M. (2001). Control of conformational and interpolymer effects in conjugated polymers. *Nature, 411*(6841), 1030-1034.

Langford, V. S., McKinley, A. J., & Quickenden, T. I. (2001). Temperature dependence of the visible-near-infrared absorption spectrum of liquid water. *The Journal of Physical Chemistry A, 105*(39), 8916-8921.

Lin, J., & Brown, C. (1992). Near-IR spectroscopic determination of NaCl in aqueous solution. *Applied Spectroscopy, 46*(12), 1809-1815.

Lin, J., & Brown, C. W. (1993). Near-IR spectroscopic measurment of seawater salinity. *Environmental Science & Technology., 27*(8), 1611-1615.

Lin, J., Zhou, J., & Brown, C. W. (1996). Identification of electrolytes in aqueous solutions from near-IR spectra. *Applied Spectroscopy, 50*(4), 444-448.

Maréchal, Y. (2006). *The hydrogen bond and the water molecule: The physics and chemistry of water, aqueous and bio-media*. Elsevier.

Martin, F., & Zipse, H. (2005). Charge distribution in the water molecule—A comparison of methods. *Journal of Computational Chemistry, 26*(1), 97-105.

Max, J. J., & Chapados, C. (2001). IR spectroscopy of aqueous alkali halide solutions: Pure salt-solvated water spectra and hydration numbers. *The Journal of Chemical Physics, 115*(6), 2664-2675.

Max, J. J., de Blois, S., Veilleus, A., & Chapados, C. (2001). IR spectroscopy of aqueous alkali halides. Factor analysis. *Canadian Journal of Chemistry, 79*, 13-21.

Max, J. J., Gessinger, V., van Driessche, C., Larouche, P., & Chapados, C. (2007). Infrared spectroscopy of aqueous ionic salt solutions at low concentrations. *The Journal of Chemical Physics, 126*(18), 184507.

Nickolov, Z. S., & Miller, J. D. (2005). Water structure in aqueous solutions of alkali halide salts: FTIR spectroscopy of the OD stretching band. *Journal of Colloid and Interface Science, 287*(2), 572-580.

Ninham, B. W., & Lo Nostro, P. (2010). *Molecular forces and self assembly: in colloid, nano sciences and biology.* Cambridge University Press.

Palmer, L. G., & Civan, M. M. (1977). Distribution of Na^+, K^+ and Cl^- between nucleus and cytoplasm in Chironomus salivary gland cells. *The Journal of Membrane Biology, 33*(1), 41-61.

Persichetti, G., Testa, G., & Bernini, R. (2013). High sensitivity UV fluorescence spectroscopy based on an optofluidic jet waveguide. *Optics Express, 21*(20), 24219-24230.

Perucca, C. F. (2003). *Potash processing in Saskatchewan - A review of process technologies.* AMEC Engineering & Construction Services Limited. CIM Bulletin.

Pestova, O. N., Kostikov, Y. P., & Khripun, M. K. (2004). X-ray phase analysis of structure of water-salt systems: NaCl-H_2O and KCl-H_2O. *Russian Journal of Applied Chemistry, 77*(7), 1082-1085.

Praprotnik, M., Janezic, D., & Mavri, J. (2004). Temperature dependence of water vibrational spectrum: A molecular dynamics simulation study. *Journal of Physical Chemistry A, 108*(50), 11056-11062.

Ravisankar, M., Reghunath, A. T., Sathianandan, K., & Nampoori, V. P. (1988). Effect of dissolved NaCl, $MgCl_2$, and Na_2SO_4 in seawater on the optical attenuation in the region from 430 to 630 nm. *Applied Optics, 27*(18), 3887-3894.

Sterner, S. M., Hall, D. L., & Bodnar, R. J. (1988). Synthetic fluid inclusions. V. Solubility relations in the system NaCl-KCl-H_2O under vapor-saturated conditions. *Geochimica et Cosmochimica Acta*, *52*(5), 989-1005.

Sullivan, J. M., Twardowski, M. S., Zaneveld, J. R., Moore, C. M., Barnard, A. H., Donaghay, P. L., & Rhoades, B. (2006). Hyperspectral temperature and salt dependencies of absorption by water and heavy water in the 400-750 nm spectral range. *Applied Optics, 45*(21), 5294-5309.

Walrafen, G. E., & Pugh, E. (2003). Raman combinations and stretching overtones from water, heavy water, and NaCl in water at shifts to ca. 7000 cm^{-1}. *Journal of Solution Chemistry, 33*(1), 81-97.

Zatula, A. S., Ryding, M. J., Andersson, P. U., & Uggerud, E. (2012). Proton mobility and stability of water clusters containing alkali metal ions. *International Journal of Mass Spectrometry, 330*, 191-199.

APPENDIX A – ADDITIONAL CALCULATIONS

Standard Error of Estimate for Figure 4-3 and 4-4

$$\sigma_{est} = \sqrt{\frac{\sum(A-A')^2}{N}} \quad \text{A-1}$$

where σ_{est} is the standard error for one set of trials at a given temperature, A is the absorbance at a given time, A' is the average absorbance at that given time for the set of trials, and N is the number of absorbance readings for a set of trials

Uncertainty for Table 5-1

$$Molality = \frac{Mass_{NaCl}}{Mass_{Water}} \quad \text{A-2}$$

$$U_{Mass_{NaCl}} = \frac{\delta Molality}{\delta Mass_{NaCl}} * u_{Mass_{NaCl}} = \frac{u_{Mass_{NaCl}}}{Mass_{Water}} \quad \text{A-3}$$

$$U_{Mass_{Water}} = \frac{\delta Molality}{\delta Mass_{Water}} * u_{Mass_{Water}} = -\frac{Mass_{NaCl} * u_{Mass_{Water}}}{Mass^2_{Water}} \quad \text{A-4}$$

$$u_{Molality} = \pm\sqrt{U^2_{Mass_{NaCl}} + U^2_{Mass_{Water}}} \quad \text{A-5}$$

where U is the partial uncertainty of the variables, and u is the uncertainty of each variable.
The same equations are used for KCl. Molarity uncertainty values are calculated with the mass of salt replaced by the moles of the salt and the mass of water replace by the total volume.

Water vs. Air Absorbance Calculation with Refractive Index
Reflection due to air/quartz interface.

$$R_{air} = \left|\frac{n_{air}-n_{quartz}}{n_{air}+n_{quartz}}\right|^2 * 100\% \quad \text{A-6}$$

$$n_{air} = 1.000293$$

$$n_{quartz} = 1.458$$

$$R_{air} = \left|\frac{1.000293-1.458}{1.000293+1.458}\right|^2 * 100\% = 3.47\%$$

Reflection due to water/quartz interface.

$$R_{water} = \left|\frac{n_{water} - n_{quartz}}{n_{water} + n_{quartz}}\right|^2 * 100\% \quad \text{A-7}$$

$$n_{water} = 1.330$$

$$R_{water} = \left|\frac{1.330 - 1.458}{1.330 + 1.458}\right|^2 * 100\% = 0.212\%$$

where R is the percentage of light reflected at each interface and n is the refractive index (Hecht, 2002).

Transmission of light through air-filled cuvette.

$$T_{air} = \left(1 - \frac{R_{air}}{100\%}\right)^4 * 100\% \quad \text{A-8}$$

$$T_{air} = \left(1 - \frac{3.47\%}{100\%}\right)^4 * 100\% = 86.8\%$$

Transmission of light through water-filled cuvette.

$$T_{water} = \left(1 - \frac{R_{air}}{100\%}\right)^2 * \left(1 - \frac{R_{water}}{100\%}\right)^2 * 100\% \quad \text{A-9}$$

$$T_{water} = \left(1 - \frac{3.47\%}{100\%}\right)^2 * \left(1 - \frac{0.212\%}{100\%}\right)^2 * 100\% = 92.4\%$$

Where T is the percent transmission through the sample.

Absorbance reading of air-filled cuvette.

$$A_{air} = 2 - \log_{10}(T_{air}) \quad \text{A-10}$$

$$A_{air} = 2 - \log_{10}(86.8) = 0.06129$$

Absorbance reading of water-filled cuvette.

$$A_{water} = 2 - \log_{10}(T_{water}) \quad \text{A-11}$$

$$A_{water} = 2 - \log_{10}(92.4) = 0.03429$$

where A is the absorbance reading of the sample.

Absorbance reading with water in the sample beam and air in the reference beam.

$$A = A_{water} - A_{air} \quad \text{A-12}$$

$$A = 0.03429 - 0.06129 = -0.027$$

95% Confidence Interval of the Estimate for Figures 7-2, 7-3, 7-8, 7-8, 7-10, and 7-11

Uncertainty

$$u = t_{v,95} * s_{yx} \quad \text{A-13}$$

Sample (Figure 7-2 a)

$\nu = N - 2 = 30$

$t_{30,95} = 2.042$

$$s_{A,c} = \sqrt{\frac{\sum_{i=1}^{N}\left(A_{measured\_i} - A_{modeled\_i}\right)^2}{\nu}} \quad \text{A-14}$$

$s_{A,c} = 0.0021$

$u = 2.042 * 0.0021$

$u = 0.0044$

Standard Error of Estimate for Table 7-3.

$$\sigma_{est} = \sqrt{\frac{\sum(T_{modeled} - T_{measured})^2}{N-2}} \quad \text{A-15}$$

where σ_{est} is the standard error of the estimate for each wavelength and T is the temperature.

Standard Error of Estimate for Table 7-4 and Table 7-5.

$$\sigma_{est} = \sqrt{\frac{\sum(C_{modeled} - C_{measured})^2}{N-2}} \quad \text{A-16}$$

where σ_{est} is the standard error of the estimate for variable and C is the molarity (for g·gwater^{-1} concentration, c would be used).

APPENDIX B – MODELLING AT CONSTANT TEMPERATURE

```
%-----------------------------------------------------------
% Peters, R. 2016. Differentiating Between NaCl(aq) and KCl(aq) in Solution
Using
% Spectral Measurements at Constant Temperature.
% Version 1.0
% Input data .txt
% [:,1] = wavelength (nm)
% [:,2:i] = spectral data for i-1 samples with air as reference (N/A)
%-----------------------------------------------------------
% Points of interest:
% A 1353 nm point of primary g·gwater-1
% B 1210 nm point of primary species differentiation
% C 1229 nm point of species specific molarity
% D 1674 nm point of molarity check
% E 953 nm point of g·gwater-1 check
%-----------------------------------------------------------

clear all
clc

% Load the spectra
filename='sample.txt';
eval(['load ',filename])
solution=sample;
x=size(sample,2);

for i=2:x

    % Pull points of interest from the sample
    A=solution(find(solution==1353,2),i);
    B=solution(find(solution==1210,2),i);
    C=solution(find(solution==1229,2),i);
    D=solution(find(solution==1674,2),i);
    E=solution(find(solution==953,2),i);

    totmolal=-1.55651*A+2.23224;

    % Species determination parameters - estimation of absorbance at 1210
    % nm based on total g·gwater-1 calculation
    Naest=totmolal*(-0.08155)+0.51455;
    Kest=totmolal*(-0.12868)+0.51447;
    % Comparison to measured value at 1210 nm
    Ntest=abs(Naest-B);
    Ktest=abs(Kest-B);

    % Determining speciation and concentrations
    if totmolal<0.01
        type='water';
        typenum=0;
        molar=0;
        molarcheck=0;
        molal=0;
        molalcheck=0;
```

```
        totmolal=0;
    else if Ntest>Ktest
        type='KCl';
        typenum=2;
        molar=(C-0.48606)/(-0.01609);
        molarcheck=(D-2.40770)/(-0.21294);
        molarerr=abs(molar-molarcheck)/abs(molar)*100;
        molal=(B-0.51447)/(-0.12868);
        molalcheck=(E-0.12849)/(-0.07959);
        molalerr=abs(molal-molalcheck)/abs(molal)*100;
    else
        type='NaCl';
        typenum=1;
        molar=(C-0.48556)/(-0.01036);
        molarcheck=(D-2.40770)/(-0.21294);
        molarerr=abs(molar-molarcheck)/abs(molar)*100;
        molal=(B-0.51455)/(-0.08155);
        molalcheck=(E-0.12849)/(-0.07959);
        molalerr=abs(molal-molalcheck)/abs(molal)*100;
        end
    end
    output(1,i)=typenum;
    output(2,i)=molar;
    output(3,i)=molarcheck;
    output(4,i)=molal;
    output(5,i)=molalcheck;
    output(6,i)=totmolal;

end
```

APPENDIX C – MODELLING WATER BETWEEN 15°C AND 95°C

```
%-------------------------------------------------------
% Peters, R. 2016. Determining Water Temperature Using Spectral Techniques.
% Version 1.0
% Input data .txt
% [:,1] = wavelength (nm)
% [:,2:i] = spectral data for i-1 samples with air as reference (N/A)
%-------------------------------------------------------
% Points of interest:
% A 1256 nm point of primary temperature determination
% B 1674 nm point of secondary temperature determination
% C 953 nm point of secondary temperature determination
% D 1135 nm point of secondary temperature determination
%-------------------------------------------------------

clear all
clc

% Load the spectra
filename='sample.txt';
eval(['load ',filename])
solution=sample;
x=size(sample,2);

for i=2:x

    % Pull points of interest from the sample
    A=solution(find(solution==1256,2),i);
    B=solution(find(solution==1674,2),i);
    C=solution(find(solution==953,2),i);
    D=solution(find(solution==1135,2),i);

    % Temperature determination at each wavelength
    temp1256=-794.871547*A+379.062427;
    temp1674=-89.302017*B+245.814552;
    temp953=1125.056228*C-117.447325;
    temp1135=981.060001*D-148.659832;

    output(1,i)=temp1256;
    output(2,i)=temp1674;
    output(3,i)=temp953;
    output(4,i)=temp1135;

end
```

APPENDIX D – MODELLING MIXED SALTS USING SINGLE-WAVELENGTH COMPARISONS

```
%-----------------------------------------------------------
% Peters, R. 2016. Differentiating Between NaCl(aq) and KCl(aq) in Dual-Salt
% Solutions Using Single-Wavelength Differences in Spectral Measurements.
% Version 1.0
% Input data .txt
% [:,1] = wavelength (nm)
% [:,2:i] = spectral data for i-1 samples with air as reference (N/A)
%-----------------------------------------------------------
% Points of interest:
% A 1353 nm point of overall g·gwater-1
% B 1210 nm point of species specific g·gwater-1
% C 1229 nm point of species specific molarity
% D 1674 nm point of overall molarity
% E 1218 nm point of species specific g·gwater-1
% F 1322 nm point of species specific molarity
% G 1203 nm point of species specific g·gwater-1
% H 1748 nm point of species specific molarity
%-----------------------------------------------------------

clear all
clc

% Load the spectra
filename='sample.txt';
eval(['load ',filename])
solution=sample;
x=size(sample,2);

for i=2:x
% Pull points of interest from the sample
    A=solution(find(solution==1353,2),i);
    B=solution(find(solution==1210,2),i);
    C=solution(find(solution==1229,2),i);
    D=solution(find(solution==1674,2),i);
    E=solution(find(solution==1218,2),i);
    F=solution(find(solution==1322,2),i);
    G=solution(find(solution==1203,2),i);
    H=solution(find(solution==1748,2),i);

% Overal g·gwater-1 and Molarity
    totmolal=(A-1.433495)/(-0.642655);
    totmolar=(D-2.397689)/(-0.205160);

% Estimating expected absorbance at 1210 nm based on total g·gwater-1 assuming
% single-salt solutions
Naest1=totmolal*(-0.08155)+0.51455;
Kest1=totmolal*(-0.12868)+0.51447;
% Comparison to measured value at 1210 nm
Namolal1=abs(B-Kest1)/abs(Kest1-Naest1)*totmolal;
Kmolal1=abs(B-Naest1)/abs(Kest1-Naest1)*totmolal;
```

```
% Converting g·gwater-1 to molarity for 1210 nm values
coNamolar1=(Namolal1+0.001154)/(0.067414);
coKmolar1=(Kmolal1-0.000886)/(0.084877);

% Estimating expected absorbance at 1229 nm based on total molarity assuming
% single-salt solutions
Nraest1=totmolar*(-0.01036)+0.48556;
Krest1=totmolar*(-0.01609)+0.48606;
% Comparison to measured value at 1229 nm
Namolar1=abs(C-Krest1)/abs(Krest1-Nraest1)*totmolar;
Kmolar1=abs(C-Nraest1)/abs(Krest1-Nraest1)*totmolar;
% Converting molarity to g·gwater-1 for 1229 nm values
coNamolal1=Namolar1*0.067414-0.001154;
coKmolal1=Kmolar1*0.084877+0.000886;

% Estimating expected absorbance at 1218 nm based on total g·gwater-1 assuming
% single-salt solutions
Naest2=totmolal*(-0.10963)+0.50419;
Kest2=totmolal*(-0.15185)+0.50429;
% Comparison to measured value at 1218 nm
Namolal2=abs(E-Kest2)/abs(Kest2-Naest2)*totmolal;
Kmolal2=abs(E-Naest2)/abs(Kest2-Naest2)*totmolal;
% Converting g·gwater-1 to molarity for 1218 nm values
coNamolar2=(Namolal2+0.001154)/(0.067414);
coKmolar2=(Kmolal2-0.000886)/(0.084877);

% Estimating expected absorbance at 1322 nm based on total molarity assuming
% single-salt solutions
Nraest2=totmolar*(-0.03801)+0.81960;
Krest2=totmolar*(-0.04717)+0.81819;
% Comparison to measured value at 1322 nm
Namolar2=abs(F-Krest2)/abs(Krest2-Nraest2)*totmolar;
Kmolar2=abs(F-Nraest2)/abs(Krest2-Nraest2)*totmolar;
% Converting molarity to g·gwater-1 for 1322 nm values
coNamolal2=(Namolar2)*0.067414-0.001154;
coKmolal2=(Kmolar2)*0.084877+0.000886;

% Estimating expected absorbance at 1203 nm based on total g·gwater-1 assuming
% single-salt solutions
Naest3=totmolal*(-0.06301)+0.52577;
Kest3=totmolal*(-0.11043)+0.52539;
% Comparison to measured value at 1203 nm
Namolal3=abs(G-Kest3)/abs(Kest3-Naest3)*totmolal;
Kmolal3=abs(G-Naest3)/abs(Kest3-Naest3)*totmolal;
% Converting g·gwater-1 to molarity for 1203 nm values
coNamolar3=(Namolal3+0.001154)/(0.067414);
coKmolar3=(Kmolal3-0.000886)/(0.084877);

% Estimating expected absorbance at 1748 nm based on total molarity assuming
% single-salt solutions
Nraest3=totmolar*(-0.17372)+3.11223;
Krest3=totmolar*(-0.21409)+3.11519;
% Comparison to measured value at 1748 nm
Namolar3=abs(H-Krest3)/abs(Krest3-Nraest3)*totmolar;
Kmolar3=abs(H-Nraest3)/abs(Krest3-Nraest3)*totmolar;
% Converting molarity to g·gwater-1 for 1748 nm values
```

```
coNamolal3=(Namolar3)*0.067414-0.001154;
coKmolal3=(Kmolar3)*0.084877+0.000886;

% Summarize findings
NarS=[coNamolar1 Namolar1 coNamolar2 Namolar2 coNamolar3 Namolar3];
NalS=[Namolal1 coNamolal1 Namolal2 coNamolal2 Namolal3 coNamolal3];
KrS=[coKmolar1 Kmolar1 coKmolar2 Kmolar2 coKmolar3 Kmolar3];
KlS=[Kmolal1 coKmolal1 Kmolal2 coKmolal2 Kmolal3 coKmolal3];

% Find averages
avgNamolar=mean(NarS(:,:));
avgKmolar=mean(KrS(:,:));
avgNamolal=mean(NalS(:,:));
avgKmolal=mean(KlS(:,:));

% Find differences to average
for j=1:6
    diffNamolar(j,:)=[abs(avgNamolar-NarS(1,j)) j];
    diffNamolal(j,:)=[abs(avgNamolal-NalS(1,j)) j];
    diffKmolar(j,:)=[abs(avgKmolar-KrS(1,j)) j];
    diffKmolal(j,:)=[abs(avgKmolal-KlS(1,j)) j];
end

% Take out least best fit point and average remaining
NarSort=sortrows (diffNamolar,1);
Namolar=sum(NarS(1,NarSort(1:5,2)))/5;

NalSort=sortrows (diffNamolal,1);
Namolal=sum(NalS(1,NalSort(1:5,2)))/5;

KrSort=sortrows (diffKmolar,1);
Kmolar=sum(KrS(1,KrSort(1:5,2)))/5;

KlSort=sortrows (diffKmolal,1);
Kmolal=sum(KlS(1,KlSort(1:5,2)))/5;

if totmolal<0.01
    Namolal=0;
    Kmolal=0;
    Namolar=0;
    Kmolar=0;
    totmolar=0;
    totmolal=0;
end

% Output
output(4,i)=Namolal;
output(5,i)=Kmolal;
output(1,i)=Namolar;
output(2,i)=Kmolar;
output(3,i)=totmolar;
output(6,i)=totmolal;

rejects(1,i)=NarSort(6,2);
rejects(2,i)=KrSort(6,2);
```

```
rejects(3,i)=NalSort(6,2);
rejects(4,i)=KlSort(6,2);
end
```

APPENDIX E – MODELLING MIXED SALTS USING DUAL-WAVELENGTH COMPARISONS

```
%-----------------------------------------------------------
% Peters, R. 2016. Differentiating Between NaCl(aq) and KCl(aq) in Dual-Salt
% Solutions Using Dual-Wavelength Comparisons in Spectral
% Measurements.
% Version 1.0
% Input data .txt
% [:,1] = wavelength (nm)
% [:,2:i] = spectral data for i-1 samples with water as reference (N/A)
%-----------------------------------------------------------
% Points of interest:
% A 1209 nm point where NaCl 1353-nm-normalized data converge
% B 1213 nm point where KCl 1353-nm-normalized data converge
% C 1353 nm point of overall salinity
%-----------------------------------------------------------

clear all
clc

% Load the spectra
filename='sampleminw.txt';
eval(['load ',filename])
solution=sampleminw;
x=size(sample,2);

% Pull points of interest from the sample
for i=2:x
A=solution(find(solution==1209,2),i);
B=solution(find(solution==1213,2),i);
C=solution(find(solution==1353,2),i);

% Determine overall g·gwater-1
totmolal=(C-0.009640)/(-0.658390);

% Normalizing absorbance at 1209 and 1213 nm
Acal=A/C;
Bcal=B/C;

% Calculating line parameters based on average values at 1213 and 1209 nm
m1=(0.219875-0.120547)/(1213-1209);
b1=0.120547-(m1*1209);

% Calcualting linear position of current spectrum
m2=(Bcal-Acal)/(1213-1209);
b2=Acal-m2*1209;
x=(b2-b1)/(m1-m2);

% Calculating NaCl and KCl concentraiton based on linear comparison
NaClmolal=totmolal*((1213-1209)-abs(1209-x))/(1213-1209);
KClmolal=totmolal*((1213-1209)-abs(1213-x))/(1213-1209);
```

```
% Converting g·gwater-1 to molarity
NaClmolar=(NaClmolal+0.001154)/(0.067414);
KClmolar=(KClmolal-0.000886)/(0.084877);

% Accounting for negative concentration readings
if NaClmolal<0
    KClmolal=totmolal;
    NaClmolal=0;
    NaClmolar=0;
end
if KClmolal<0
    NaClmolal=totmolal;
    KClmolal=0;
    KClmolar=0;
end

totmolar=NaClmolar+KClmolar;

output(1,i)=NaClmolar;
output(2,i)=KClmolar;
output(3,i)=totmolar;
output(4,i)=NaClmolal;
output(5,i)=KClmolal;
output(6,i)=totmolal;
end
```